SANDIA REPORT
SAND2006-0091
Unlimited Release
Printed January 2006

Development and Testing of a Mudjet-Augmented PDC Bit

David W. Raymond and James W. Grossman

Prepared by
Sandia National Laboratories
Albuquerque, New Mexico 87185 and Livermore, California 94550

Sandia is a multiprogram laboratory operated by Sandia Corporation,
a Lockheed Martin Company, for the United States Department of Energy's
National Nuclear Security Administration under Contract DE-AC04-94AL85000.

Issued by Sandia National Laboratories, operated for the United States Department of Energy by Sandia Corporation.

Available to DOE and DOE contractors from
U.S. Department of Energy
Office of Scientific and Technical Information
P.O. Box 62
Oak Ridge, TN 37831

Telephone: (865) 576-8401
Facsimile: (865) 576-5728
E-Mail: reports@adonis.osti.gov
Online ordering: http://www.osti.gov/bridge

Available to the public from
U.S. Department of Commerce
National Technical Information Service
5285 Port Royal Rd.
Springfield, VA 22161

Telephone: (800) 553-6847
Facsimile: (703) 605-6900
E-Mail: orders@ntis.fedworld.gov
Online order: http://www.ntis.gov/help/ordermethods.asp?loc=7-4-0#online

SAND2006-0091
Unlimited Release
Printed January 2006

Development and Testing of a Mudjet-Augmented PDC Bit

David W. Raymond
dwraymo@sandia.gov

James W. Grossman
jwgross@sandia.gov

Sandia National Laboratories
P.O. Box 5800
Albuquerque, NM 87185-1033

Georges Chahine and Ken Kalumuck, DynaFlow, Inc.
Oliver Matthews, Security DBS
Alan Black, TerraTek, Inc.
Ken Bertagnolli and Michael Vail, US Synthetic

ABSTRACT

This report describes a project to develop technology to integrate passively pulsating, cavitating nozzles within Polycrystalline Diamond Compact (PDC) bits for use with conventional rig pressures to improve the rock-cutting process in geothermal formations. The hydraulic horsepower on a conventional drill rig is significantly greater than that delivered to the rock through bit rotation. This project seeks to leverage this hydraulic resource to extend PDC bits to geothermal drilling.

This page intentionally left blank

CONTENTS

Page

List of Figures

List of Tables

1. Introduction

With a broad science and engineering charter to meet our national security needs, including energy security, Sandia National Laboratories has been tasked by the U.S. Department of Energy with a programmatic mission to develop technology that improves development and use of our nation's renewable energy resources to help ensure a secure base-load electrical energy supply for our future. Specifically, with funding from the DOE Office of Geothermal Technologies, our objective is to improve drilling technology to reduce drilling costs and thereby foster exploration and development of geothermal resources. In the short term, this means improving the penetration rate and life of conventional drill bits used by the drilling industry for geothermal well-field construction.

Notable among the conventional bits currently used by the drilling industry at large are polycrystalline diamond compact (PDC) drill bits. These bits are comprised of a myriad of synthetic cutting elements, or PDCs, mounted in an array on a bit substrate. Application of torque to the bit, resulting in rotation of the bit face against a geologic formation, allows the polycrystalline diamond elements to "cut" the rock. Although polycrystalline diamond technology was originally developed by General Electric, Sandia has had a long-standing presence in the development of PDC bit technology including contributions in materials development, resolution of substrate bonding anomalies, laboratory testing and development of empirical relationships to predict cutting loads, and computational modeling of the integrated bit response. While originally heralded as a significant technology for drilling hard-rock formations characteristic of geothermal resources, it is primarily the oil and gas drilling industry that has profited from the development of PDC bits since their inception. The abrasiveness and high compressive strength of geothermal formations have exceeded the capabilities of PDC bits for the first twenty years of their existence.

As a possible complement to PDC bits, Sandia has considered the energy resident in the drilling fluids pumped to the bit for cooling and cuttings removal as a possible synergistic-collaborator in advancing the wellbore. Towards this objective, Sandia worked with Tracor Hydronautics and then with DynaFlow, to whom ownership of the technology and principal investigators were transferred, to develop cavitating jet technology in the late seventies and early eighties specifically for this application. That work resulted in advances in the technology of passively pulsating-cavitating jets and their applications. The work described herein seeks to blend these two complementary technologies, PDC bits and pulsating cavitating jets, to improve the performance of polycrystalline diamond compact bits so that they may be utilized for exploration and production of geothermal resources.

1.1 Background

Most geothermal wells today are drilled using roller cone bits (*Figure 1*). Although robust, these bits drill at slow penetration rates in hard rock. Rotation of the cones is required to crush the rock, and these moving parts are prone to fail in the hot, hard, abrasive environment typical of geothermal drilling, rendering the entire bit inoperative. The seals that protect the bearings have also been known to fail when exposed to the high temperatures of geothermal formations. Roller cone bit technology is mature and few major improvements are likely.

Figure 1: Roller Cone Bit (IADC Code 6-2-7). Photo courtesy of Reed Hycalog.

Figure 2: PDC Bit. Photo Courtesy of Security DBS.

Conversely, polycrystalline diamond compact bits (*Figure 2*) have an aggressive cutting structure but have not found widespread use in drilling hard rock. PDC bits have no moving parts and they possess high-temperature resistance by virtue of the materials of which they are constructed. Today's PDC bits are drilling harder, more abrasive formations than ever before [1]. Nevertheless, PDC bits are not without their limitations in hard-rock formations.

It is the wear resistance of PDC bits in the hard, abrasive formations characteristic of geothermal drilling that has traditionally been the concern. While laboratory cutter wear testing confirms the abrasion resistance of PDC cutters has improved to where drag bits are economically viable for drilling abrasive formations, improper operation of synthetic diamond bits can still lead to accelerated wear of the individual cutters. Furthermore, many PDC bits returning from the field exhibit impact type damage resulting from dynamic instability of the drill string. Bit bounce, whirl, and stick-slip are some of the types of dynamic instability that can occur. The effects of abrasion and impact-types of failure can be reduced by improved use of the hydraulic energy in the drilling fluid.

Many attempts have been made over the years to commercialize high-pressure (>10,000 psi) water or mudjet drilling systems. These attempts have invariably failed because of the

difficulties of using such high pressures on a drill rig. Equipment maintenance is a costly nuisance when an abrasive fluid like drilling mud is pumped at high pressure. Instead of high-pressure, this project seeks to use existing drilling fluid pressures more effectively down hole. Several investigators have studied the reduction in cutting forces that occurs when a moderate-pressure (<10,000 psi) water jet is directed at the rock surface ahead of a drag cutter. Hood [2] found that a 7,000-psi waterjet reduced cutting forces on a tungsten carbide cutter in Norite (44,000-psi compressive strength) by about 50%. Dubugnon [3] showed 10-20% reductions in drag cutter forces with nozzle pressures as low as 1,000 psi in Bohus Granite (29,000-psi compressive strength). Single-cutter test data generated by Glowka [4] shows that when a 4500-psi high-pressure jet is directed at a PDC cutter there is a 50-65% reduction in the penetrating stress required to cut the rock. Some of Glowka's results for Sierra White Granite are shown in *Figure 3*. These cutter force reductions are thought to be caused by two mechanisms: 1) the jet blasts away the very fine rock flour (debris) created by the surface-crushing action of the cutter against the rock, increasing the stress concentrations in the rock and decreasing the forces required to cut the rock; and 2) the fluid enters rock fractures created by the cutter, hydraulically extending the fractures and reducing the mechanical forces required to form a rock chip.

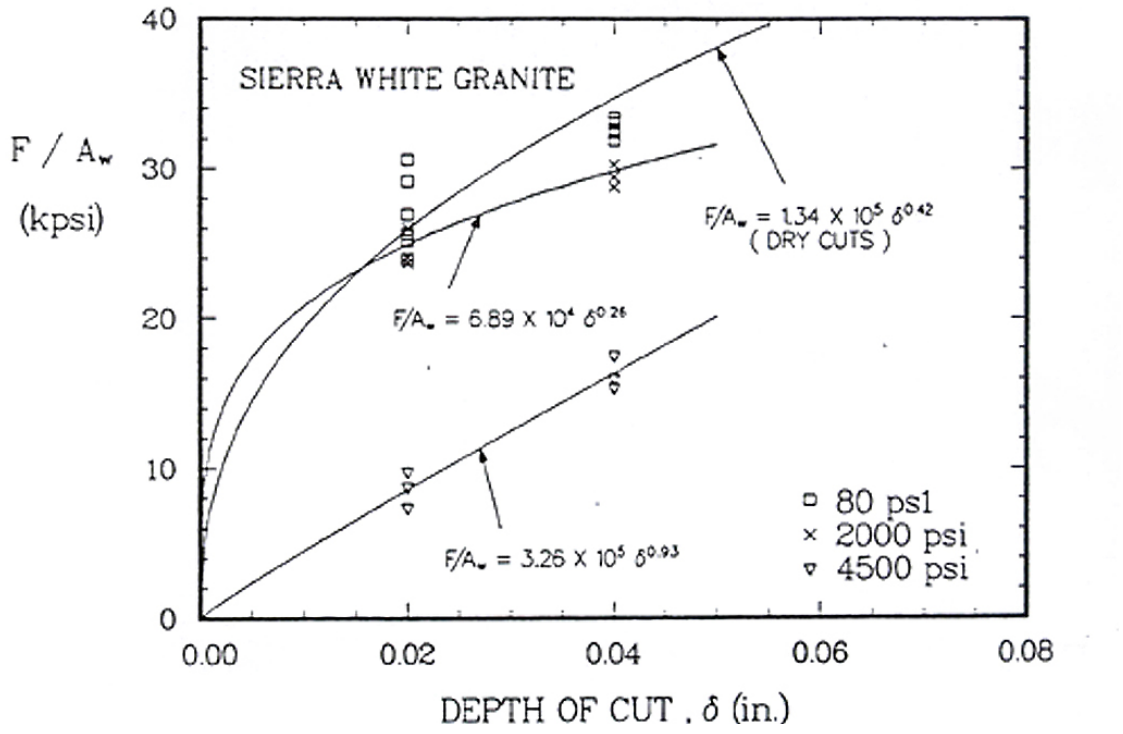

Figure 3: Single cutter test data with moderate pressure augmentation [from reference 4].

Another way to make effective use of this synergistic interaction using moderate pressures and mechanical cutters is by hydraulic design that induces cavitation at the rock surface. Cavitation can lead to increased penetration rates by improved hole cleaning at the bit/rock interface, through weakening or direct erosion of the rock, or a combination of these effects. Cavitation can be generated using a nozzle that produces low pressure regions in the flow. Radtke & Cohn conducted comprehensive research demonstrating that cavitating jets are more efficient than non-cavitating nozzles in kerf cutting tests in the high ambient pressures typical of deep hole drilling environments [5]. Generation of organized vortical structures in the jet can further enhance cavitation in pulsating cavitating jets [6, 7].

The principle behind the cavitating jet technology used in this project, denoted STRATOJET®, is shown in *Figure 4*. Pulsations are produced by acoustic reflections at the entrance to an "organ pipe" internal to the nozzle waterway. The pulsations produce a structured flow regime at the nozzle exit that collapses against the rock spawning high velocity microjets. Research conducted by DynaFlow has suggested that very high impact pressures can result as these bubbles collapse against the rock surface.

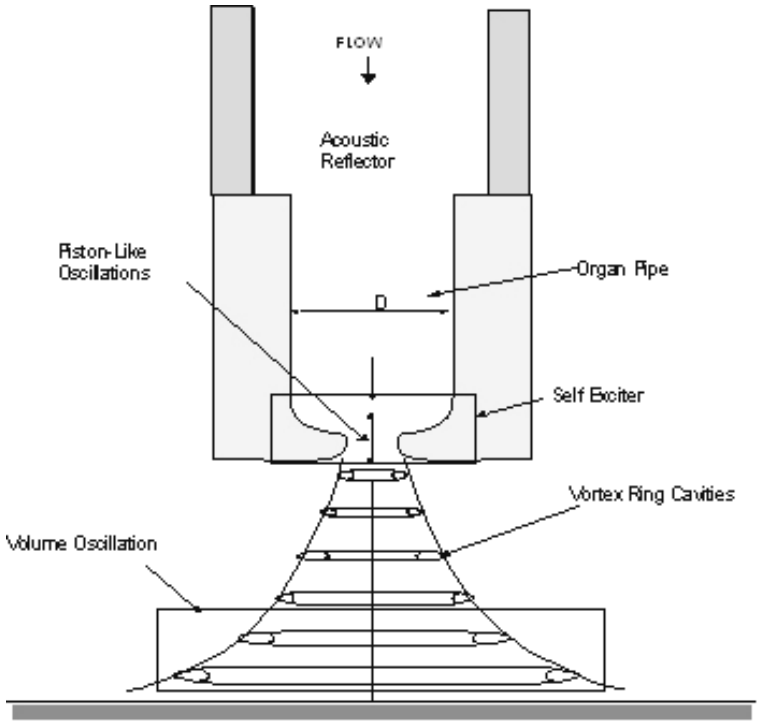

Figure 4: Cavitating Jet Concept.

Sandia sponsored considerable work by Tracor Hydronautics on these cavitating jets, the result of which was an improved understanding of the factors governing the formation of organized structures in the self-resonating jets [6]. From Reference 6, structured cavitating jets hold several benefits over conventional nozzles in regard to drilling applications. *Figure 5* shows that these jets will develop incipient cavitation at greater ambient pressures than conventional jets [7]. DynaFlow has conducted erosion tests with these nozzles at elevated ambient pressures. *Figure 6* shows these jets are also more erosive than conventional jets at the ambient pressures below which conventional nozzles begin to

cavitate [8]. Additionally, computational modeling by DynaFlow has demonstrated that Stratojets® create negative pressure pulsations along the bottom of the wellbore as the flow moves outward from the nozzle [7]. These pulsations help to reduce hold-down forces on cuttings that coat the bottom of the wellbore and resist its advancement.

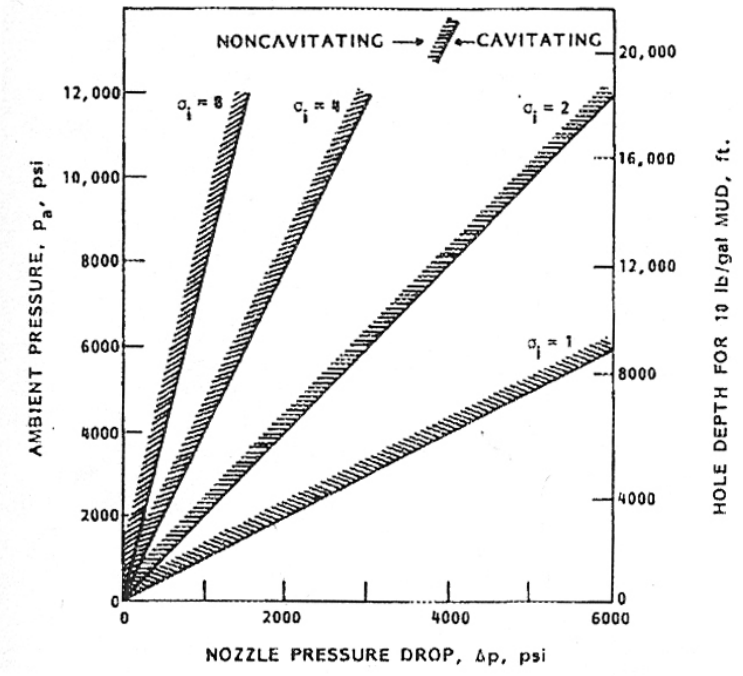

Figure 5: Stratojets® cavitate at greater depths than conventional jets [from reference 7].

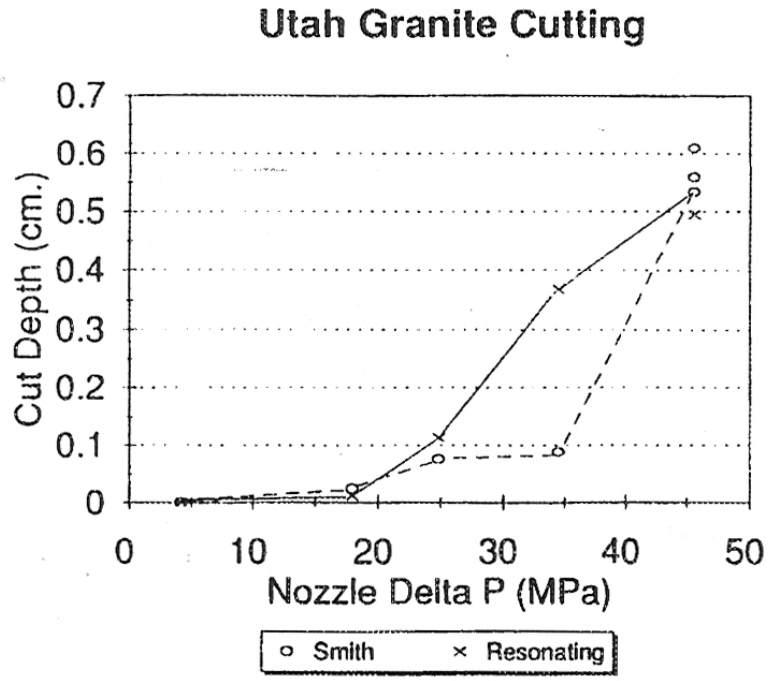

Figure 6: Stratojets® are more erosive than conventional jets [from reference 8].

Using cavitating jets with PDC bits can reduce cutting forces on drag cutters in hard rock to help extend use of PDC bits to the formations characteristic of geothermal reservoirs. If PDC bits could be made more robust by improved hydraulic design such that these bits could be used for geothermal drilling, we can take advantage of the more efficient cutting mechanism and higher penetration rates achievable with these bits. Cost savings of $20,000 to $400,000 per bit run have been reported in the petroleum drilling literature on PDC bits. Extending such costs savings to geothermal drilling may be possible with mudjet augmentation because of the cutter force reductions that are achievable with this technique. Smaller cutter forces would reduce both abrasive wear and the dynamic bit behavior that leads to cutter impact damage. PDC bits are currently not used in geothermal drilling because of the catastrophic failure caused by these damage mechanisms. Nevertheless, while this project is directly relevant to geothermal drilling, it is expected that this technology could be applied to drilling other rock formations as well.

1.2 Overall Approach

This work proceeded in two phases. In the first phase of the project, we sought to demonstrate that a mudjet augmented PDC bit could be built that drills with increased penetration rate in hard rocks. This was accomplished by designing, fabricating, and laboratory testing a prototype bit. The laboratory testing was conducted under elevated ambient pressures so that meaningful penetration-rate data could be obtained and the effect of cavitation suppression at simulated depth could be evaluated. Data related to bit life was recorded during Phase I, but an adequate evaluation of expected improvements in bit life could not be conducted in a laboratory test program. Bit life, therefore, will be evaluated during later field-testing opportunities.

Phase II was to be conducted only if Phase I was successful in demonstrating that a mudjet-augmented PDC bit could be designed and fabricated that drills faster in hard rock than both a conventional PDC bit and a roller cone bit. The objective of Phase II was to improve our understanding of the various parameters that contribute to enhanced performance using the synergistic combination of drag cutters and cavitating jet technology.

To take advantage of the benefits offered by incorporating resonating cavitating jets in fixed cutter bits, the work was approached in four areas:

1) Specification of Nozzle Configurations and Operating Conditions
2) Development of Cavitation-Resistant Orifices
3) Integration of Nozzles into PDC Bits, and
4) Characterization of Performance (Bit Response and Nozzle/Cutter Interaction)

These topics are addressed in both Phase I and Phase II.

1.3 Technical Objectives

The technical objectives of each phase of the project are as follows:

- Phase I: Develop and demonstrate a PDC bit with cavitating jets fed by conventional rig pressures (less than 6,000 psi) that produces enhanced penetration rates, reduced bit loads, and demonstrates that resonating cavitating jets are not suppressed at depth.

- Phase II: Characterize the relationships between parameters involved in the nozzle/cutter interaction.

1.4 Sponsorship

This project was originally funded through the National Advanced Drilling and Excavations Technologies (NADET) Program. The NADET program was started in 1995 with funding provided by the geothermal division of the Department of Energy (DOE). Initial funding covered the work of the contractors under Phase I of the work described herein. The DOE Office of Geothermal Technologies provided follow-on funding for Sandia and the contractors engaged in Phase II of the work activities.

This page intentionally left blank

2. Phase I – Demonstration of Feasibility

The objective in Phase I is to develop and demonstrate a PDC bit that incorporates cavitating jet technology. To be representative of field drilling conditions, the demonstration testing is conducted under realistic hydrostatic pressures that would be encountered in field drilling so that meaningful penetration-rate data can be obtained and the effects of cavitation suppression can be evaluated. It is desired to compare the performance of such an augmented bit to an identical bit incorporating conventional nozzles. It was unclear at the beginning of the project if this would be accomplished through identical bits with different hydraulics or in a single bit with interchangeable nozzles. It was also not clear if the orifices would each have their own resonating chambers or if they would share a central chamber – the approach would be resolved as part of the nozzle/bit integration.

To develop a demonstration bit incorporating this technology, a cooperative team was formed consisting of DynaFlow, Inc. - owner of the Stratojet® patent, Security DBS – a PDC bit manufacturer, TerraTek, Inc. – an indoor drilling laboratory, and Sandia National Laboratories – overall project integrator. The principal investigators from each of these organizations for this phase of the work are: Georges Chahine and Ken Kalumuck, DynaFlow, Inc; Oliver Matthews, Security DBS; Alan Black, TerraTek, Inc.; and David Raymond, Sandia National Laboratories.

DynaFlow conducted design studies and laboratory testing to optimize nozzle performance for this application, designed nozzles, and provided specifications to Sandia and Security DBS for integration into the demonstration bit. Security DBS integrated the nozzle design with the bit design, designed and fabricated the prototype bit, and participated in laboratory testing activities. TerraTek, Inc. conducted full-scale laboratory testing of the prototype bit under simulated downhole conditions using their Drilling Research Laboratory (DRL). Sandia National Laboratories provided parameters for the overall bit specification, assisted in the design of the prototype bit, and coordinated joint work activities including planning and design reviews, laboratory testing, and reporting.

2.1 Approach

The project team selected many of the design and operating parameter specifications during preparation of the proposal to NADET; others were selected in the course of the project. The rationale for many of these parameter selections is described below.

2.1.1 Bit Selection

A bit diameter of 8-1/2 inches was selected for the Phase I demonstration to be applicable to geothermal well bore construction. While a range of bit diameters is certainly required, the well profile at total depth in a geothermal reservoir is often near this size. It is noted that the general approach to development of the Phase I bit will be applicable to other bit diameters given sufficient latitude in cutter/nozzle interaction geometries and overall hydraulic design.

It was decided in the proposal stage of this project that the approach would include modification of a PDC bit from the existing product line available at Security DBS. In so doing, the Phase I development could focus upon modification of the waterway in an existing bit design to accommodate the organ pipes that feed the cavitating nozzles. It was also decided that the bit would be of the matrix body type; i.e., cast tungsten-carbide material, for superior erosion resistance to that offered by steel-bodied bits.

Security DBS considered various cutting structures for the demonstration bit encompassing PDC bit designs with five to nine blades. The cutter distribution of a five-blade, medium-set, matrix body PDC bit was chosen as it was presumed that a lighter cutter distribution would show a more favorable response when subject to jet augmentation. The cutting structure is a track-set bit; meaning the cutters run in "tracks" that may be redundant with other cutters on the bit. This bit is a Security DBS Model No. FM2546 which corresponds to an IADC Code M434 [9]. It includes 37 primary cutters (4-19mm diameter and 33-13 mm diameter compacts) and eight (8) gage cutters. The cutting structure of the bit is described in *Table 1*. The cutter numbers generally increase radially outward. *Figure 7* shows the cutter layout on the face of the bit. Note that the second column of *Table 1* is used to identify the cutter ID in *Figure 7*. The conventional implementation of this bit incorporates one nozzle per blade, which as we shall see, fit favorably with integration of the organ pipes into the bit body.

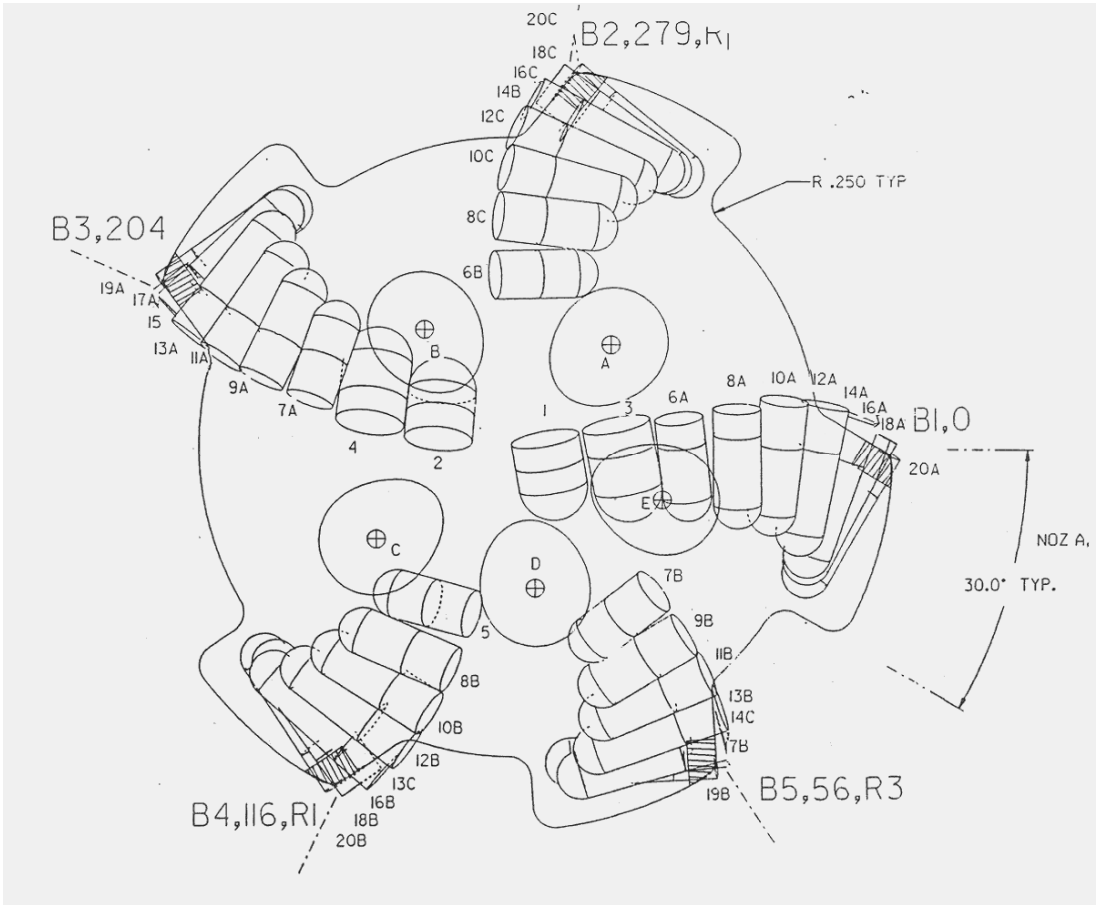

Figure 7: Phase I Bit Cutting Structure.

Table 1: Cutting Structure of the Phase I Demonstration Bit.

Cutter No.	Cutter ID	PDC wafer (in)	Cutter radius (in)	Back rake (deg)	Side rake (deg)	Prof angle (deg)	Long pos. (in)	Ang. Pos. (deg)
1	1	0.3800	0.4060	12.000	-8.22	-25.00	0.627	12.72
2	2	0.3800	0.7865	20.000	-7.73	-25.00	0.822	173.73
3	3	0.3800	1.2033	12.000	-6.09	-25.00	1.002	10.59
4	4	0.3800	1.5593	20.000	-6.38	-22.00	1.186	170.38
5	5	0.2695	1.8954	20.000	-5.00	-7.00	1.416	257.50
6	6A	0.2695	1.8964	15.000	-5.00	-7.00	1.409	9.50
7	6B	0.2695	1.8964	15.000	-5.00	-7.00	1.409	94.50
8	7A	0.2695	2.2557	15.000	-5.00	5.50	1.426	167.00
9	7B	0.2695	2.2564	20.000	-5.00	5.50	1.433	315.00
10	8A	0.2695	2.5543	15.000	-5.00	16.50	1.360	9.50
11	8B	0.2695	2.5543	15.000	-5.00	16.50	1.360	255.50
12	8C	0.2695	2.5543	15.000	-5.00	16.50	1.360	92.50
13	9A	0.2695	2.8377	15.000	-5.00	27.40	1.216	165.00
14	9B	0.2695	2.8377	15.000	-5.00	27.40	1.216	313.00
15	10A	0.2695	3.0921	20.000	-5.00	36.90	1.035	9.50
16	10B	0.2695	3.0921	20.000	-5.00	36.90	1.035	253.50
17	10C	0.2695	3.0921	20.000	-5.00	36.90	1.035	90.50
18	11A	0.2695	3.3282	20.000	-5.00	46.70	0.811	163.00
19	11B	0.2695	3.3282	20.000	-5.00	46.70	0.811	311.00
20	12A	0.2695	3.5365	20.000	-5.00	53.40	0.562	7.50
21	12B	0.2695	3.5365	20.000	-5.00	53.40	0.562	251.50
22	12C	0.2695	3.5437	25.000	-5.00	53.40	0.567	88.50
23	13A	0.2695	3.7141	20.000	-5.00	60.20	0.289	161.00
24	13B	0.2695	3.7141	20.000	-5.00	60.20	0.289	309.00
25	13C	0.2695	3.8593	20.000	-5.00	66.90	-0.003	249.00
26	14A	0.2695	3.8668	25.000	-5.00	66.90	0.001	5.00
27	14B	0.2695	3.8668	25.000	-5.00	66.90	0.001	86.00
28	14C	0.2695	3.9683	20.000	-5.00	73.70	-0.311	306.50
29	15	0.2695	3.9765	25.000	-5.00	73.70	-0.307	158.50
30	16A	0.2695	4.0600	30.000	-5.00	80.40	-0.624	2.50
31	16B	0.2695	4.0600	30.000	-5.00	80.40	-0.624	246.50
32	16C	0.2695	4.0600	30.000	-5.00	80.40	-0.624	83.50
33	17A	0.2695	4.0953	30.000	-5.00	87.20	-0.950	156.00
34	17B	0.2695	4.0953	30.000	-5.00	87.20	-0.950	304.00
35	18A	0.2695	4.0986	30.000	-5.00	90.00	-1.276	360.00
36	18B	0.2695	4.0986	30.000	-5.00	90.00	-1.276	244.00
37	18C	0.2695	4.0986	30.000	-5.00	90.00	-1.276	81.00

2.1.2 Hydraulic Design

A high differential pressure across the orifices was desired to ensure the advantage introduced by the cavitating jets would be apparent in the bit performance. Accordingly, a differential pressure of 5000 psi was chosen as an operating condition for the Phase I bit. This was based upon testing conducted by Glowka [4] that showed significant cutter force reductions in hard rock (Sierra White Granite) when the pressure drop across the nozzle reached 4500 psi (see *Figure 3*). Based upon the 8-1/2 inch bit diameter, a flowrate of 300 gpm was selected as a nominal flowrate for the full bit. The hydraulic design would be based upon a 10 lb/gal water-based drilling fluid as it is commonly used in geothermal drilling. Based upon laboratory test experience at DynaFlow, a standoff distance of three (3) orifice diameters from the orifice exit to the formation was targeted for the demonstration bit.

There was considerable discussion at the beginning of the project regarding the minimum orifice size that should be employed for the nozzles. The minimum orifice diameter traditionally used in the drilling industry is a #8 (i.e., 8/32 = 0.25 inch diameter) as smaller orifices are presumed to be subject to blockage [10]. Conversely, the limitation of larger orifice sizes is they require a larger flowrate at a given pressure differential. Hence, larger orifice sizes reduce the total number of nozzles that can be distributed across the face of the bit.

The number of nozzles to use in the Phase I bit eventually became a judgment call for Sandia. Given our flowrate limitation for the testing at TerraTek (300 gpm), the options were five nozzles at 60 gpm per nozzle using a 0.194-inch diameter orifice, or three nozzles at 90 gpm per nozzle using a 0.25-inch diameter orifice. However, a prevailing consideration was the similarity in nozzle layout between the baseline and augmented bits since any performance enhancement realized on the augmented bit will be evaluated with respect to the baseline bit. Significant variations in nozzle layout may modify the overall bit hydraulics so as to complicate the evaluation of the augmented bit.

Since the conventional implementation of the baseline bit has one nozzle for each of the five blades, Sandia recommended that five nozzles (0.194 orifice diameter) be incorporated in the augmented bit, with an identical placement on the baseline bit, so the performance enhancement of the augmented bit may be directly attributed to the performance of the cavitating nozzles and not complicated by the number of cavitating nozzles. Since Phase I does not include field-testing, the risk of nozzle blockage introduced by using the smaller orifice size can be effectively mitigated at TerraTek by appropriately filtering the drilling fluids to remove any large particulates which may pose a threat to nozzle blockage.

2.1.3 Wellbore Conditions

The Drilling Research Laboratory at TerraTek is capable of enforcing simulated wellbore pressures on the drill sample. Since the objective of this work is to show that the passively pulsating jets are beneficial at depth and that their cavitation is not suppressed in the presence of higher hydrostatic pressures, the TerraTek test plan was developed to include a range of wellbore ambient pressures (atmospheric, 2000 and 4000 psi) for these investigations.

2.1.4 Formation

To address formation requirements pertinent to geothermal drilling, a sample of Crab Orchard Sandstone was chosen for the Phase I demonstration testing. This rock, with slight permeability and porosity, has a compressive strength (21,000 psi UCS) that is representative of the rocks currently drillable with PDC bits in production operations. To demonstrate the potential of the combined bit technology in harder rock formations, additional plans were made to test the bit in Sierra White Granite (28,000 psi UCS), a rock with negligible permeability and porosity.

These specifications established a basis for the ensuing bit design, but the nozzle/orifice configuration had to be fully specified first.

2.2 Specification of Nozzle/Orifice Configurations

DynaFlow conducted hydrodynamic analysis and testing to specify organ pipe and orifice configurations for development of the integrated bit. DynaFlow uses a high-pressure cell to conduct testing at elevated ambient pressures (up to approximately 2600 psi) to design passively pulsating-cavitating nozzles and characterize their erosive potential. Testing was done in their high-pressure cell using a 0.06-inch diameter orifice. The principle of similitude is used to extend these configurations to other designs and operating conditions. Using this facility, organ pipe and orifice configurations for the Phase I bit were specified. The nozzle/orifice configurations were chosen to maximize the magnitude of pressure fluctuations at the hydraulic operating condition of the bit. The details of the nozzle and orifice specifications are documented in DynaFlow's letter report; this is included in Appendix A.

In summary, DynaFlow considered two organ pipe geometries: single and stepped. The stepped configuration (see Appendix A, *Figure 2*) incorporates an additional stepped reduction in the organ pipe diameter resulting in two organ pipes in series. *Figure 8* shows DynaFlow's measurements of the pressure fluctuations of these two configurations as measured in the feed pipe upstream of the nozzle and normalized to the pressure differential across the orifice (DynaFlow measured resonant frequencies of 16, 31, and 47 kHz for the single organ pipe configuration with the 0.06-inch diameter orifice [11]). As shown, the single organ pipe configuration has a peak performance centered on the operating condition of 5000 psi. The stepped organ pipe configuration, however, produces a more uniform response across a range of operating conditions. For this reason, the stepped configuration merits additional consideration for use in a bit since precise control of the operating condition at the nozzle may not be possible in the field. For Phase I, however, the single organ pipe configuration was chosen for integration into the demonstration bit since the operating conditions are precisely controlled in the laboratory and the value of the pressure fluctuations is greater. The stepped organ pipe configuration was the subject of additional research by DynaFlow, as described in Section 4.1 of this report. *Figure 9* (from Appendix A) shows the pertinent design parameters for the organ pipe and orifice for the single organ pipe configuration that DynaFlow specified to be integrated into the Phase I bit.

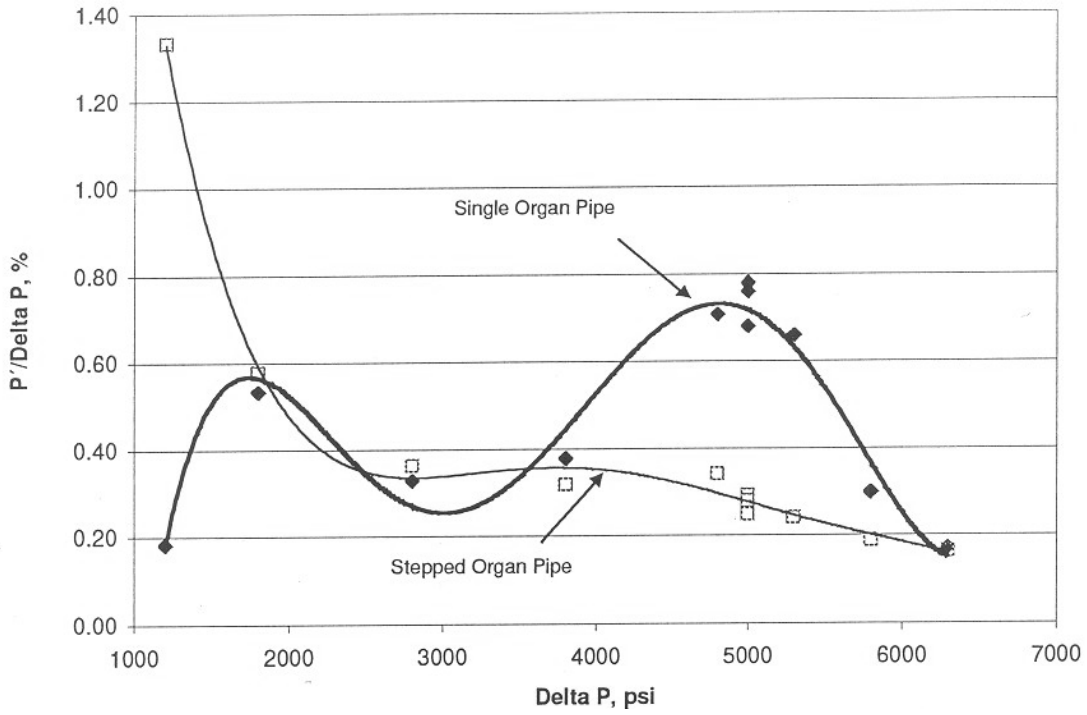

Figure 8: Comparison of normalized rms pressure fluctuations for the Single & Stepped Organ Pipes as a function of the pressure drop across the nozzle.

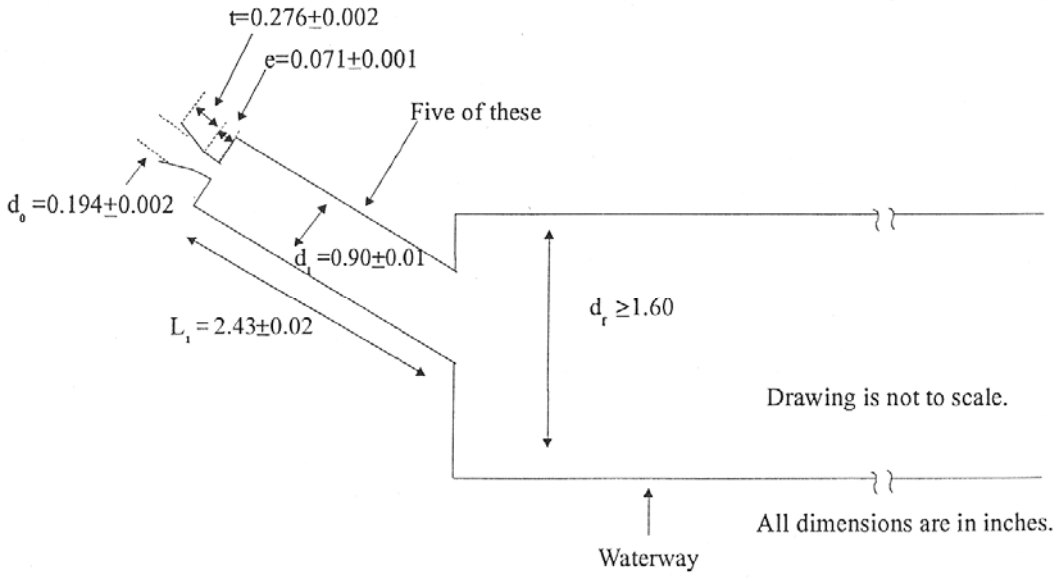

Figure 9: Organ pipe and orifice design dimensions for the Phase I bit.

2.3 Development of Cavitation-Resistant Orifices

DynaFlow encountered significant erosion in the throat of the nozzle orifices used in their laboratory testing to characterize the nozzle configurations. The orifices were machined from a variety of conventional materials including tungsten carbide, stainless steel, and sapphire. All of these experienced significant erosion that eventually lead to a reduction in nozzle performance. These low lifetimes for the orifices mandated an attempt to identify a longer lasting material.

Sandia initiated an effort to identify an abrasion-resistant material that would withstand the effects of cavitation within the orifice. After a literature search and consultation with personnel in the abrasives industry, it was decided that the orifices could be fabricated from a product consisting of sintered polycrystalline diamond (PCD) supported by an annular ring of tungsten carbide. *Figure 10* shows tungsten carbide supported polycrystalline diamond as fabricated by GE Superabrasives, one of several manufacturers. This product is commonly used for dies throughout the wire drawing industry by cutting a central hole through the product using plunge EDM (electro-discharge machining) or a laser method [12]. The material can be machined via EDM because of trace amounts of cobalt distributed throughout the PCD matrix.

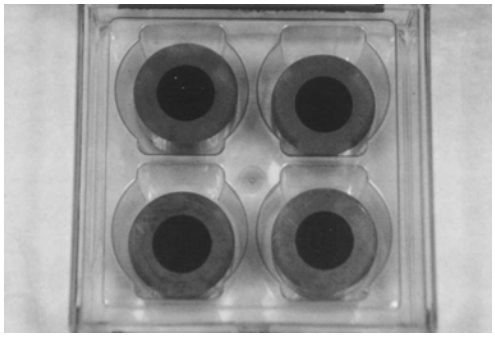

Figure 10: Tungsten carbide supported polycrystalline diamond manufactured by GE Superabrasives.

Since these products are used throughout the wire die drawing industry, a variety of diameters and thickness are available from various polycrystalline diamond manufacturers (e.g., GE Superabrasives, De Beers, and Sumitomo Electric). The GE Superabrasives product is available in 3, 5, 25, and 50 micron diamond grain sizes. The 25 micron grain size was chosen for good abrasion resistance and because existing product dimensions allowed for immediate integration of the orifice profile. This approach to produce the orifices for this project is particularly attractive since the hardness of the PCD material makes it well suited to the harsh cavitation environment. Additionally, the tungsten carbide ring forms a convenient interface for mounting it to the surrounding bit body. Tungsten carbide is esteemed for its high operating temperature capacity and for its abrasion resistance. This approach was selected to manufacture the orifices for the Phase I demonstration bit.

Figure 11 shows the design envelope for the GE P/N 5211 tungsten carbide supported polycrystalline diamond with the Phase I orifice profile introduced. As shown in the drawing, the orifice geometry is well suited to the wire die design as there is sufficient material surrounding the polycrystalline diamond to accommodate a circumferential braze to install the orifice into an outer housing. The outer surface of the tungsten carbide orifice can be turned down from the original raw stock size (1 inch diameter) to the requisite dimension by centerless grinding.

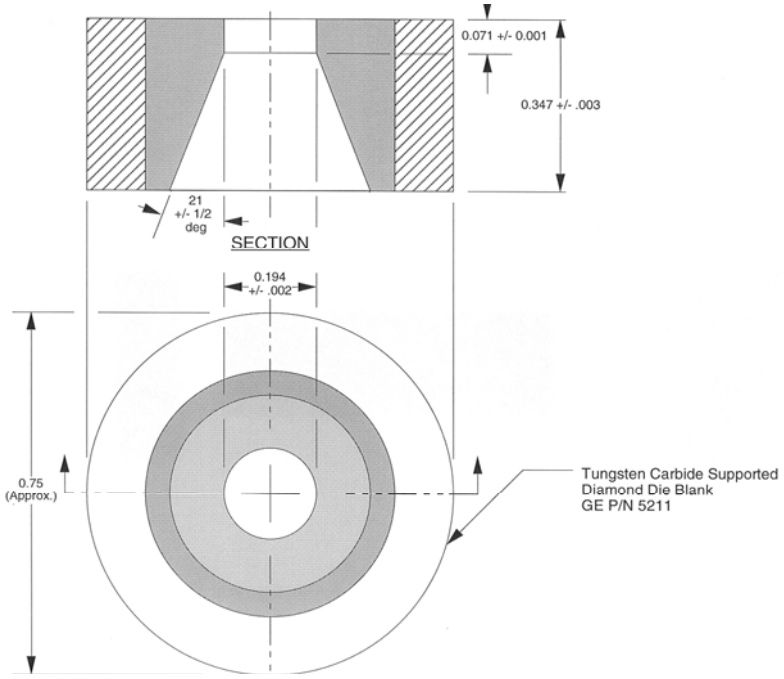

Figure 11: Phase I orifice profile within the tungsten carbide supported polycrystalline diamond.

Although various companies throughout the United States have the capability to machine the profile of these orifices using EDM, Sandia decided to machine these products in house to prove the process for this application and control tolerances on the finished product. The central hole through the orifice was created with plunge EDM using the graphite electrodes shown in *Figure 12*. *Figure 13* shows the electrode that was fabricated to create the diverging cone. Various electrode materials were used to create the orifice taper using the plunge EDM approach including graphite, copper tungsten, and silver tungsten. Ongoing problems with wear on the electrode caused considerable difficulties in maintaining the requisite dimensions of the orifice. The electrical parameters in the plunge EDM approach were adjusted to control the current at the electrode tool/part interface in an attempt to control the wear of the electrode. The electrode had to be re-surfaced often to maintain the orifice taper.

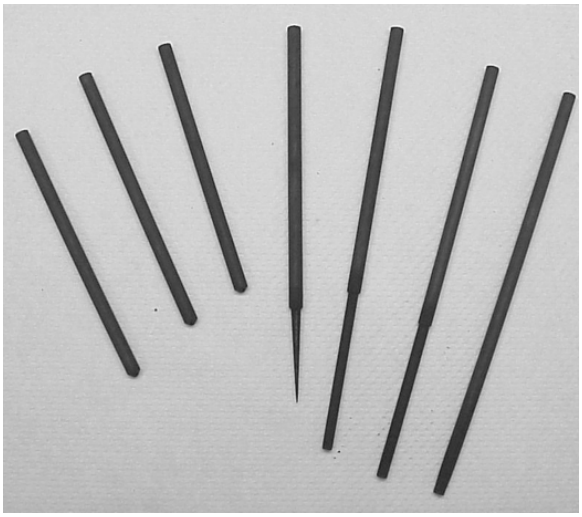

Figure 12: Photograph of electrodes used to machine central hole in PCD orifice using plunge EDM.

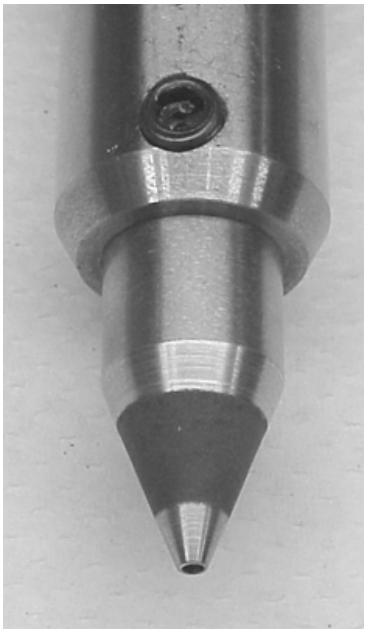

Figure 13: Photograph of electrode used to machine diverging cone in PCD orifice using plunge EDM.

Fortuitously, the machine shop at Sandia received shipment of a new wire EDM machine that had sufficient electrical capacity to wire EDM the die. This approach was used to produce the final parts. The central hole was still created using plunge EDM, but then the parts were set up on the wire EDM machine where the final profiling was completed. This gave us much better control over the tolerances in the final product. *Figure 14* shows the five orifices produced in this manner. *Figure 15* shows close-up views of the entrance and exit to one of these orifices (orifice #1). The orifices were inspected using a coordinate measuring machine and approved or sent back to the wire EDM machine for finer resolution. Appendix B contains the CMM orifice inspection results.

Figure 14: All five Phase I orifices after EDM machining and inspection.

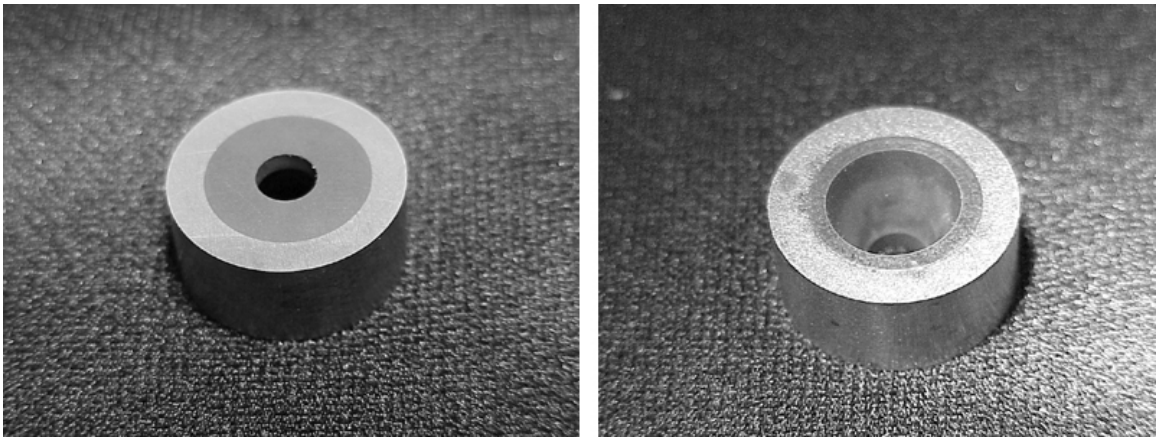

Figure 15: Orifice #1 – entrance and exit views.

One disadvantage of fabricating these orifices via EDM is their cost as machining the orifices to the required profile turned out to be a very time intensive process. It took 25 hours alone to plunge EDM the central hole through the die. The cost to produce a single orifice is shown in *Table 2*. As a means of making this orifice technology affordable, Sandia and US Synthetic, a manufacturer of polycrystalline diamond, addressed an alternate approach to fabricate the diamond orifices in Phase II of this project. US Synthetic is currently conducting research to produce these polycrystalline diamond orifices using a direct-sintered approach. This is described in section 4 of this report.

Table 2: Approximate Cost of Each Phase I Orifice Produced from Tungsten Carbide Supported Polycrystalline Diamond.

Description	Hours	Machining Cost	Cost
Die Blank	-	-	$1,000
Central Hole (Plunge EDM)	25	$2500	$2,500
Profile throat (Wire EDM)	6	$600	$600
Inspection	1	$100	$100
Total Cost			**$4,200**

The orifices produced by the EDM method had good surface finishes and appeared to be structurally sound for the application, although one orifice did exhibit a radial crack presumably due to residual stresses from the sintering resulting in high tensile stresses when the interior diamond material was subsequently removed. No comprehensive testing was conducted to qualify the orifices for integration into the bit. However, the orifices were subject to a "disaster screening" by subjecting them to flow tests, at the conditions to be encountered during drilling (see Section 2.5.2), before committing them to a full drilling test. Having presumably solved the materials orifice problem, development of the bit proceeded.

2.4 Prototype Bit Development

2.4.1 Selection of Augmented Cutters (PDCWEAR Modeling)

To decide which cutters on the bit should be augmented by the cavitating jets, Sandia analyzed the Security DBS five-blade bit using PDCWEAR, an analysis code developed at Sandia to evaluate PDC bit performance [see reference 4]. Using the limited single cutter data from *Figure 3* for high-pressure augmentation of PDC cutters, Sandia selected the cutters to be augmented with the objective of providing the greatest improvement in penetration rate. The analysis predicted that the augmented bit would drill faster and further than an equivalent un-augmented bit.

Sandia identified two methodologies to select cutters for mudjet augmentation. Mudjet assistance is modeled in the PDCWEAR computer code as a reduction in the penetrating force required to achieve a given depth of cut. The first approach to cutter selection is to augment the cutters that have the highest wear rate. Since augmentation reduces the required cutting forces, the work performed by these cutters is reduced and hence they wear at a reduced rate. This reduced wear approach extends the bit life.

The second method is to augment the cutters that have the highest axial force components. The benefit of jet augmentation in this case is to reduce the penetrating forces that predominantly contribute to weight on bit (WOB), and hence a reduction in the overall weight on bit required to achieve a given rate of penetration (ROP). The reserve weight on bit is redistributed throughout the bit and the increased cutter forces will act to increase the rate of penetration at a given WOB. The reduced wear approach has the advantage of also increasing the rate of penetration, but at a lesser rate than the reduced WOB approach early

in the wear pattern for the subject bit. The reduced WOB method does not appear to extend the life of the selected bit significantly, as modeled in PDCWEAR, since the cutters that have the greatest wear rate limit bit life.

The reduced WOB method was deemed a better choice for the Phase I feasibility demonstration since it results in a greater increase in rate of penetration early in the wear pattern. Cutter wear is difficult to measure when drilling to shallow depths, as in laboratory testing. Selecting cutters based upon the reduced wear method may actually compromise the performance of the bit as the cutters which see the greatest wear are further out radially and nozzle placement here could negatively affect cutter cooling elsewhere on the bit. A bit that incorporates both selection methodologies would have to be integrated into an overall new bit design as opposed to the current constraint of augmenting an existing bit. Given the approach in this phase of the project, Sandia recommended that the feasibility demonstration emphasize the benefits of improved ROP (i.e., reduced WOB method) as the benefit of improved bit life can be borne out in the PDCWEAR analysis. Improved bit life will also be more suitably demonstrated in a field test where more significant cutter wear can develop with the accumulation of extended drilling depth as compared to a laboratory demonstration.

The axial and penetrating loads on the cutters comprising the un-augmented bit, as predicted by the PDCWEAR analysis, are shown in *Figure 16* for the bit in a sharp condition operating at 110 RPM in Sierra White Granite at a rate of penetration of 15 ft/hr (solution A2B). The cutter distribution after the bit has worn very slightly is shown in *Figure 17*. As shown in these figures, cutter numbers 1 & 2 actually have the greatest loads early in the wear pattern, yet the adjacent cutters wear at faster rates to where cutters 3 & 4 eventually have comparable or greater cutting loads. Consistent with the reduced WOB approach, Sandia recommended Cutter IDs 3, 4, 6B, 7B, and 8B (Cutter Nos. 3, 4, 7, 9 & 11) (*Figure 7*) be considered as candidates for mudjet assistance. The recommended cutters allow five different ‘tracks’ in the cutting structure to be augmented. Augmentation of five separate tracks will allow the benefits of both cutter force reductions and bottom hole cleaning to be realized.

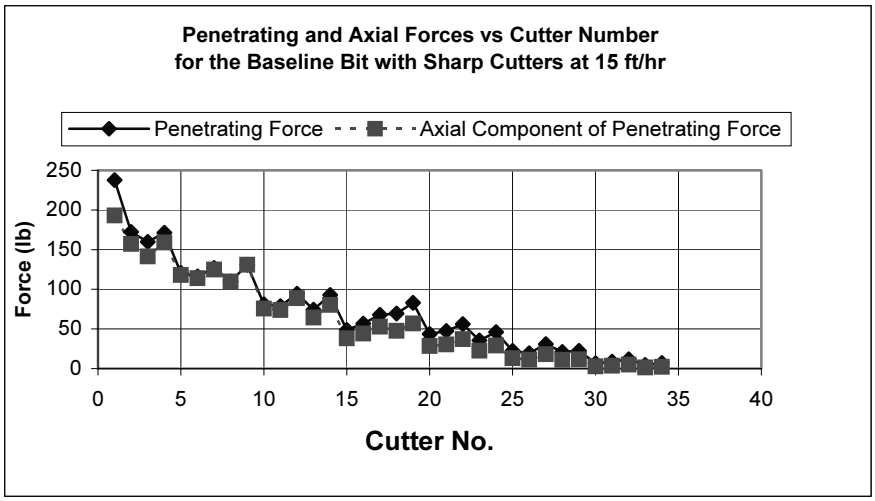

Figure 16: PDCWEAR Results: Cutter loads without augmentation.

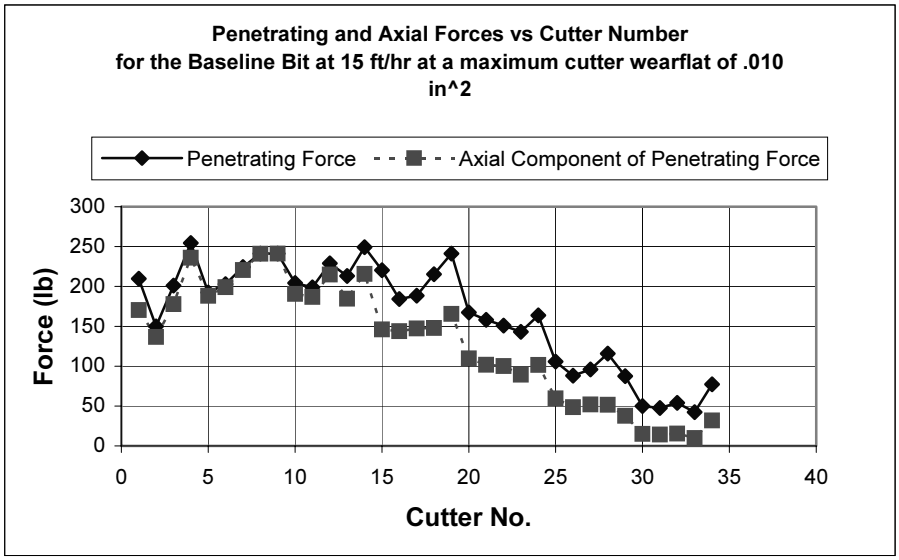

Figure 17: PDCWEAR Results: Cutter loads without augmentation at slightly worn condition.

However, as described in the following section, this cutter selection was troublesome to the nozzle/bit integration and Security DBS suggested that cutters 5, 6A, 6B, 7A & 7B (Cutter Numbers 5, 6, 7, 8 & 9) be augmented instead (*Figure 18*). This cutter selection was investigated in PDCWEAR as well (solution B1A). This is a comparable augmentation plan to the previous one as each blade is still augmented. However, the augmentation is spread over a smaller area of the bottom hole pattern as only two tracks are augmented instead of five (*Figure 19*). The reduction in penetrating loads for all the cutters on the bit is shown in *Figure 20* for sharp cutters when Cutter IDs 5, 6A, 6B, 7A & 7B (Cutter Nos. 5, 6, 7, 8 & 9) are subject to mudjet augmentation. This revision in cutter selection is necessary to accommodate integration of the nozzles into the existing cutting structure. The integrated effect of this cutter augmentation is to reduce the WOB, torque, and sideload for the overall bit. These results are summarized in *Table 3*.

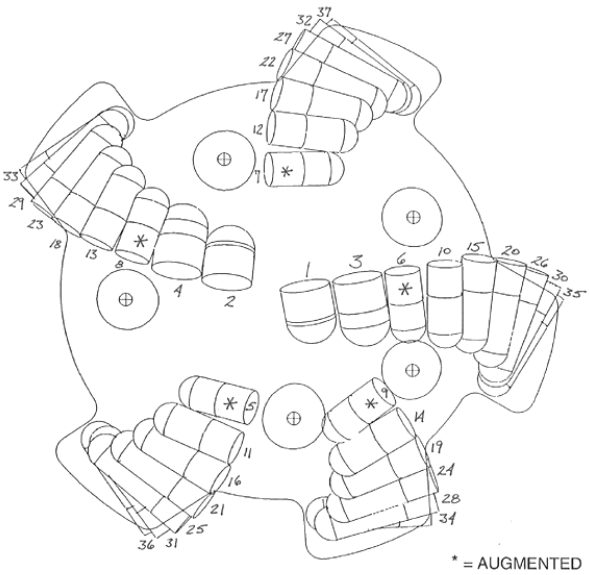

Figure 18: Phase I Bit Cutting Structure

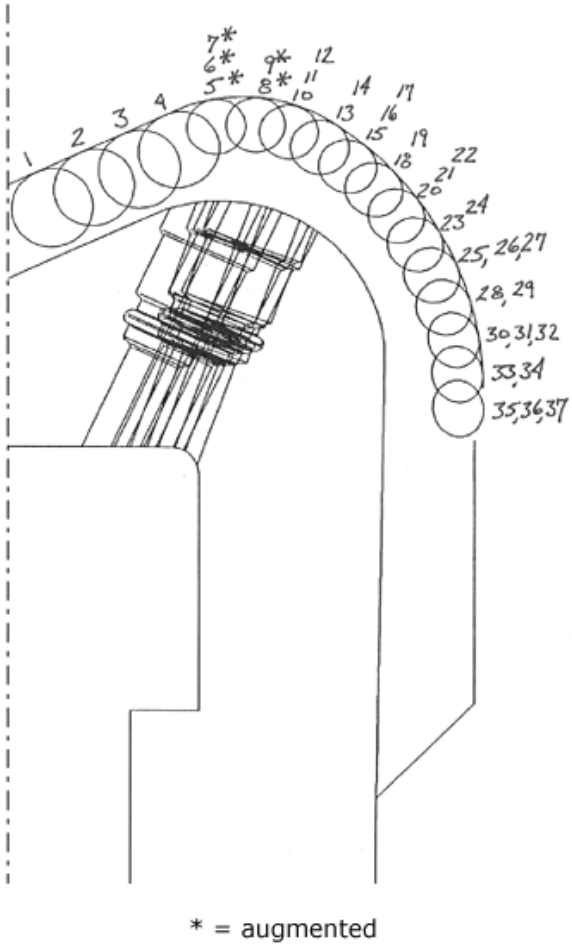

Figure 19: Phase I Bit Cutting Profile

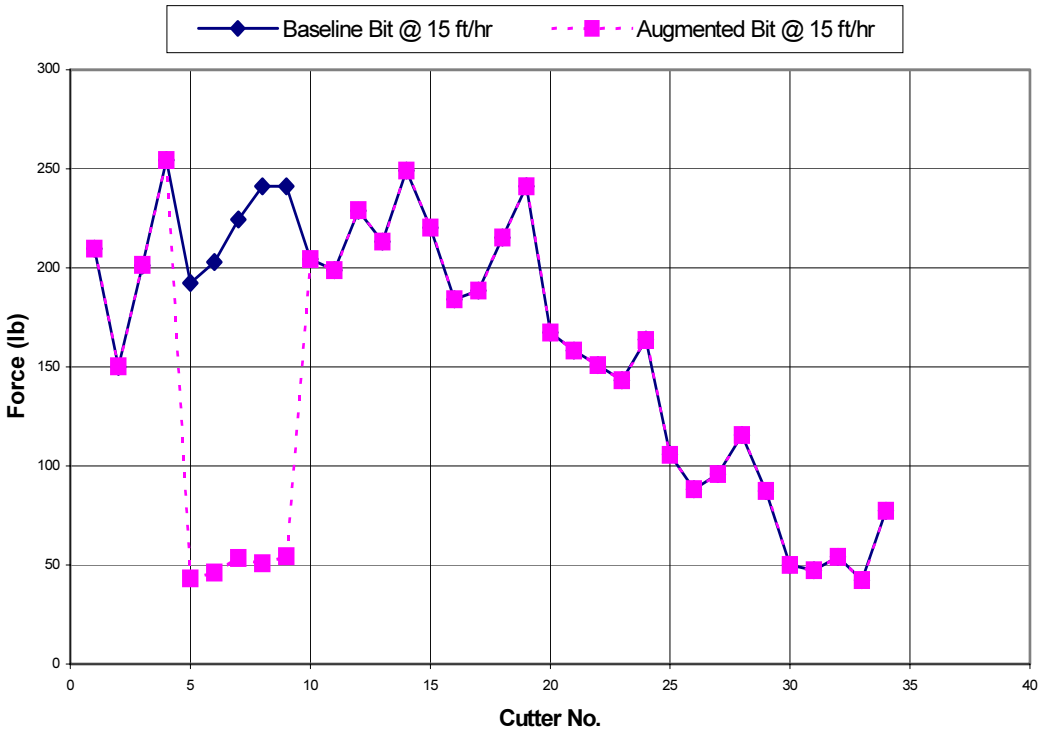

Figure 20: PDCWEAR Results: Cutter loads with augmentation on cutter Nos. 5-9.

Table 3: Effect of Mudjet Augmentation on Integrated Bit Loads.

	WOB [lb]	Torque [ft-lb]	Resultant Sideload [lb]
Baseline @ 15 fph	2099	347	95
Baseline @ 30 fph	3577	585	90
Baseline @ 60 fph	7028	1147	153
Augmented @ 15 fph	1777	306	88
Augmented @ 30 fph	3135	529	100
Augmented @ 60 fph	6419	1069	184

The integrated effect of the mudjet augmentation on the life of the bit as predicted by the PDCWEAR analysis is shown in *Figure 21*. As shown in the figure, the WOB for the augmented bit operating at 15 ft/hr is significantly less than the baseline bit operating at the same ROP. Also shown is the WOB profile for the augmented bit operating at 30 ft/hr, which coincidentally lays atop the WOB profile for the baseline bit at 15 ft/hr. Hence, as the cutters wear the mudjet augmentation results in a doubling in penetration rate of the augmented bit over the baseline bit, while wearing at essentially the same rate as the un-augmented bit.

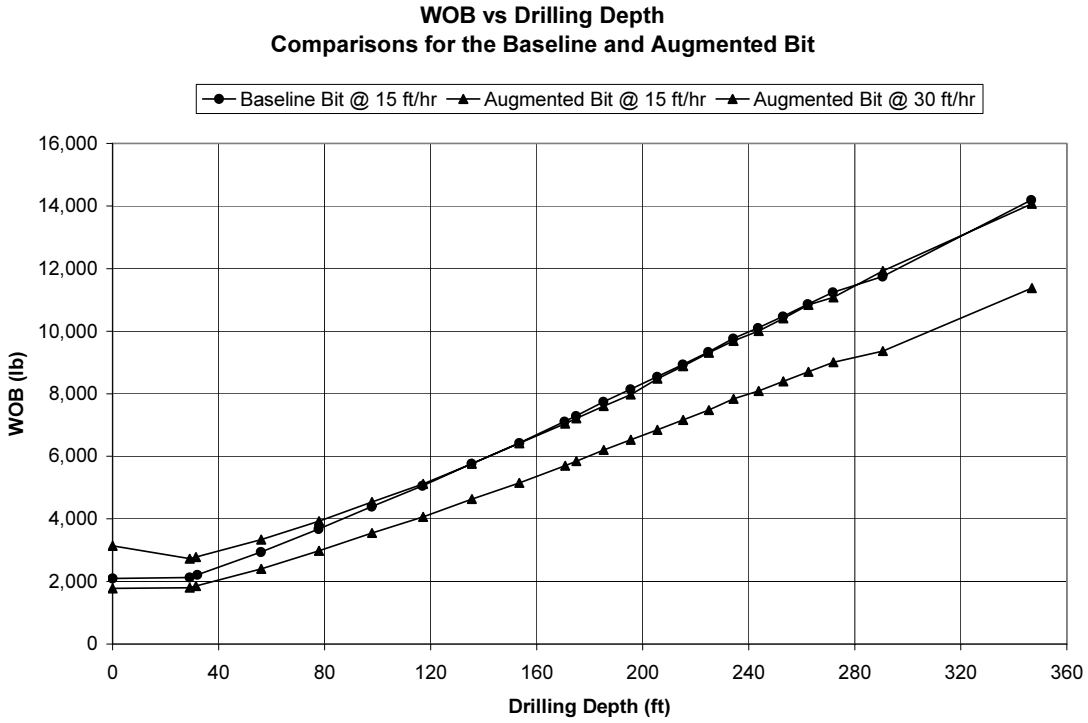

Figure 21: PDCWEAR Results: Comparison of WOB profile for conventional bit with augmentation on cutter nos. 5-9.

2.4.2 Bit/Organ Pipe Design Integration

Security DBS integrated the design of the organ pipes and nozzles into the cutting structure comprising the PDC bit design subject to the following criteria: DynaFlow nozzle design requirements, Sandia nozzle placement requirements, and Security DBS nozzle and fixed cutter bit design requirements. The nozzle design was an iterative process taking into account the requirements of all three parties in this phase of the project. The goal of the integrated design is to create a design that will not only work in the laboratory service environment but can also possibly withstand a field environment. This integration process addressed the following items.

2.4.2.1 Interchangeable Nozzles

In order to evaluate the performance enhancements introduced by the cavitating jets, the bit was designed with removable nozzle assemblies such that it can be used with either structured cavitating jets (enhanced) or conventional nozzles (standard) to allow the relative benefit of high-pressure jets to be evaluated within a single bit. This provided one bit and two sets of nozzles (standard & enhanced) for the best comparison of the effect of enhanced hydraulics. An alternative approach would have been to independently specify the nozzle hydraulics and layout. This, however, would require two bits for testing, possibly complicating the comparison of bit performance between augmentation and conventional nozzles as slight differences in bit design may result during bit manufacture.

The approach to integrate the nozzle design into the bit is illustrated in Figure 22 [13]. Based upon this interchangeable nozzle approach, a "mandrel" was designed to form both the organ pipe, and an internal thread to accommodate nozzle installation, during casting of the tungsten carbide matrix body bit. The mandrel is made out of graphite as it maintains the thread form during casting of the bit body [14]. A 3D model of the mandrel was used to determine if the nozzles would fit into the bit in the manner prescribed by DynaFlow and Sandia. This bit with the mandrels in place is shown in *Figure 23.* A side view of the bit and mandrel are shown in *Figure 24*. A three dimensional view of the mandrels and bit cutting structure is shown in *Figure 25*.

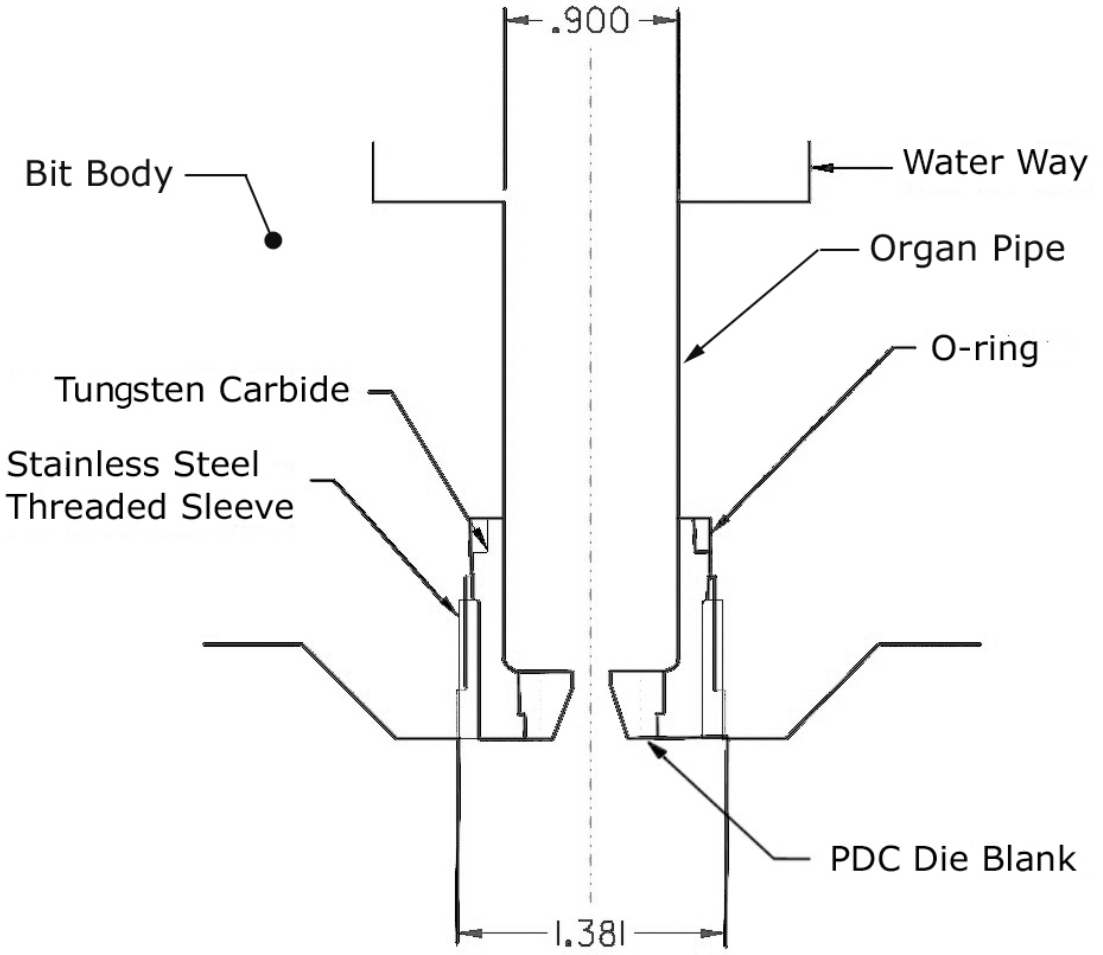

Figure 22: Approach to integrate an interchangeable nozzle design with an organ pipe cast into the bit body.

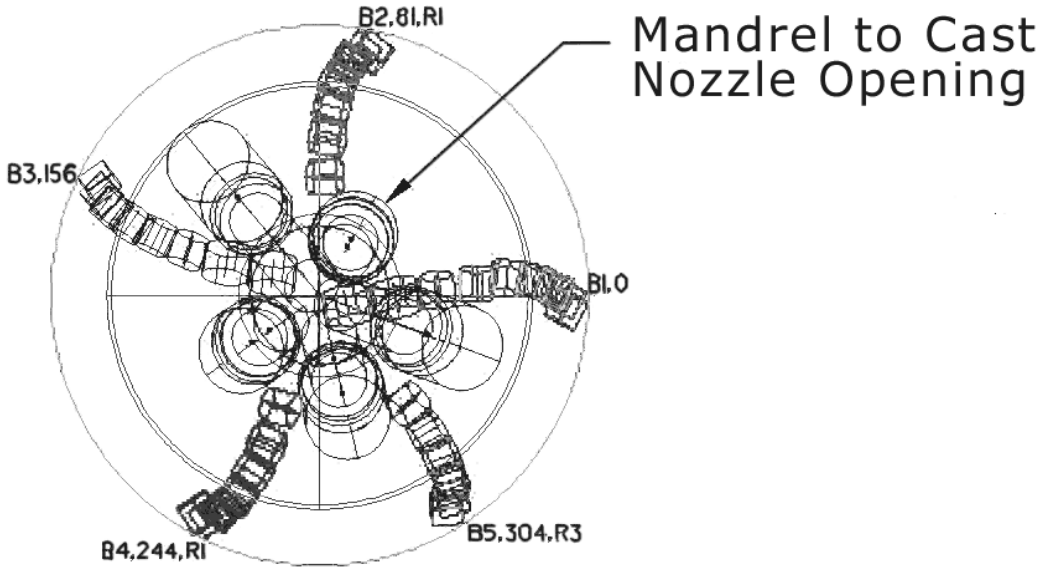

Figure 23: Face view of the bit cutting structure and the mandrel used to cast the organ pipes.

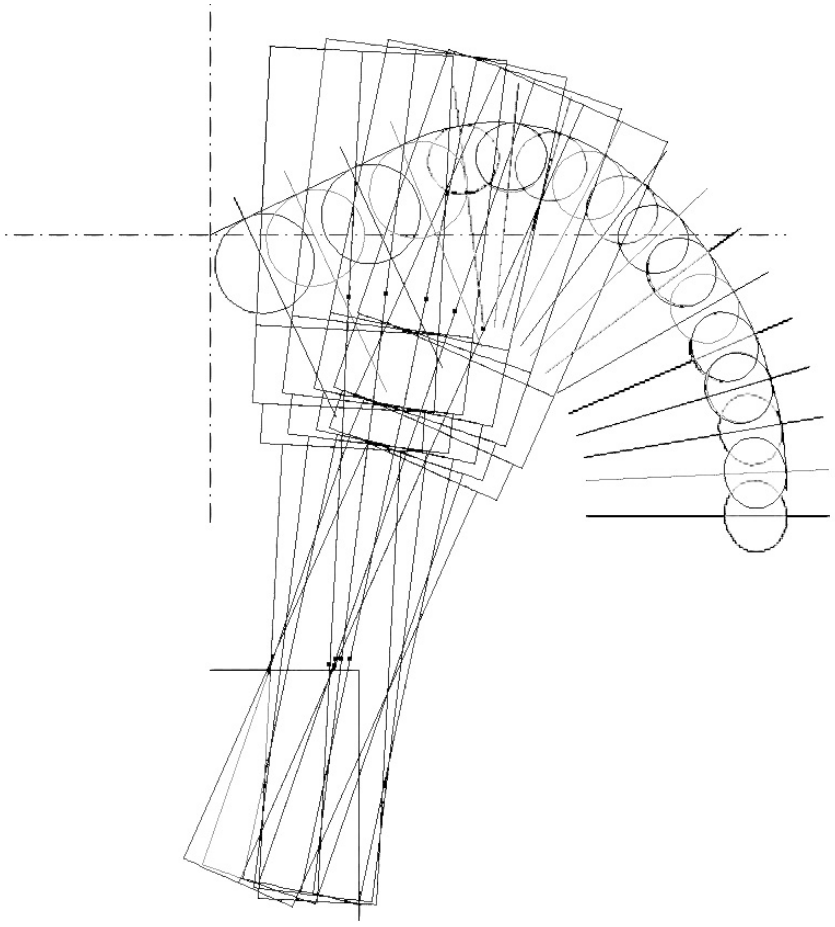

Figure 24: Sideview of the Bit Profile & the various mandrels used to cast the organ pipe.

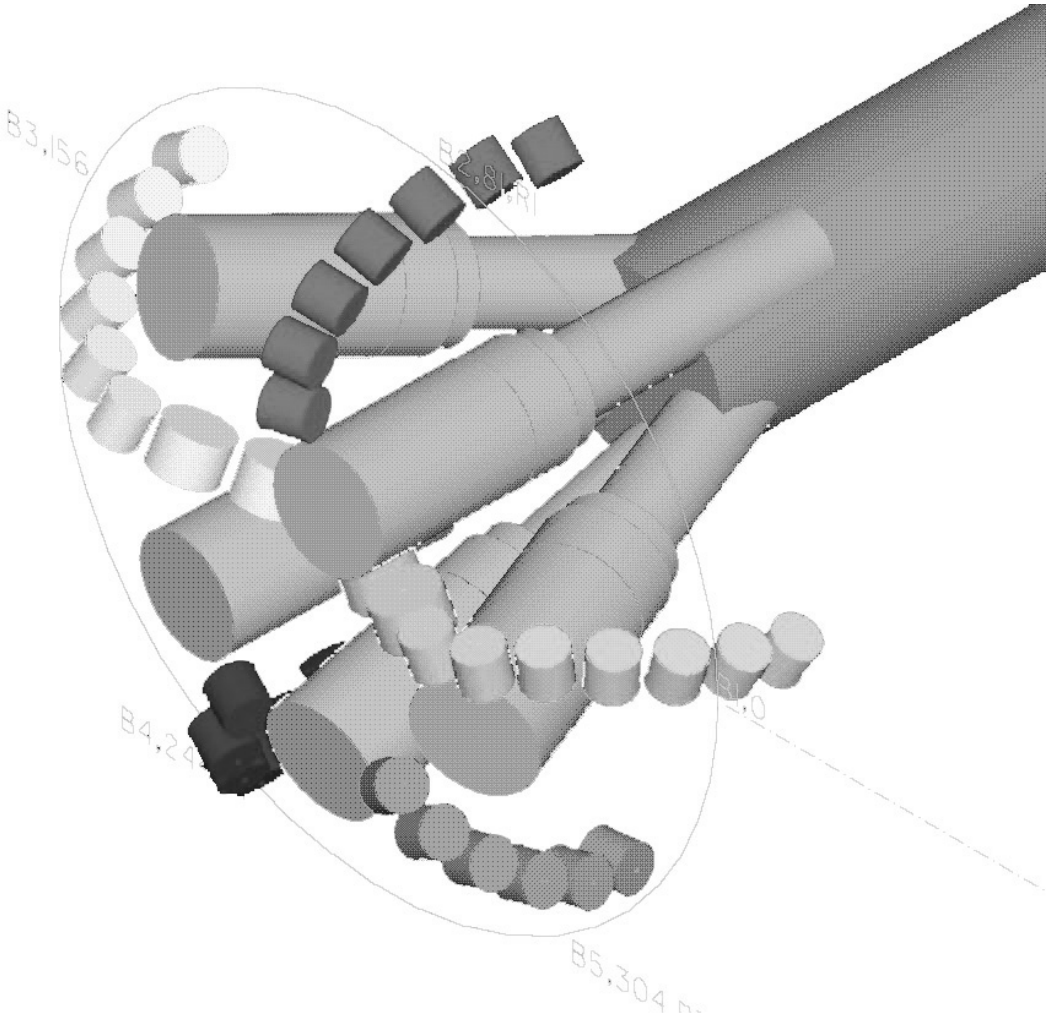

Figure 25: Three-dimensional view of the cutting structure & mandrels extending back into the central waterway of the bit.

2.4.2.2 Organ pipe modifications

Figure 26 shows that the organ pipe specified by DynaFlow was too large to allow five of them to merge in the available waterway without interference, i.e., the waterway available in the bit is too small in diameter (1.6 - 2.25 inch) compared to the organ pipe diameter (0.9 inch). DynaFlow approved a reduction in the organ pipe diameter from 0.9 inch to 0.73 inch to allow five organ pipes to fit within the available waterway diameter [15]. The dimension of 0.9 inch was conservatively based upon a ratio of organ pipe diameter to orifice diameter of 4.5, although DynaFlow has successfully used a ratio of 3.5 before. It was presumed this reduction would not negatively influence the nozzle performance.

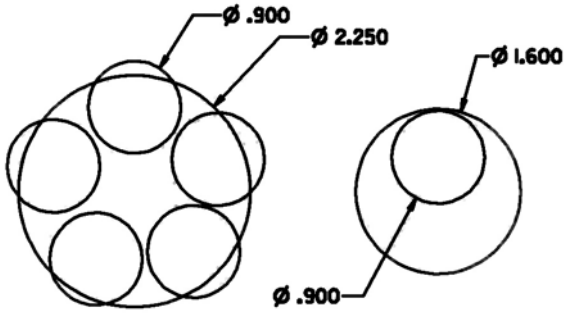

Figure 26: This figure illustrates that the original organ pipe would not fit in the available bit waterway opening (1.6in min – 2.25 max)

2.4.2.3 Revision of augmented cutters

As stated, Security DBS had difficulty incorporating Sandia's preferred cutter augmentation. The prevailing approach had been to have a nozzle on each blade and augment separate tracks [16]. Augmenting each track, however, was not possible. Since the organ pipe length on all nozzles is the same, they must intersect the central waterway at the same radius. Security DBS noted that with cutter nos. 5-9 augmented it is possible to get a nozzle on each blade since these cutters are approximately equidistant radially from the centerline of the bit. Cutter nos. 5-9 in the PDCWEAR analysis have approximately the same average forces as the other combinations considered in the PDCWEAR analysis. These should allow comparable standoff distances and approach what DynaFlow requested. Since they also use different blades, the advantages of cleaning will still be realized.

2.4.2.4 Orifice standoff distances

In the absence of data to guide the specific details of the nozzle/cutter interaction, engineering judgment was used as a guide to integrate the nozzles into the bit. As per DynaFlow's specification, the nozzles should have a standoff distance of approximately three (3) orifice diameters; i.e., approximately 0.6 inches for the 0.194-inch diameter nozzle. Using the new organ pipe diameter of 0.730", Security DBS was able to reduce the nozzle standoff distances to the range of 0.550 – 0.650 inches [17].

2.4.2.5 Integrated Bit & Nozzles

After consulting with DynaFlow, Security DBS implemented a hemispherical end to the waterway. This produces a smooth transition for the flow between the waterway and each individual organ pipe. Subject to these revisions, Security DBS came up with a "workable design" [17]. A three dimensional view of the nozzles and bit cutting structure is shown in *Figure 27*.

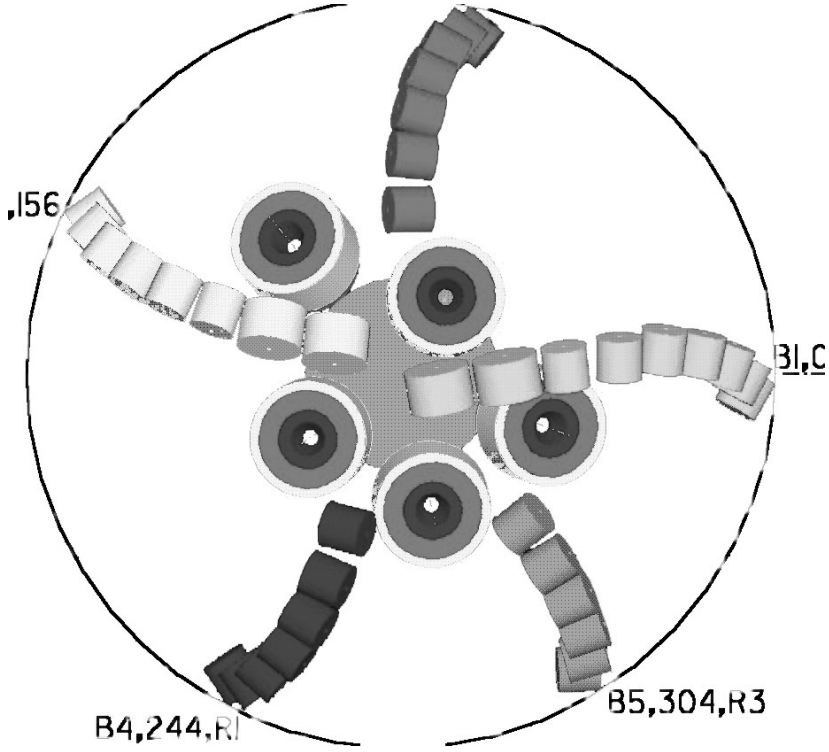

Figure 27: Three dimensional view of the orifices and the bit cutting structure.

2.4.3 Orifice/Nozzle Design Integration

The integration of the organ pipe into the bit body, as described above, had to be completed first since the overall organ pipe length must be accounted for in the dimension from the central waterway to the entrance to the orifice. As such, the orifice/nozzle design grew out of the integration of the organ pipe with the overall bit design. Since the nozzle body itself must make up part of the organ pipe, the balance of the organ pipe is cast within the body of the tungsten-carbide bit using the mandrel described in the previous section.

2.4.3.1 Enhanced Nozzle Design

The nozzle design is detailed in the Security DBS drawing shown in *Figure 28*. The nozzle housing includes a counterbore on the leading surface for installation of the PCD orifice. Since the nozzle bodies must be threaded into the bit body, the nozzle assembly includes a stainless steel threaded sleeve that is brazed onto the nozzle body. The flats on the nozzle body match tines on an installation tool that seats the nozzles in the bit body.

When the nozzle assemblies are installed into the thread form that is cast into the bit, the orifices are directed at the appropriate cutters to be augmented. *Figure 29* is an isometric view of the nozzles and waterway. *Figure 30* is the view looking up from the rock formation.

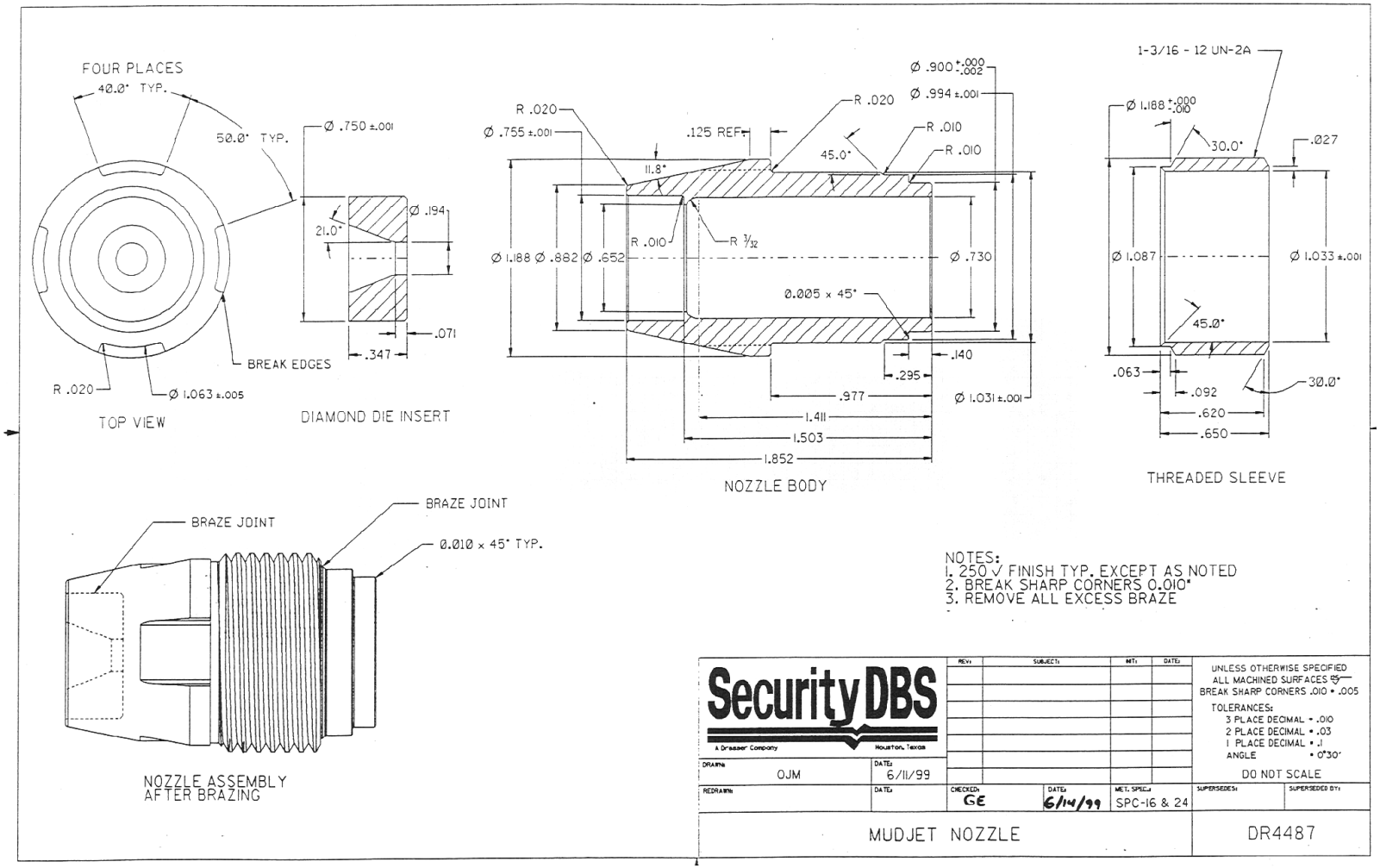

Figure 28: Phase I Nozzle/Orifice Assembly.

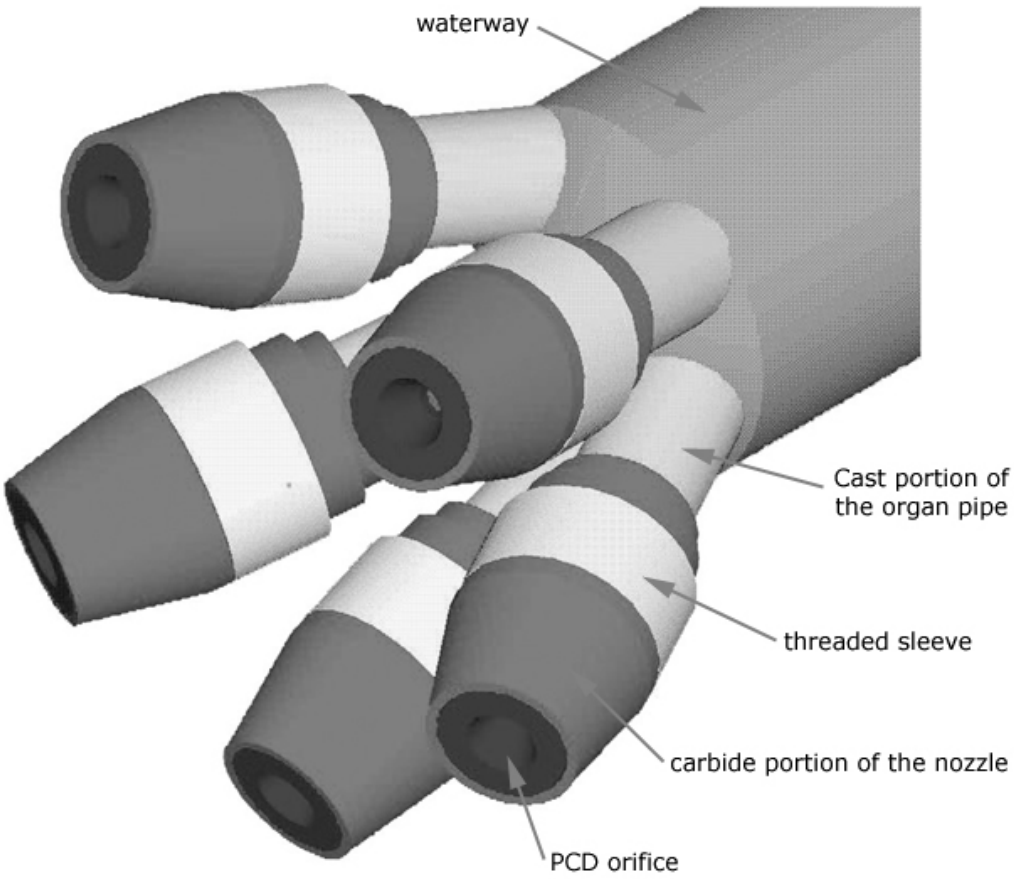

Figure 29: Isometric view of the nozzles, organ pipes, and central waterway of the bit.

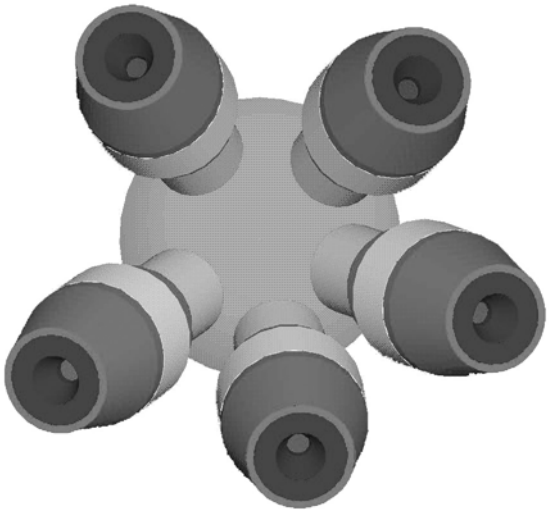

Figure 30: View looking up at the nozzles from the formation.

The seal design used with the nozzle assembly incorporates a combination of an O-ring and backup. These are a Parker P/N 2-020 O-ring and a Parker Parbak 8-020 backup. The nominal inner diameter for the O-ring is 0.864 with a nominal cross-section of 0.070 inches. The Parbak inner diameter is 0.893 inches. This combination, with the proper clearance of 0.001-0.002 inch will provide a good seal to 10,000 psi based upon the Parker Design Criteria. The O-ring detail is shown in *Figure 31* [18].

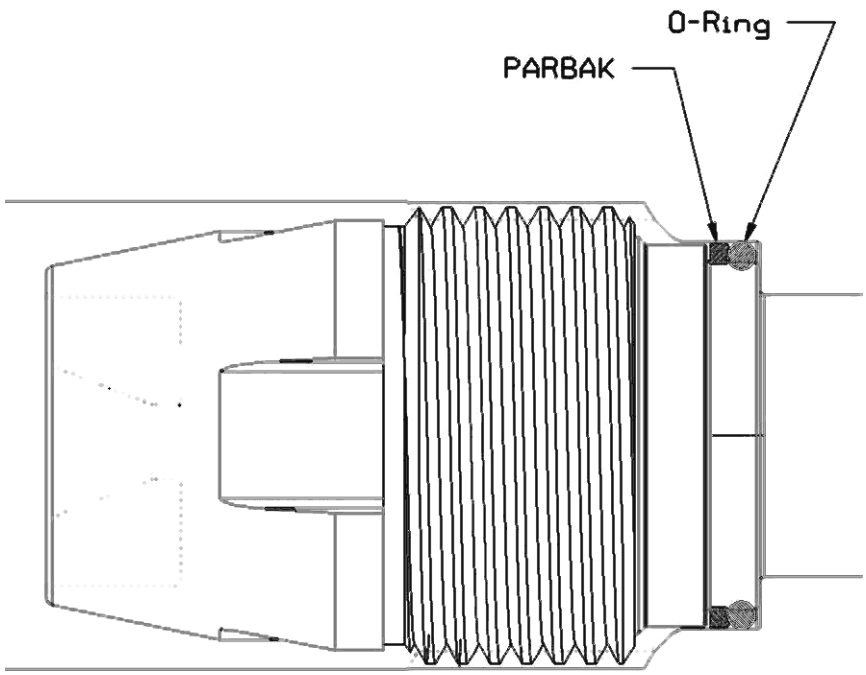

Figure 31: O-ring detail in the nozzle installation.

The nozzle bodies are sintered from tungsten carbide. They were made by Fansteel, a subcontractor to Security DBS. Considerable discussion ensued regarding the procedure to braze the tungsten carbide supported polycrystalline diamond orifices into the tungsten carbide nozzles. During these discussions and unbeknownst to the project team, Fansteel proceeded to braze the polycrystalline diamond orifices into the sintered tungsten carbide nozzle bodies using a low temperature flame-based braze. The uncertainty associated with the quality of this installation braze provided the justification for conducting a flow test at full scale pressures before committing the bit to drilling demonstrations. Photos of three of these nozzles following assembly are shown in *Figure 32*.

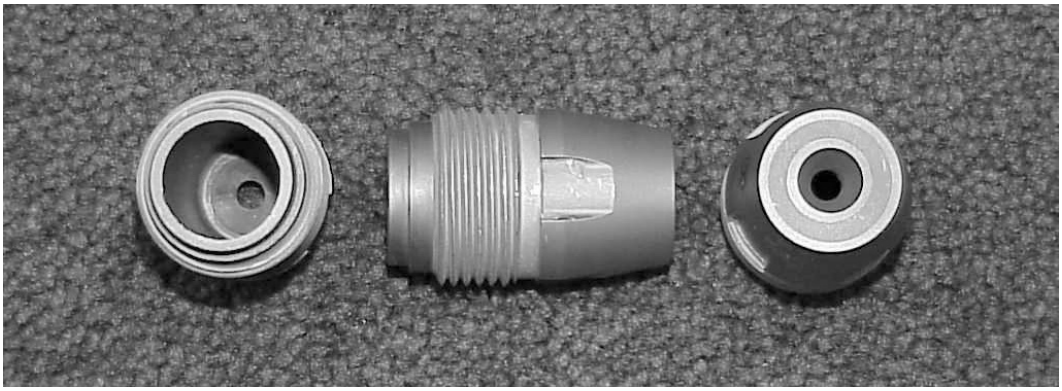

Figure 32: Phase I Nozzle assemblies consisting of a tungsten carbide body with brazed-in PCD orifice.

2.4.3.2 Standard Nozzle Design

The standard nozzle was designed to have an outside geometry comparable to the enhanced nozzle, also with the threaded stainless steel ring, so they could be installed in place of the enhanced nozzles. The orifice of these nozzles is designed to have a #8 diameter (8/32 inch) orifice. The taper of the converging section is 17.5 degrees, which is the standard for Security DBS. The overall length is 1.5 inches. This change in length will move the jet back 0.352 inches from the formation as compared to the enhanced nozzle. The standard nozzles are shown in the Security DBS drawing given in *Figure 33* [19]. These nozzles were also fabricated by Fansteel.

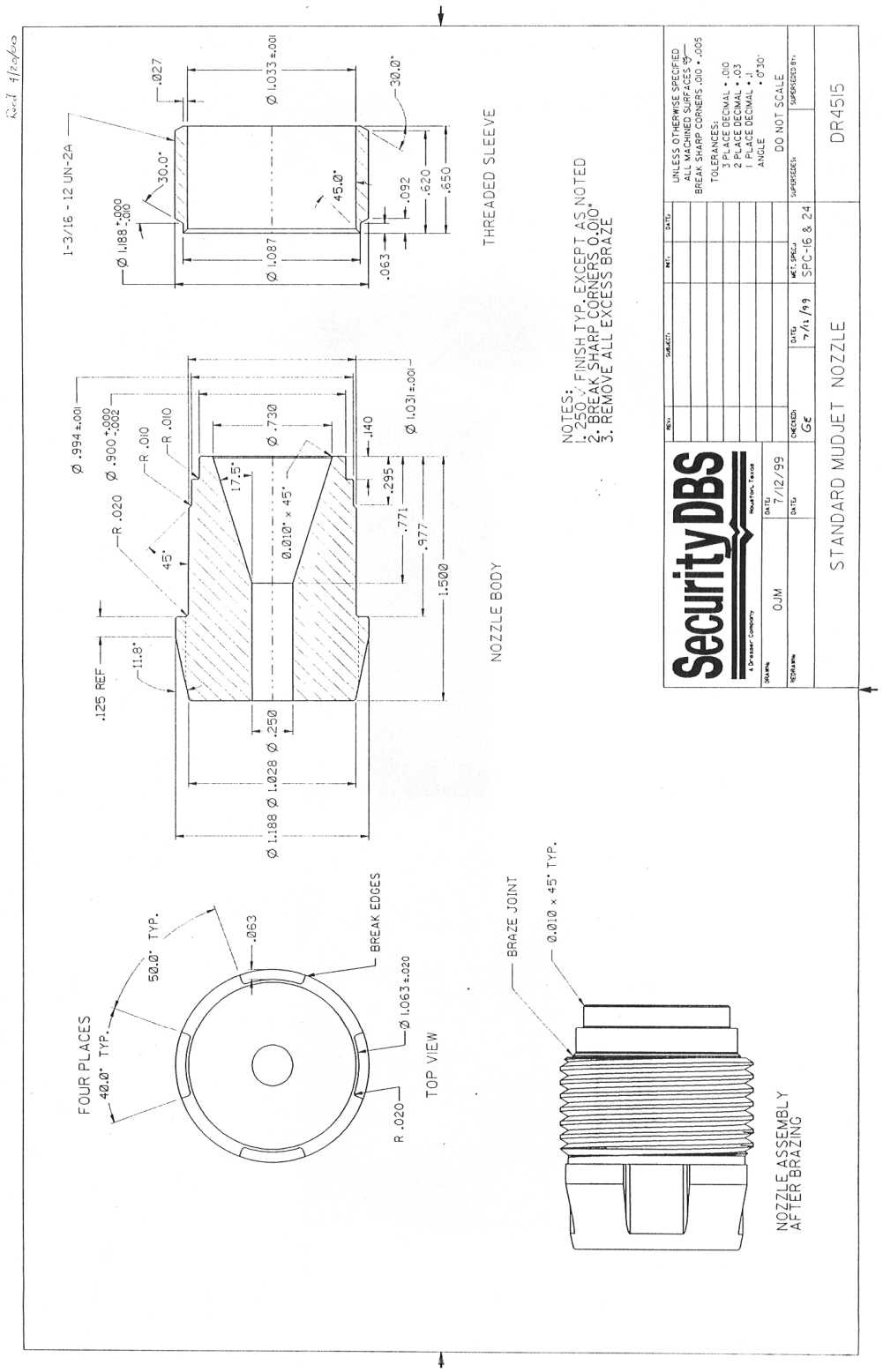

Figure 33: Standard Nozzle/Orifice Assembly.

2.4.4 Completed Bit

A solid model of the design-integrated bit, which uses either standard or enhanced nozzles, is shown in *Figure 34*. Five enhanced or standard type nozzles may be used with the bit. The design and placement of the nozzles are such that the inner tube length (i.e., organ pipe) is at the specified dimension given by DynaFlow (i.e., 2.43 inches). The tubes were measured by dividing the three dimensional tube into ten segments, measuring the length of each segment and then averaging these lengths. Nozzles corresponding to cutters five through seven have a standoff distance from nozzle exit to formation of 0.54 inches. Nozzles corresponding to cutters eight and nine have a standoff distance from nozzle exit to formation of 0.65 inches [20].

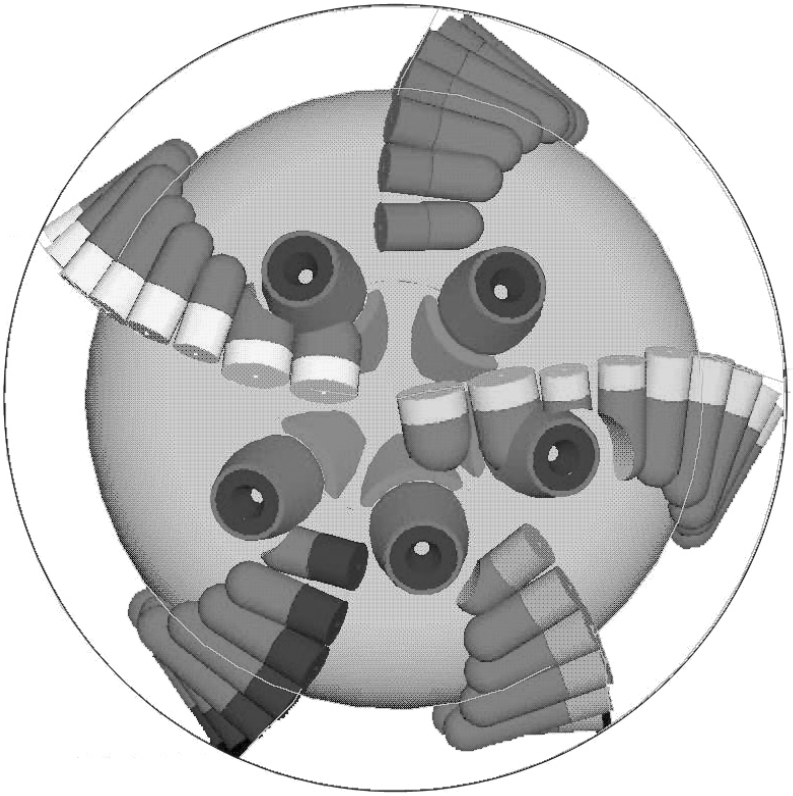

Figure 34: Final model of the integrated bit design; outer circle shows available junk slot.

The standoff distance requirement coupled with the physical dimensions of the nozzle necessitated close proximity of the nozzle body to the formation (approximately 1/8 inch). A kinematics analysis was done on the possibility of the formation hitting the nozzles during drilling. It was determined that the bit could drill to about 100 ft/hr at 110 rpm without *theoretically* coming into contact with the formation, which is to say, barring any non-concentric movement of the bit during testing.

The bit design incorporating the organ pipes is documented in Security DBS Drawings DC2293, DL1476, DR4493, DR4494, DR4495, DR4496, and DY1619. Non-standard items include the domed waterway, the nozzle dummy (DR4488), and the boss used to allow the nozzles to extend out of the junk slot surface.

The bit was manufactured along with the nozzles following a project-team design review. Security DBS had a little trouble with the positioning of the nozzles (i.e., mandrel) during manufacture of the bit body [21]. Consequently the tube lengths and nozzle position relative to the cutting structure are off by a maximum of 1/16 inch (nozzle C). Final dimensions are shown in *Table 4*. Note that a short leg refers to the cast portion of the organ pipe.

Table 4: Measurements of Organ Pipe in Manufactured Phase I Bit.

Meas.\Nozzle	A	B	C	D	E
Total tube length	2.404	2.417	2.396	2.404	2.426
Tube diameter	0.726	0.725	0.724	0.725	0.723
Short Leg cast	1.060	1.080	1.122	1.070	Unavailable

A face view of the bit with the polycrystalline diamond orifices installed is shown in *Figure 35*; a side photo is shown in *Figure 36*. *Figure 37* shows a face view of the bit with the standard nozzles installed. A photograph taken down the central waterway of the bit is shown in *Figure 38* and reveals the entrance to each of the several organ pipes cast into the bit. The bit with the nozzles removed, threads exposed, and a view of the cast organ pipe is shown in *Figure 39*. A close-up of the cast organ pipe and threads is shown in *Figure 40*.

The cutters used on the Phase I Demonstration bit are as follows [22]:

Long substrate 13mm x 13mm: DeBeers Lot # 253052
Short Substrate 13mm x 8mm: US Synthetic Lot #003977
Short Substrate 19mm x 8mm: US Synthetic Lot #003932
Drop Ins 13mm x 8mm: US Synthetic Lot #003946

Appendix C includes details on the Coordinate Measuring Machine (CMM) inspection of the bit.

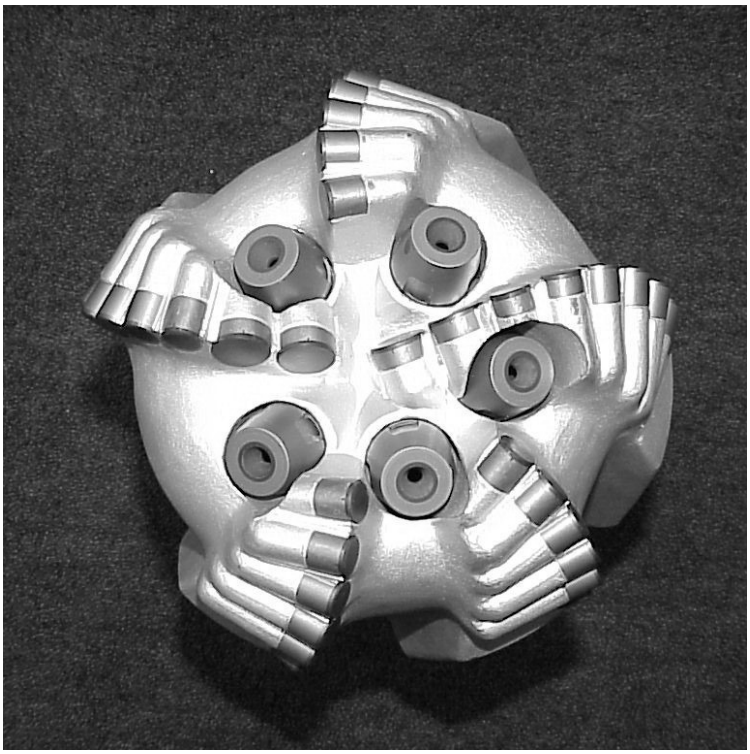

Figure 35: Face view photograph of the phase I Bit with cavitating nozzles installed.

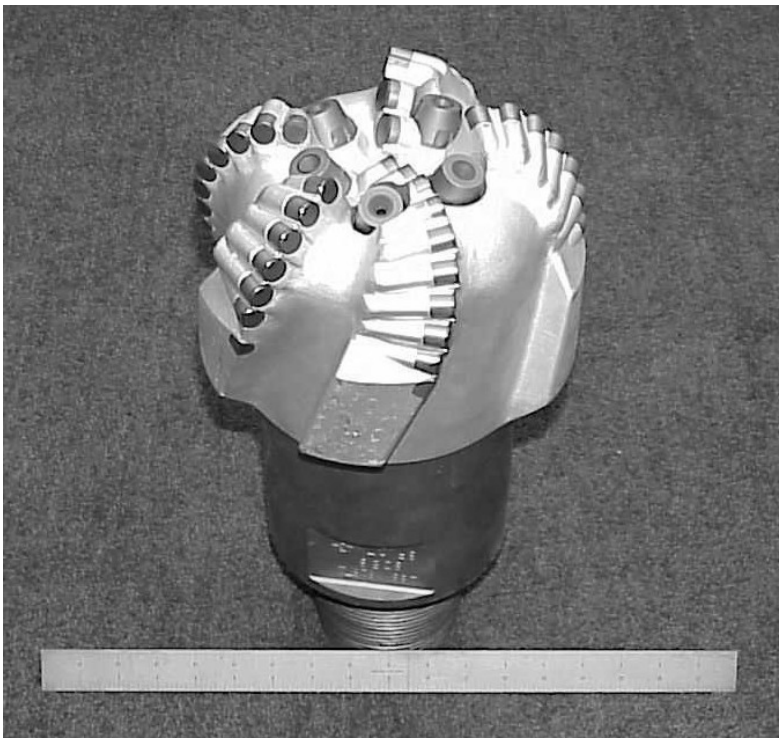

Figure 36: Side view photograph of the Phase I Bit with cavitating nozzles installed.

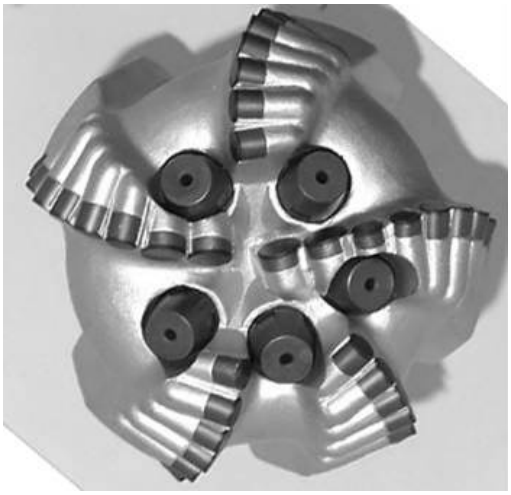

Figure 37: Photograph of the Phase I Bit with the standard nozzles installed.

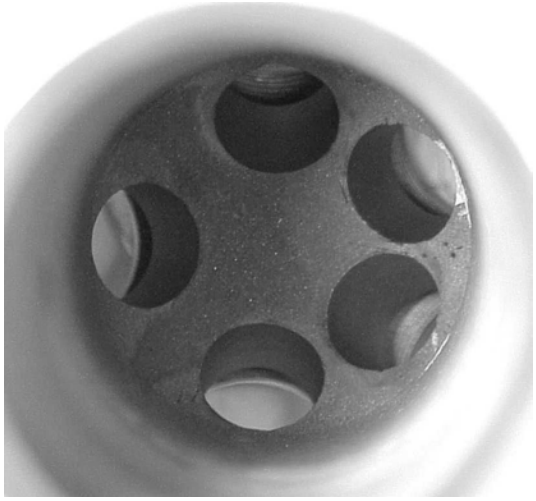

Figure 38: Photograph of the Phase I Bit looking down the central waterway showing the hemispherical intersection with the individual organ pipes.

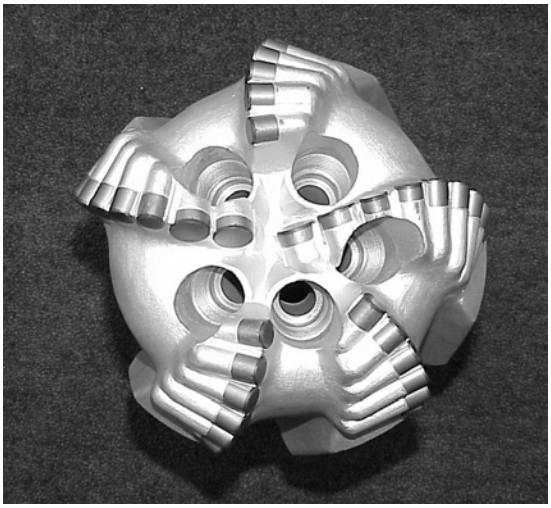

Figure 39: Face view photograph of the Phase I bit showing the threads in the bit body and the short leg of the organ pipes.

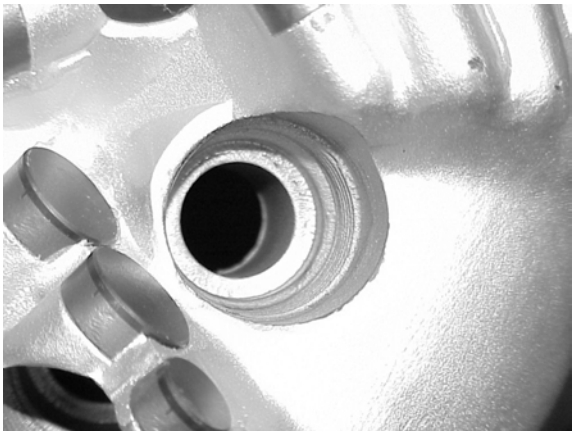

Figure 40: Close-up photograph of the threads cast into the bit body, the O-ring seat, and the short leg of a single organ pipe.

2.5 Phase I Demonstration Testing

The Phase I demonstration bit was tested at the Drilling Research Laboratory (DRL) at TerraTek with both standard nozzles and cavitating jet nozzles. Two conventional roller cone bits were also tested for comparison. The TerraTek rig is shown in *Figure 41*. The DRL also includes the Wellbore Simulator (lower left corner of *Figure 41*), into which the rock samples are placed for the flow and drilling tests.

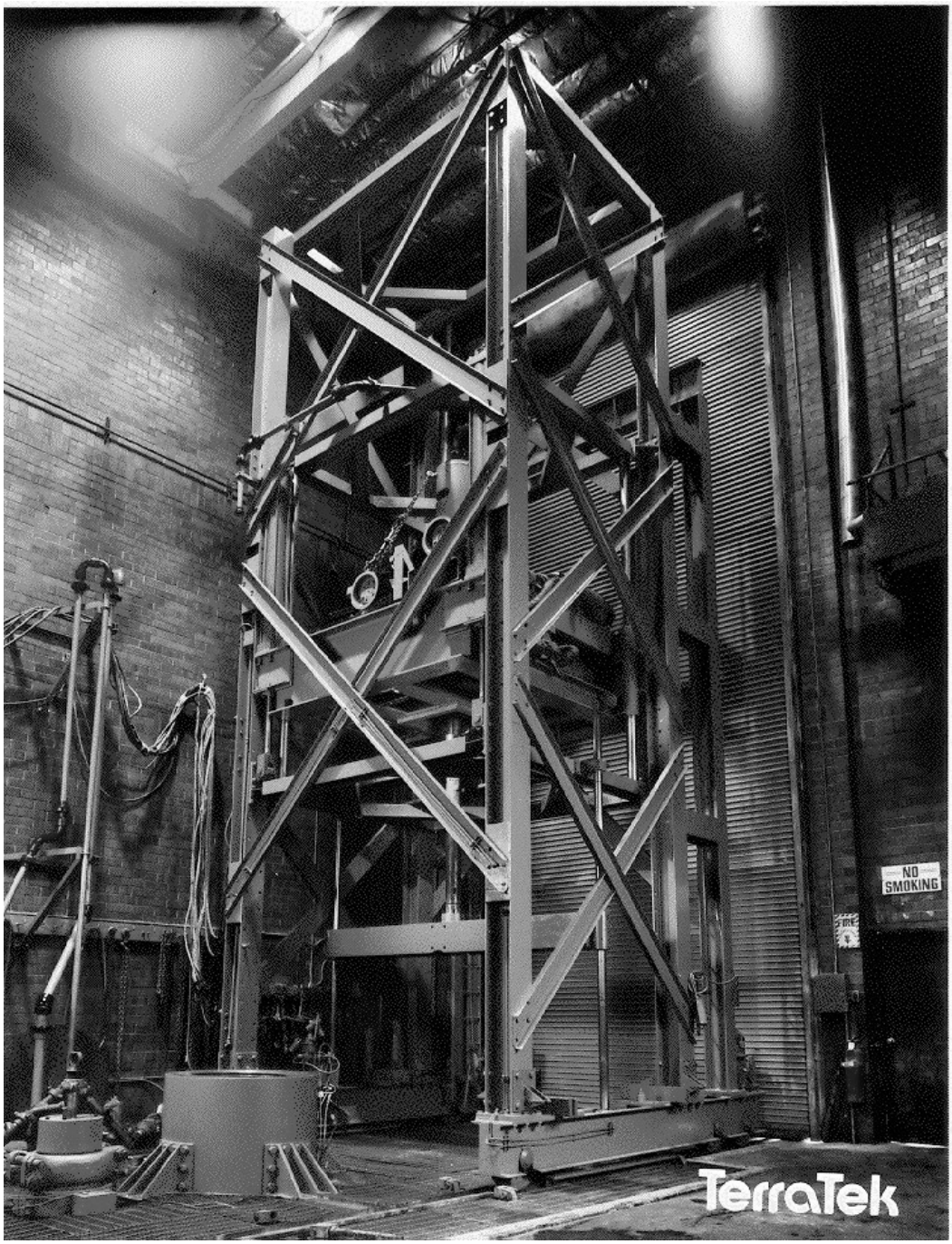

Figure 41: Drilling Research Laboratory at TerraTek, Inc.

2.5.1 Test Plan

The test plan is included in Appendix D. The TerraTek Drilling Research Laboratory is described in this appendix as well. The test plan refers to testing with a current-technology hard rock PDC bit – this is the prototype bit with the conventional nozzles installed. As noted in Appendix D, a Smith F3 (IADC code 5-3-7) roller cone bit was also tested in Crab Orchard Sandstone. It is shown in *Figure 42*. A hard-formation roller cone, Reed Hycalog HP62A (IADC code 6-2-7), was also tested in Sierra White Granite; it is shown in Figure 1.

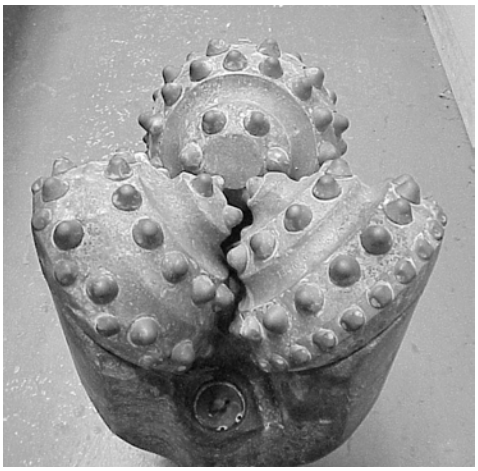

Figure 42: Smith F3 (IADC code 5-3-7) roller cone bit also tested at TerraTek.

2.5.2 Flow Test

Since new orifice materials were developed for this project, it was decided that they should be flow tested under the operational conditions to be expected during drilling before committing the bit to drilling tests. This flow testing was conducted at TerraTek in the DRL at the hydraulic operating conditions anticipated in the drilling tests, i.e., 300 gpm at a 5000 psi pressure drop. The bit was spudded into a sample of Nugget sandstone to a total depth of 7 inches. This also allowed the bottom hole pattern created by the bit to be observed. The bit was pulled off bottom and the orifices were flow tested for several minutes. Then the bit was set down on the Nugget Sandstone and the nozzles were allowed to impinge upon the rock sample for 30 seconds, resulting in significant rock erosion. *Figure 43* shows the damage done to the rock during this time interval. The depth of each of these cavities is on the order of 1 ±1/8 inches. Nugget sandstone has a compressive strength of 18000 psi UCS. No anomalies were observed during this flow test. The bit was thereby qualified for subsequent drilling tests.

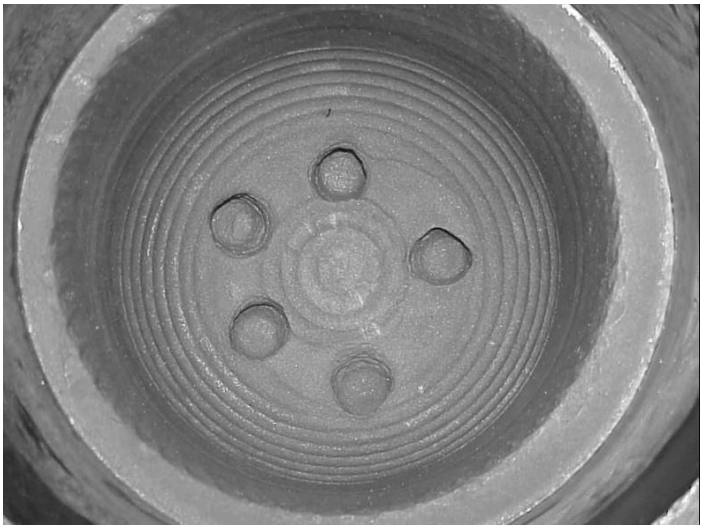

Figure 43: Erosion pattern created in Nugget Sandstone during flow test.

2.5.3 Drilling Tests

The test conditions evaluated at the Drilling Research Laboratory at TerraTek in the Phase I demonstration are summarized in *Table 5*. Generally, the Phase I bit was tested in Crab Orchard Sandstone at atmospheric pressure and at elevated well bore pressures of 2000 and 4000 psi. A conventional roller cone bit (Smith F3, IADC code 5-3-7) was also tested in this rock formation at atmospheric pressure; TerraTek had previously tested this bit at these elevated pressure conditions and made that data available to Sandia for inclusion in this comparative analysis as well. The Phase I bit was also tested in Sierra White Granite at elevated well bore pressures of 2000 and 4000 psi. Again a roller cone bit (Reed Hycalog, IADC code 6-2-7) was tested at comparable conditions. As described in the test plan in Appendix D, TerraTek monitored various drilling parameters throughout this testing. Appendix E contains the record of each of the drilling parameters measured during the drilling tests; mud properties during each of these tests are also reported in this appendix.

The drilling tests conducted at atmospheric pressure used large rock samples secured beneath the rig (outside the well bore simulator). As described in Table 5, the first sample of Crab Orchard Sandstone fractured during the testing, requiring an additional rock sample be used to complete the testing in this rock type. A disparity was observed in the bit response between these rock samples, presumably due to variable rock properties between samples. Consequently, the Phase I bit was tested with both standard and enhanced nozzles in each rock sample to clarify the differences observed in performance. Bit comparisons for this formation can be made by comparing tests 1A, 2 & 4.

The drilling tests conducted at elevated well bore pressures used rock samples housed in a urethane bladder and installed in the well bore simulator. The pressure in the well bore simulator is controlled by a choke valve downstream of the pressure vessel. Hence, to obtain a 4000-psi well bore pressure, the drilling fluid must be pumped at 9000 psi to achieve a 5000-psi pressure differential across the bit. Since the mud pumps at TerraTek are limited to a total flow of approximately 180 gpm at the peak operating pressures anticipated during the drilling tests (9000 psi), TerraTek coordinated with Halliburton to supplement the flow rate at the higher pressures simulated in the wellbore (2000 & 4000

psi). *Figure 44* shows the pumper truck and frac truck back to back outside the TerraTek Drilling Research Laboratory. The pumper truck was used to provide flow from the DRL mud system to the frac truck, shown in *Figure 45*. The frac truck boosted the pressure of this flow, and then it was combined with the primary flow from the TerraTek mud pumps and delivered to the bit.

Figure 44: Pumper truck and Frac truck at TerraTek's Drilling Research Laboratory.

Figure 45: Frac truck receiving flow input from pumper truck to augment TerraTek pumps.

The Phase I demonstration bit performed well throughout all the testing. The interchangeable nozzle approach proved viable as it was not difficult to interchange the nozzles during the test program. The standard nozzles functioned normally at their lower differential pressure. Hence, the influence of enhanced and standard nozzles could be compared within a single bit.

The polycrystalline diamond orifices incorporated in the enhanced nozzles survived the cavitation environment and performed flawlessly throughout all the testing. No wear was observed in the throat of the orifice throughout the Phase I testing interval. A high-pitched audible tone was clearly discernible when the resonating cavitating nozzles were active in the bit, corresponding to the resonance in the organ pipes and the higher jet velocity achieved across the orifices. In addition to the data in Appendix E, high sample rate data was recorded by Sandia using the TerraTek pressure transducer installed near the swivel on the TerraTek rig.

Some erosion was observed on the upper surfaces of some of the PDC cutters comprising the bit. This is seen in the face view photograph of the bit following test #7 (*Figure 46*). While this phenomenon has the capacity to eventually erode the carbide substrate of the PDC away, it didn't appear to affect the drilling performance during this limited test series. No appreciable wear was observed on the cutting surfaces of the PDC cutters at the completion of the test program.

Figure 46: Photograph of Phase I bit near the completion of testing; note erosion on bit near cutters 4, 7A and 7B.

Table 5: Summary of Phase I Drilling Tests[1]

Test	Date	Bit	RPM	Wellbore pressure	Rock Sample	Notes
1	12/04/00	Roller Cone (IADC 5-3-7)	110	Atmospheric	Crab Orchard Sandstone Block (Rock #1)	At the second operating condition, a large section of rock broke off terminating the test.
1A	12/04/00	Roller Cone (IADC 5-3-7)	110	Atmospheric	Crab Orchard Sandstone Block (Rock #1)	The rock was relocated beneath the drill rig and the drilling continued.
2	12/04/00	PDC with standard nozzles	110	Atmospheric	Crab Orchard Sandstone Block (Rock #1)	
3	12/04/00	PDC with high-pressure nozzles	110	Atmospheric	Crab Orchard Sandstone Core, 17" Diameter x 36" Lg. (Rock #2)	Due to the rock fracture in Test 1, insufficient rock was available for testing in Rock #1. Hence, testing continued in Rock #2.
4	12/05/00	PDC with high-pressure nozzles	110	Atmospheric	Crab Orchard Sandstone Block (Rock #1)	Rate of penetration of the bit equipped with the high-pressure nozzles in Test 3 was less than the performance of the un-augmented bit in Test 2. Hence, the high-pressure nozzles were tested in a small sample of Rock #1 to investigate the anomaly.
5	12/05/00	PDC with standard nozzles	110	Atmospheric	Crab Orchard Sandstone Core, 17" Diameter x 36" Lg. (Rock #2)	To further clarify the difference in rock properties, the performance of the bit equipped with the standard nozzles was tested in Rock #2.
6a	12/07/00	PDC with standard nozzles	110	2000 psi	Crab Orchard Sandstone Core, 17" Diameter x 48" Lg.	-------
6b				4000 psi		
7a	12/07/00	PDC with high-pressure nozzles	110	2000 psi	Crab Orchard Sandstone Core, 17" Diameter x 48" Lg.	-------
7b				4000 psi		
8a	12/08/00	PDC with standard nozzles	110	2000 psi	Sierra White Granite, 17" Diameter x 48" Lg.	-------
8b				4000 psi		
9a	12/08/00	PDC with high-pressure nozzles	110	2000 psi	Sierra White Granite, 17" Diameter x 36" Lg., with pre-existing 8-1/2" hole	-------
9b				4000 psi		
10a	3/27/01	Roller Cone (IADC 6-2-7)	70	500 psi	Sierra White Granite	-------
10b			110	500 psi		
10c			70	2000 psi		
10d			110	2000 psi		
10e			70	4000 psi		
10f			110	4000 psi		

[1] TerraTek also provided data from previous roller cone testing in Crab Orchard Sandstone at 2000 and 4000 psi wellbore pressures.

2.6 Phase I Data Analysis

The data in Appendix E are analyzed and compared below. Data points with common operating conditions are averaged and various plots prepared to display results. These comparisons are contained in *Figures 47* through *56* and consist of ROP versus WOB & ROP versus Bit Power at a given well bore pressure in a specific rock type.

Generally, the rate of penetration of the Phase I bit equipped with the STRATOJET® nozzles exceeded all comparable conditions with the standard nozzles. Specifically, in Crab Orchard Sandstone with a 2000-psi wellbore pressure, the rate of penetration of the PDC bit with jet-augmentation increased more than 40 percent over that achieved with standard nozzles. At a given penetration rate, the jet augmentation reduced the requisite weight on bit, and hence the component cutter forces, by 20 percent or more.

The PDC bit was also used with both cavitating and conventional nozzles to drill Sierra White Granite at rates in excess of 40 feet per hour. In this rock type, the cavitating jets increased the ROP by up to 20% at the highest well bore ambient conditions addressed. These data additionally show the performance advantages of PDCs over roller cones in these hard formations as significantly more power is delivered to the rock by the PDC bit resulting in ROP enhancement factors up to two or three.

The data from the Phase I demonstration testing in Sierra White Granite is further analyzed following a procedure put forth by Detournay and Defourny [23]. This procedure involves computing the Specific Energy and Drilling Strength and plotting these two terms against one another. (The reader is referred to this reference for details regarding this procedure.) These results are plotted in Figures 57 & 58. Also plotted are trend lines based upon a linear regression through the available data points. According to this analysis procedure, the intersection of this friction line (trend line) with a “cutting locus” is representative of the compressive strength of the formation. Also plotted in these figures is a cutting locus that Sandia has developed based upon single cutter testing in Sierra White Granite. By comparing the intercepts of the trend lines resulting from the linear regressions, it is apparent that the enhanced nozzles reduce the effective strength of the formation, even in a hard rock such as Sierra White Granite. In Figure 57 the intercept is reduced by 20% at a 2000 psi well bore pressure; in Figure 58, at a 4000 psi well bore pressure, the intercept is reduced by 13%. Even though the ROP enhancements are not appreciable in Sierra White Granite, this apparent softening of the rock with the Stratojets® may have far reaching implications in reducing the effects of bit damage introduced by abrasion and impact loading when fielding PDC bits in these hard formations.

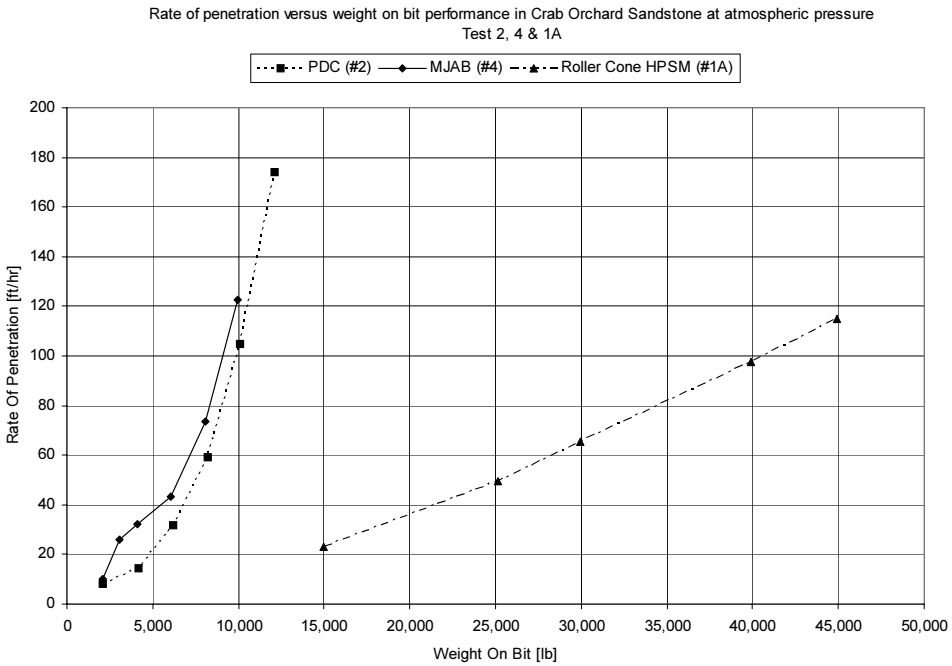

Figure 47: Rate of penetration versus weight on bit performance in Crab Orchard Sandstone at atmospheric pressure.

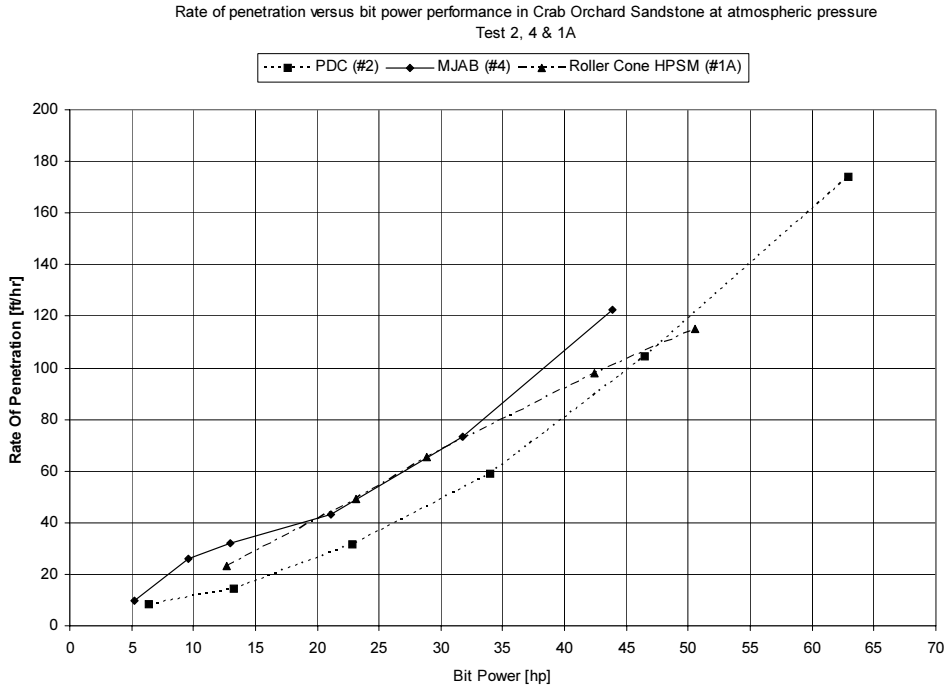

Figure 48: Rate of penetration versus bit power performance in Crab Orchard Sandstone at atmospheric pressure.

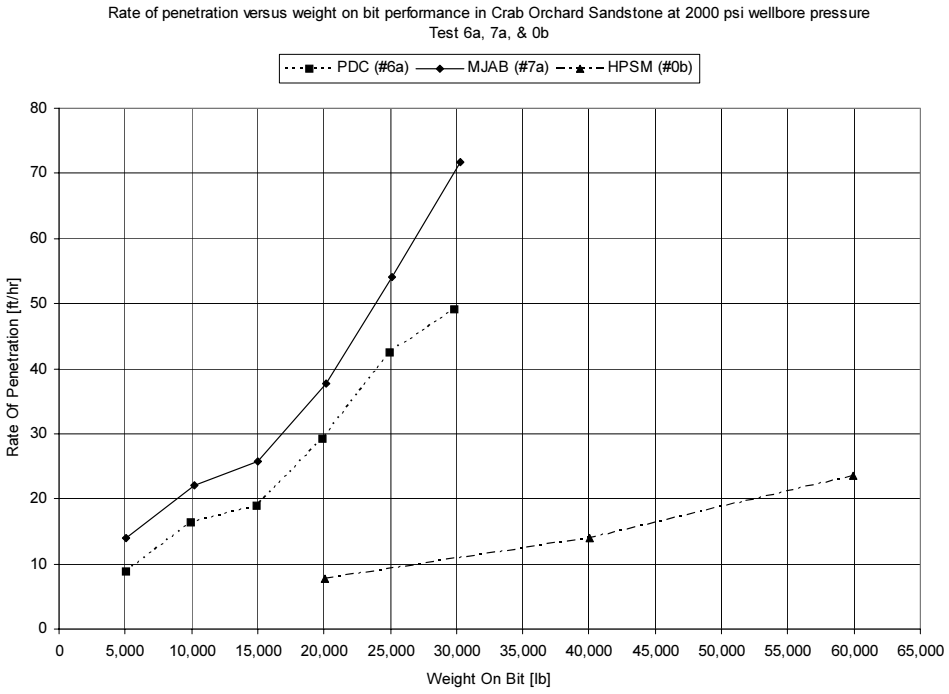

Figure 49: Rate of penetration versus weight on bit performance in Crab Orchard Sandstone at 2000 psi wellbore ambient pressure.

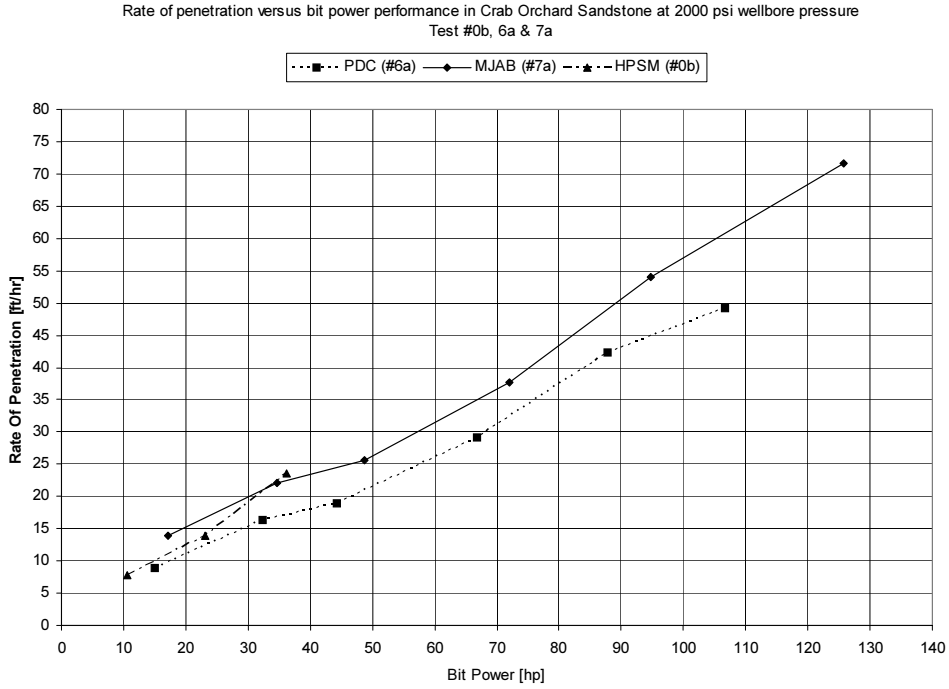

Figure 50: Rate of penetration versus bit power performance in Crab Orchard Sandstone at 2000 psi wellbore pressure.

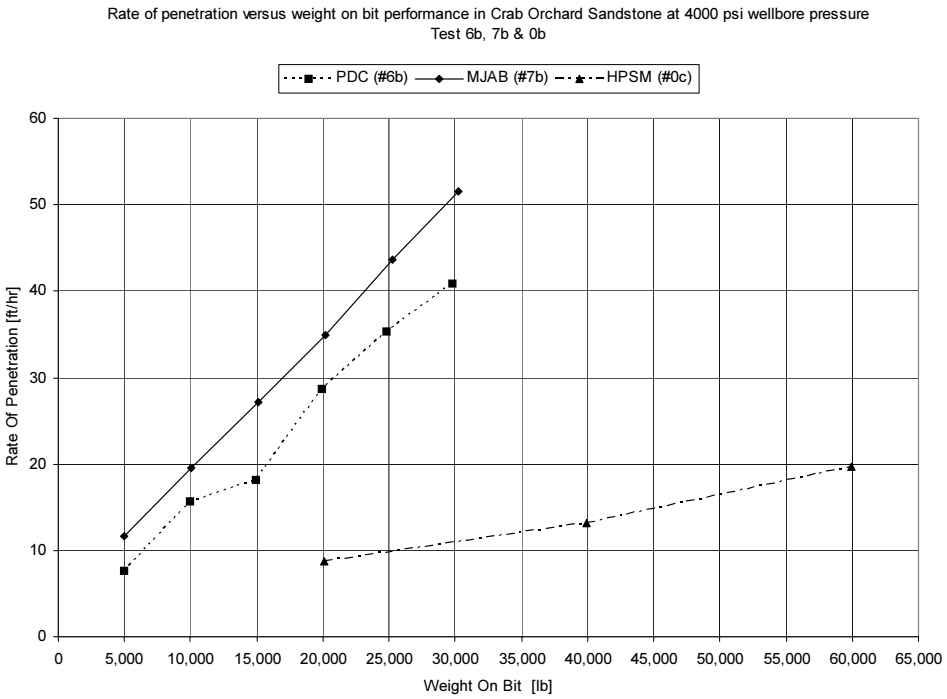

Figure 51: Rate of penetration versus weight on bit performance in Crab Orchard Sandstone at 4000 psi wellbore pressure.

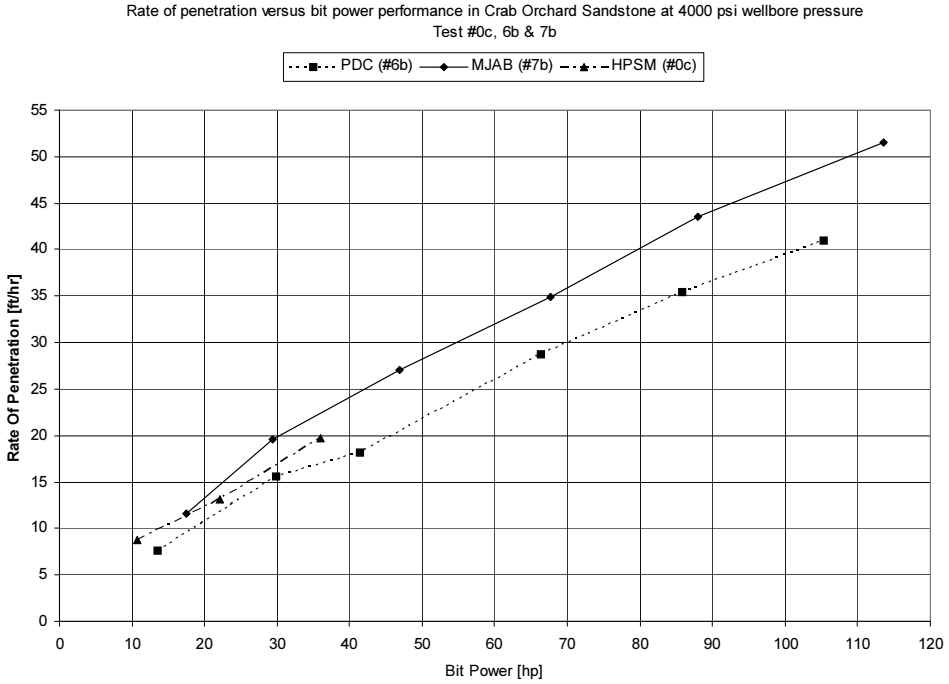

Figure 52: Rate of penetration versus bit power performance in Crab Orchard Sandstone at 4000 psi wellbore pressure.

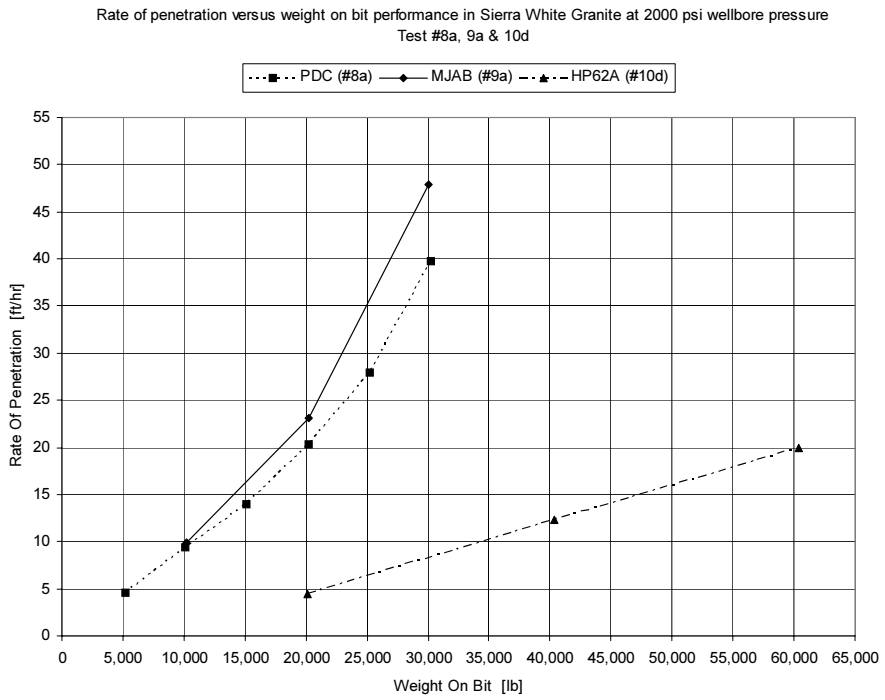

Figure 53: Rate of penetration versus weight on bit performance in Sierra White Granite at 2000 psi wellbore pressure.

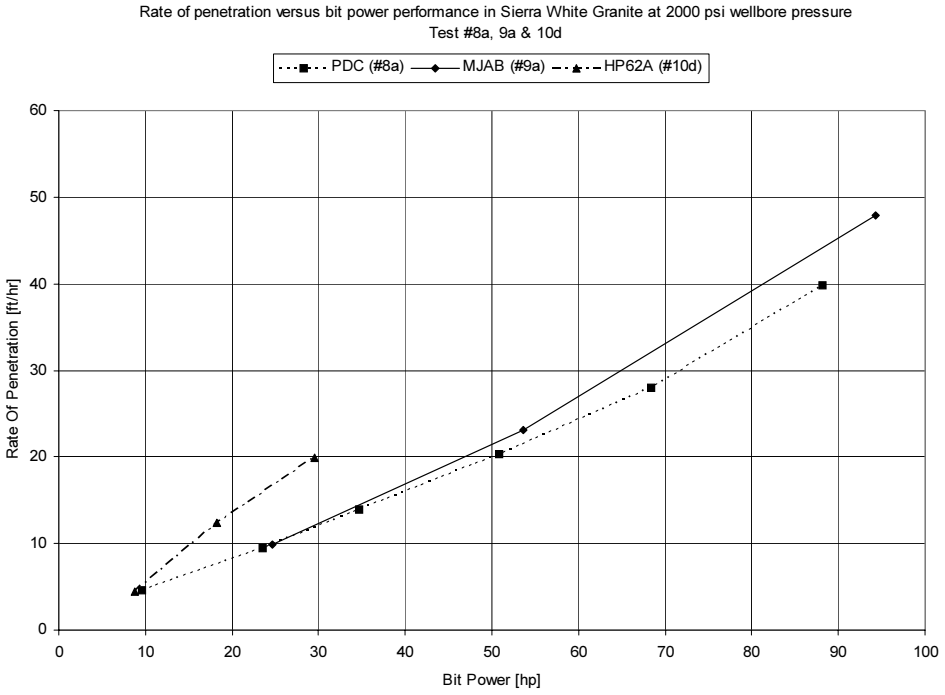

Figure 54: Rate of penetration versus bit power performance in Sierra White Granite at 2000 psi wellbore pressure.

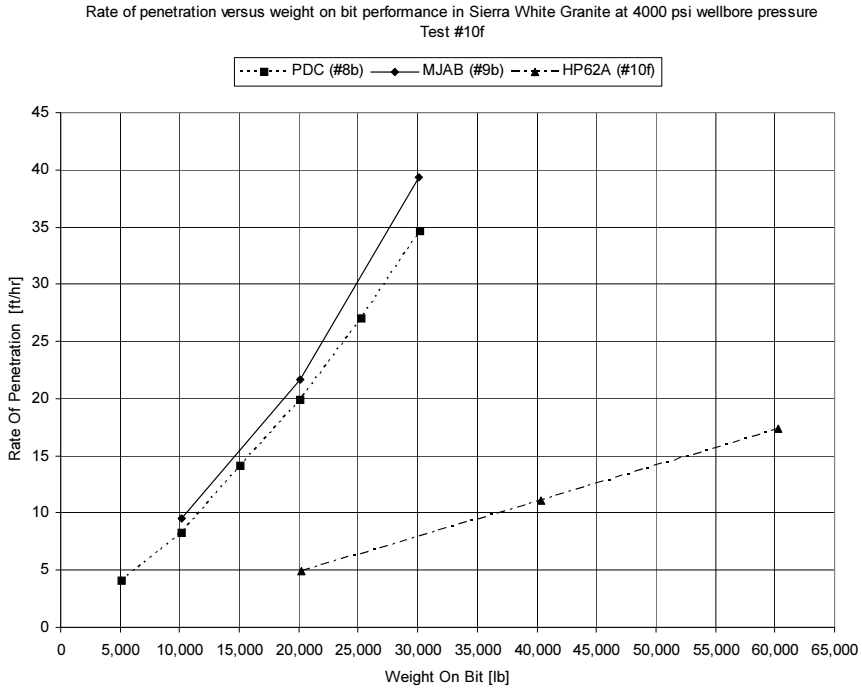

Figure 55: Rate of penetration versus weight on bit performance in Sierra White Granite at 4000 psi wellbore pressure.

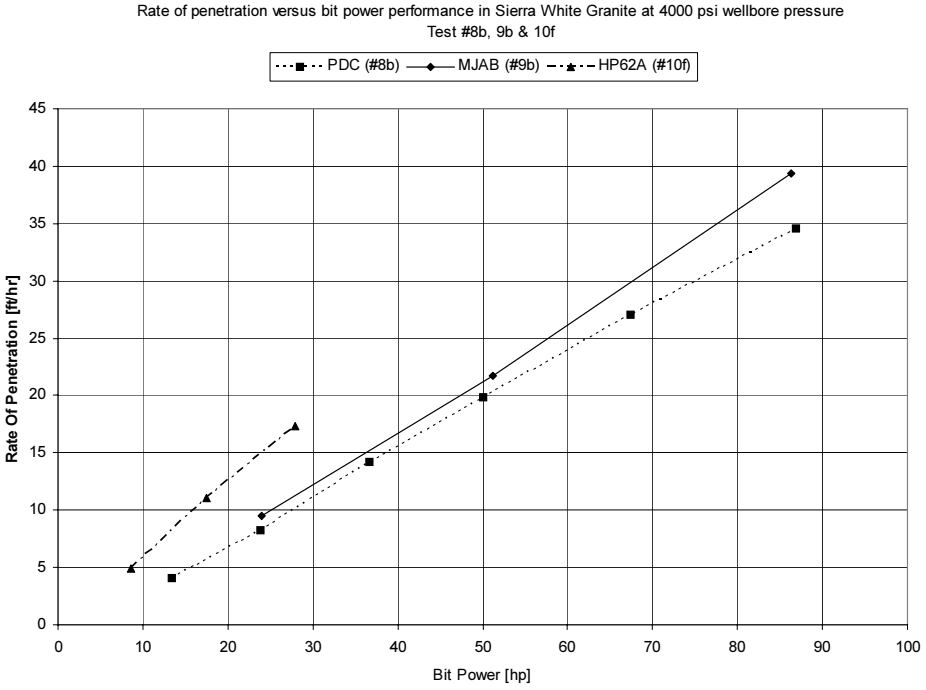

Figure 56: Rate of penetration versus bit power performance in Sierra White Granite at 2000 psi wellbore pressure.

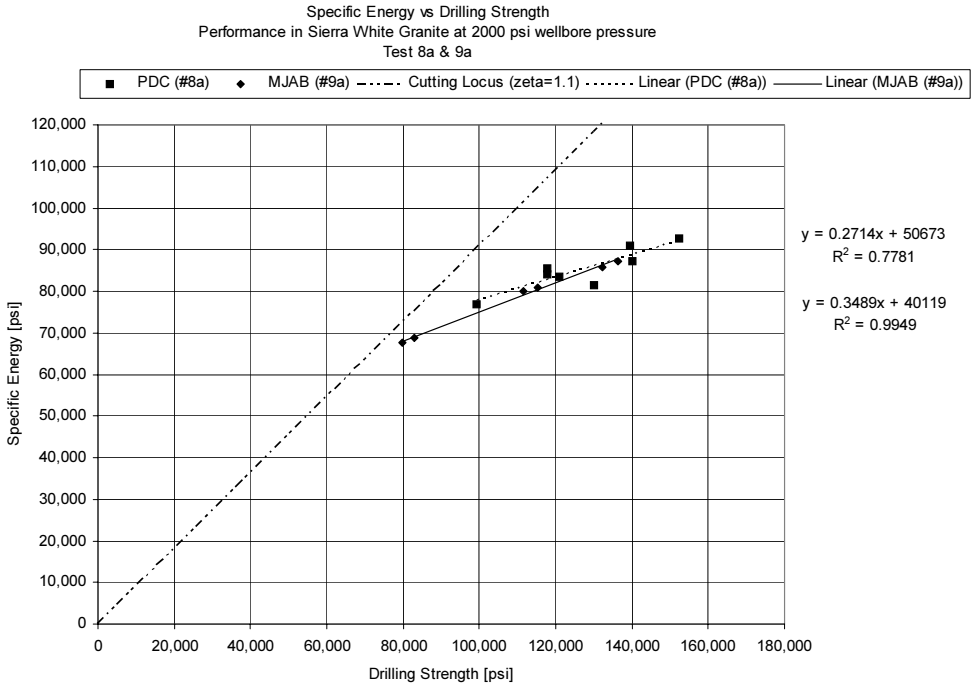

Figure 57: Specific Energy vs. Drilling Strength in Sierra White Granite at 2000 psi wellbore pressure.

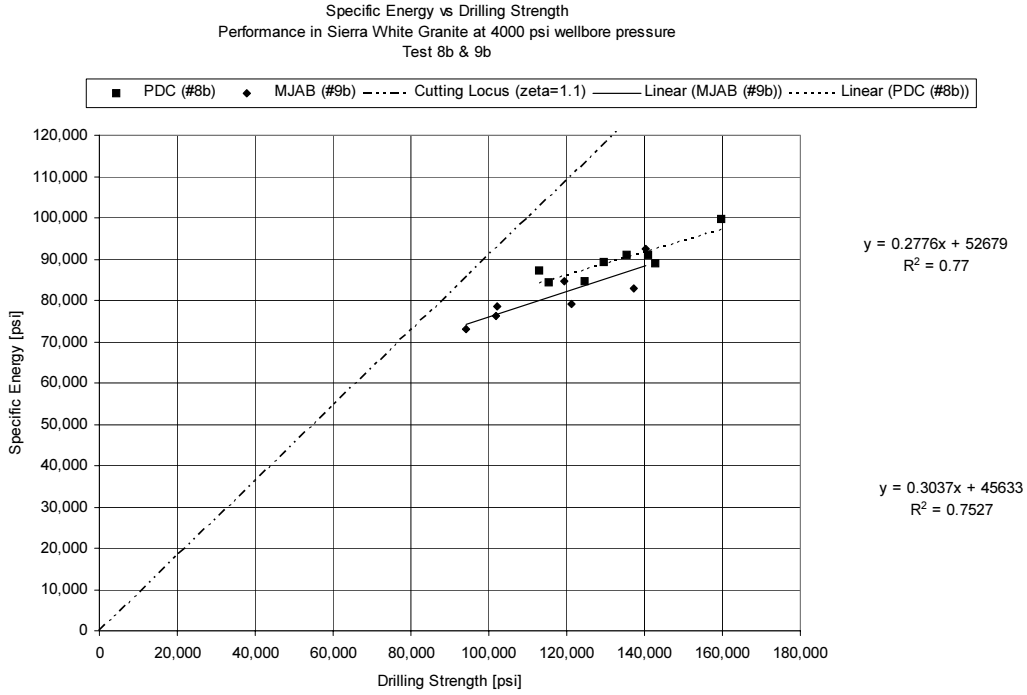

Figure 58: Specific Energy vs. Drilling Strength in Sierra White Granite at 4000 psi wellbore pressure.

3. Phase II - Characterization of Nozzle/Cutter Interaction

Work commenced on Phase II activities following the successful Phase I demonstration. The approach in Phase II was to conduct parameter testing to characterize the interaction between a single nozzle and one or more cutters comprising the bit cutting structure by testing a single nozzle with a single or multiple cutters. The testing allowed the nozzle's formation standoff, cutter lead, and inclination angle to be adjusted, in addition to pressure/flow conditions, to characterize the influence of each of these parameters upon the cutting forces. The design of the hardware was predicated on testing over a range of pressure differentials up to 8000 psi (higher than in Phase I) with the rock cutting at atmospheric pressure. Components were designed and procured based on the pressure safety requirements of the high-pressure system.

This laboratory work was conducted at Sandia National Laboratories in Albuquerque. James Grossman acted as Principal Investigator during Phase II of the project. DynaFlow supported this work through specification of nozzle/orifice designs and configurations. Prior to the system assembly, a budget reduction forced temporary postponement of the project. When the project resumed, time and budget reductions limited the scope of testing. Testing was focused on the large orifices (#10 and #12) because they were the easiest to test and their range of operation (2000 to 3000 psi) is within the capabilities of existing geothermal drilling rigs making them the most feasible for immediate commercialization. In the end the time and budget constraints, forced the project to evolve into more of a single-point investigation rather than an overall characterization effort. Nonetheless, much of the report detailing the Phase II development has been included to provide a record of the effort.

3.1 Approach

The parameters that govern the relationship between cutter and nozzle performance are:

- Cutting Structure: cutter diameter, depth of cut, linear speed, backrake angle, siderake angle, and cutter wearflat area. The interaction of a single nozzle with multiple cutters should also be investigated.
- Nozzle Hydraulics: organ pipe configuration (single or stepped), orifice diameter, flowrate, ambient pressure, pressure drop, fluid density, normalized rms pressure fluctuations.
- Interaction between Cutting Structure & Nozzle Hydraulics: standoff, jet impact distance ahead of the cutter, nozzle inclination angle, and nozzle tilt angle.
- Formation: rock properties including compressive strength, permeability, and porosity.

Data is needed on these parameters in order to achieve an integrated approach to all aspects of bit design. In order to optimize the performance gains possible with these directed nozzles, Sandia planned to conduct testing to determine the relationship between nozzle design/operating parameters and bit design/operating parameters. The test fixtures necessary to complete this work were fabricated and assembled in the Linear Cutter Test Facility (LCTF) at Sandia (*Figure 59*). The LCTF supports research on the cutting loads for various drag cutter designs. The facility consists of a horizontal mill that has been

fitted with a three-axis dynamometer to measure orthogonal cutting forces. For the present study, test fixtures were fabricated to straddle the LCTF to support the nozzle assembly independent of the milling machine so the cutting loads could be measured independent of the hydraulic reactions on the fixtures. Sandia built several prototype nozzles and conducted testing to measure the variation in cutting loads as a function of the following parameters:

Figure 59: Photo of the Linear Cutter Test Facility

3.1.1 Cutting Structure Design

A cutter holder developed for the LCTF housed a stud-type PDC cutter. The actual implementation of the augmented cutter technology, of course is not limited to this cutter type. However, this configuration is more readily amenable to the LCTF configuration with augmentation. Rather than investigate a variety of cutter configurations, cutter diameters were limited to 13mm (0.53 inch) as this is one of the more common cutter configurations deployed throughout the bit industry. Likewise, the investigation was limited to backrake angles of 20 degrees and siderakes of 0 degrees. The depth of cut was varied between 0.010, 0.020, 0.040, and 0.080 inches.

3.1.2 Hydraulic Design

Hydraulic design can be subdivided into nozzle design and overall bit hydraulic design. While the emphasis here was on the performance of a single nozzle and its interaction with a single cutter or a suite of cutters, the overall bit hydraulic design introduces practical constraints on the extent of this investigation. The sensitivity of the nozzle's erosive potential needs to be addressed in regard to flowrate, pressure drop, and the magnitude of the pressure fluctuations. Yet the number of nozzles that can be placed across the bit face will be constrained by the geometry of the layout and the operating conditions for a full-scale bit.

The diameter of the orifice governs the pressure drop and flow rate. Nozzle orifice diameters were chosen to be reasonably consistent with current practice in the bit industry. As stated in Section 2, current trends are to use orifice diameters in excess of a #8 nozzle size (0.25 inch diameter) to avoid plugging with particulates entrained in the drilling fluid. However, the design condition of the Phase I bit (5000 psi at 300 gpm) and the decision to augment five blades using five nozzles dictated a smaller orifice diameter of 0.194 inches (equivalent orifice size 6.2). This condition was targeted in the present research as well. Larger orifice sizes, #10 and #12 diameter (0.313 & 0.375 inch, respectively), were included to evaluate the most likely pressure regime on conventional drilling rigs. Smaller orifice sizes, #4 and #5 (0.125 & 0.156 inch, respectively), were selected to investigate the benefit of operating at high pressure.

Subject to the orifice diameter selections above, Sandia requested that DynaFlow conduct design and analysis to specify the single organ pipe and orifice configurations to operate at the conditions shown in *Table 6*. The nozzle/orifice operating conditions corresponding to these conditions are shown in *Table 7*. The orifice properties for each of the configurations, as specified by DynaFlow, are summarized in *Figure 60*.

Table 6: Phase II Orifice Design Conditions.

Orifice Size (#/32 inches)	Orifice Diameter (inches)	Pressure Drop (psi)
4	0.125	8000, 7000, 6000 & 5000
5	0.156	7000, 6000, 5000 & 4000
6.2	0.194	6000, 5000, 4000 & 3000
8	0.250	4000, 3000 & 2000
10	0.313	3000, 2000, & 1500
12	0.375	2000 & 1500

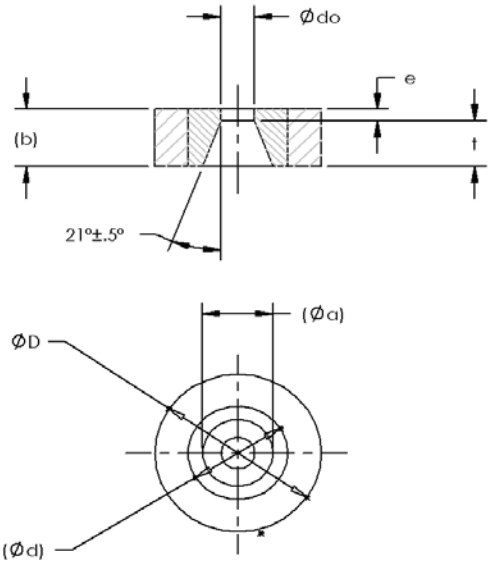

Part Number	Die P/N	Øα Ref Nominal	b Ref Nominal	Ød Ref Nominal	ØD	Ødo±.0005	e±.001	t±.001
MJAB002-1	GE5211	.262	.224	.500	.751/.749	.125	.046	.178
MJAB002-2	GE5211	.326	.279	.500	.751/.749	.156	.057	.222
MJAB002-3	GE5211	.406	.347	.500	.751/.749	.194	.071	.276
MJAB002-4	WD470	.523	.447	.787	1.379/1.377	.250	.091	.356
MJAB002-5	WD470	.655	.560	.787	1.379/1.377	.313	.115	.445
MJAB002-6	WD480	.785	.671	1.102	1.851/1.849	.375	.137	.534

Figure 60: Properties of orifices used in Phase II testing.

Table 7: Possible Nozzle/Orifice Operating Conditions to be Evaluated in Phase II.

Orifice Size (#/32 inches)	Orifice Diameter (in)	Orifice Area (in^2)	Organ Pipe Diameter (in) [Note 1]	Organ Pipe Length (in)	Delta P (psi)	Flow Rate (GPM)	Velocity (ft/s)	Frequency [0.3*V/d] (Hz)	Hydraulic Horse Power	Momentum Force (lb)
4	0.125	8.52E-05	0.58	1.15	8000	28.3	741.0	21340	132.3	93.5
4	0.125	8.52E-05	0.58	1.23	7000	26.5	693.1	19962	108.3	81.8
4	0.125	8.52E-05	0.58	1.33	6000	24.5	641.7	18481	85.9	70.1
4	0.125	8.52E-05	0.58	1.45	5000	22.4	585.8	16871	65.4	58.4
5	0.156	1.33E-04	0.72	1.53	7000	41.4	693.1	15970	169.2	127.8
5	0.156	1.33E-04	0.72	1.66	6000	38.4	641.7	14785	134.3	109.6
5	0.156	1.33E-04	0.72	1.82	5000	35.0	585.8	13497	102.1	91.3
5	0.156	1.33E-04	0.72	2.03	4000	31.3	524.0	12072	73.1	73.0
6.2	0.194	2.05E-04	0.90	2.06	6000	59.0	641.7	11923	206.4	168.4
6.2	0.194	2.05E-04	0.90	2.26	5000	53.8	585.8	10885	157.0	140.4
6.2	0.194	2.05E-04	0.90	2.52	4000	48.1	524.0	9735	112.4	112.3
6.2	0.194	2.05E-04	0.90	2.92	3000	41.7	453.8	8431	73.0	84.2
8	0.250	3.41E-04	1.16	3.25	4000	80.2	524.0	7545	187.1	187.0
8	0.250	3.41E-04	1.16	3.76	3000	69.4	453.8	6534	121.5	140.2
8	0.250	3.41E-04	1.16	4.60	2000	56.7	370.5	5335	66.1	93.5
10	0.313	5.33E-04	1.45	4.70	3000	108.5	453.8	5227	189.9	219.1
10	0.313	5.33E-04	1.45	5.76	2000	88.6	370.5	4268	103.3	146.1
10	0.313	5.33E-04	1.45	6.65	1500	76.7	320.9	3696	67.1	109.6
12	0.375	7.67E-04	1.74	6.90	2000	127.5	370.5	3557	148.8	210.3
12	0.375	7.67E-04	1.74	7.97	1500	110.5	320.9	3080	96.7	157.8

Notes: 1: The greater the diameter change between the orifice and organ pipe and between the organ pipe and the feed tube, the stronger the resonance. Regarding the organ pipe ID's, scaling from DynaFlow's Phase I design provides a factor of 4.64 times the orifice diameter [24]. This value is used as a design guide.

2: Based upon a fluid density of 8.6 lb/gal.

3: DynaFlow uses a discharge coefficient of 0.69 in the nozzle calculations.

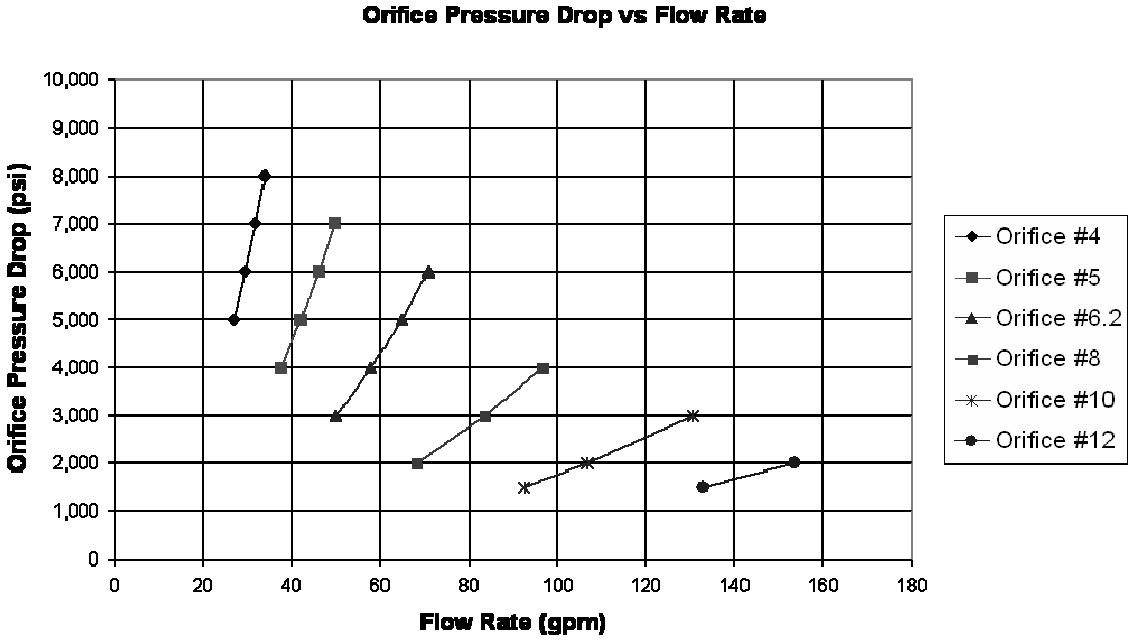

Figure 61: Phase II Nozzle Operating Conditions.

The nozzle designs allow investigation of both high pressure drop/low flowrate and high flow rate/low pressure drop. The nozzles are designed to use water during the cutter interaction testing. The nozzle operating conditions are plotted in *Figure 61*.

Presumably, the reduction in cutting forces due to augmentation will be strongly dependent upon the source pressure at the orifice. To reduce the number of pressures that must be tested with a given orifice size, the orifice set is reduced by selecting the orifice configurations that produce the greatest flowrate at a given pressure (greatest hydraulic horsepower); i.e., the operating conditions corresponding to the upper right-hand range of each orifice diameter in *Figure 61*. Hence, the matrix of orifices that must be tested and their respective operating conditions can be reduced to those highlighted in *Table 7*.

3.1.3 Interaction between Cutting Structure & Hydraulics

As previously noted, many of the parameters that govern the interaction between a given nozzle and the cutting structure are coupled with the overall hydraulic design of the bit. Accordingly, analysis is required to determine the possible combinations of suitable parameters. Reference 25 details geometric calculations that govern the inclination angle and tilt angle for a nozzle integrated into a bit as a function of the standoff distance, lead distance, and other pertinent parameters illustrated in *Figure 62*. The tilt angle is the rotation of the nozzle laterally across the face of the cutter. Subject to the analysis in this reference, the values shown in *Table 8* resulted from the presumed installation of these orifices in an 8-1/2 inch diameter bit as a function of the organ pipe configuration, lead and standoff distances. Nozzle inclination and tilt angles were computed for all orifices for a lead of 1.5 inches and a standoff of 1.0 inch, which are reasonable values based upon the Phase I bit development. The test fixtures were designed to accommodate this range of parameter interaction.

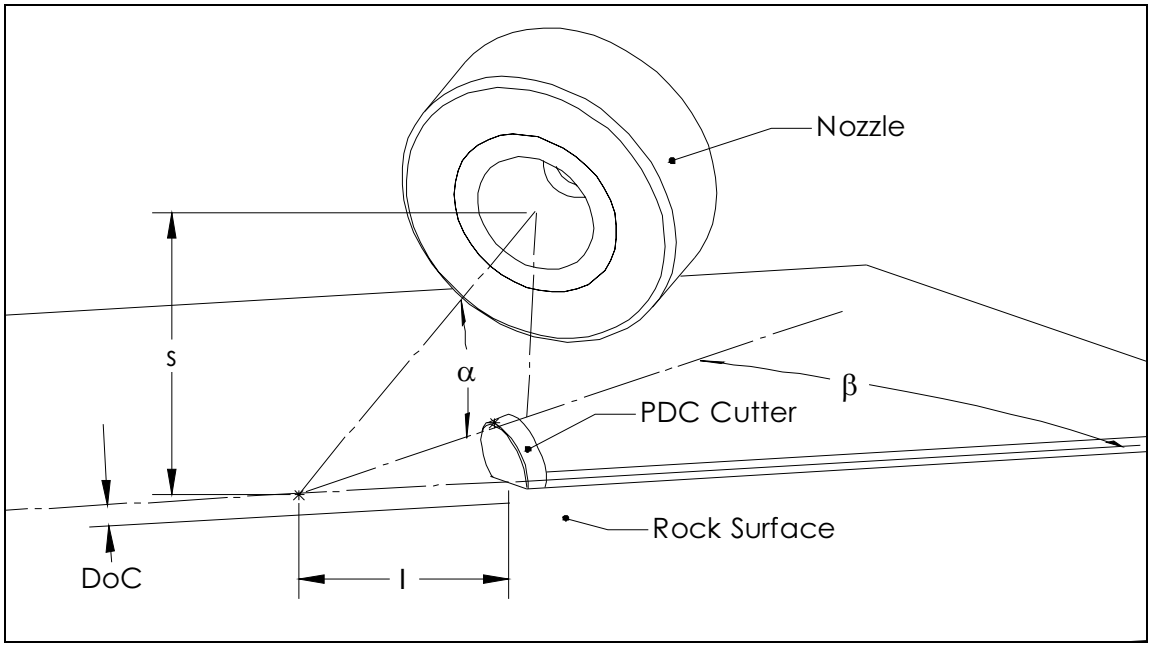

Figure 62: Illustration of cutting/nozzle interaction.

Table 8: Interaction Geometries.

Orifice No.	Organ pipe diameter [in]	Organ pipe length [in]	e [in]	t [in]	radius on bit [in]	lead [in - l]	standoff [in - s]	θ	waterway diameter [in]	α (Incl.)	β (Tilt)
4	0.58	1.23	0.05	0.18	2.50	1.50	1.00	34.9	2.20	19.7	27.2
5	0.72	1.66	0.06	0.22	2.50	1.50	1.00	34.9	2.05	17.3	24.0
6.2	0.90	2.26	0.07	0.28	2.50	1.50	1.00	34.9	2.22	13.1	18.4
8	1.16	3.25	0.09	0.36	2.50	1.50	1.00	34.9	2.20	10.0	14.1
10	1.45	4.70	0.12	0.45	2.50	1.50	1.00	34.9	2.76	5.8	8.3
12	1.74	6.90	0.14	0.53	2.50	1.50	1.00	34.9	3.31	3.4	4.8

The interaction between the hydraulics and the cutting structure on a full-scale bit also has limitations due to volumetric flow constraints. The annular flow rate for water-based drilling fluids is constrained to an annular velocity of 80-180 feet per minute. Using the nominal diameter and flow rate for the Phase I bit, the limitation on the number of nozzles for an 8-1/2" diameter bit operating at 300 gpm is shown in *Table 9*.

Table 9: Limitation on Number of Nozzles for an 8 ½ inch Diameter Bit.

Orifice Size (#/32 inches	Delta P (psi)	No. Of Nozzles	Hydraulic Horsepower per square inch (HSI)
4	8000	8	22.5
4	7000	8	18.4
5	6000	6	17.1
6.2	5000	5	16.7
8	4000	3	11.9
10	3000	2	8.1
12	2000	2	6.3

Note: 8.5 in diameter bit, 8.6 lb/gal fluid density @ 300 gpm.

This table may be used as a guide in interpreting the cutting force reduction achieved from a given nozzle/cutter combination and its influence on bit performance. The low pressure/high flowrate orifices must provide a force reduction across a plurality of cutters since the nozzles are more constrained in quantity. The high pressure/low flowrate nozzles, however, could be used in larger quantity on a given bit to achieve cutter force reductions.

3.1.4 Formation

Since the focus of this work is penetration of hard rock for geothermal formations, all testing was conducted in Sierra White Granite. This rock is a hard, abrasive formation with an unconfined compressive strength of 28,000 psi and negligible porosity and permeability. While this testing admittedly should have been done at elevated borehole pressures, it was not. To simplify the test protocol and reduce the cost of testing, all testing was conducted at atmospheric pressure. It has been assumed that the relative performance of the nozzles will scale to full-scale pressures. The benefit of cavitating nozzles has been demonstrated at pressure in Phase I of this project; the objective here is to characterize the reduction in drag cutting forces as a function of cutter interaction and hydraulic operating characteristics.

3.2 Test Fixture Description

The test fixtures for accomplishing this research consisted of several sub assemblies. These are illustrated in the drawing tree shown in *Figure 63*. It consists of the following assemblies representing the Cutting Structure, Nozzle Hydraulics, Interaction Between Cutting Structure & Nozzle Hydraulics, and Flow Loop. These are described in the following sections.

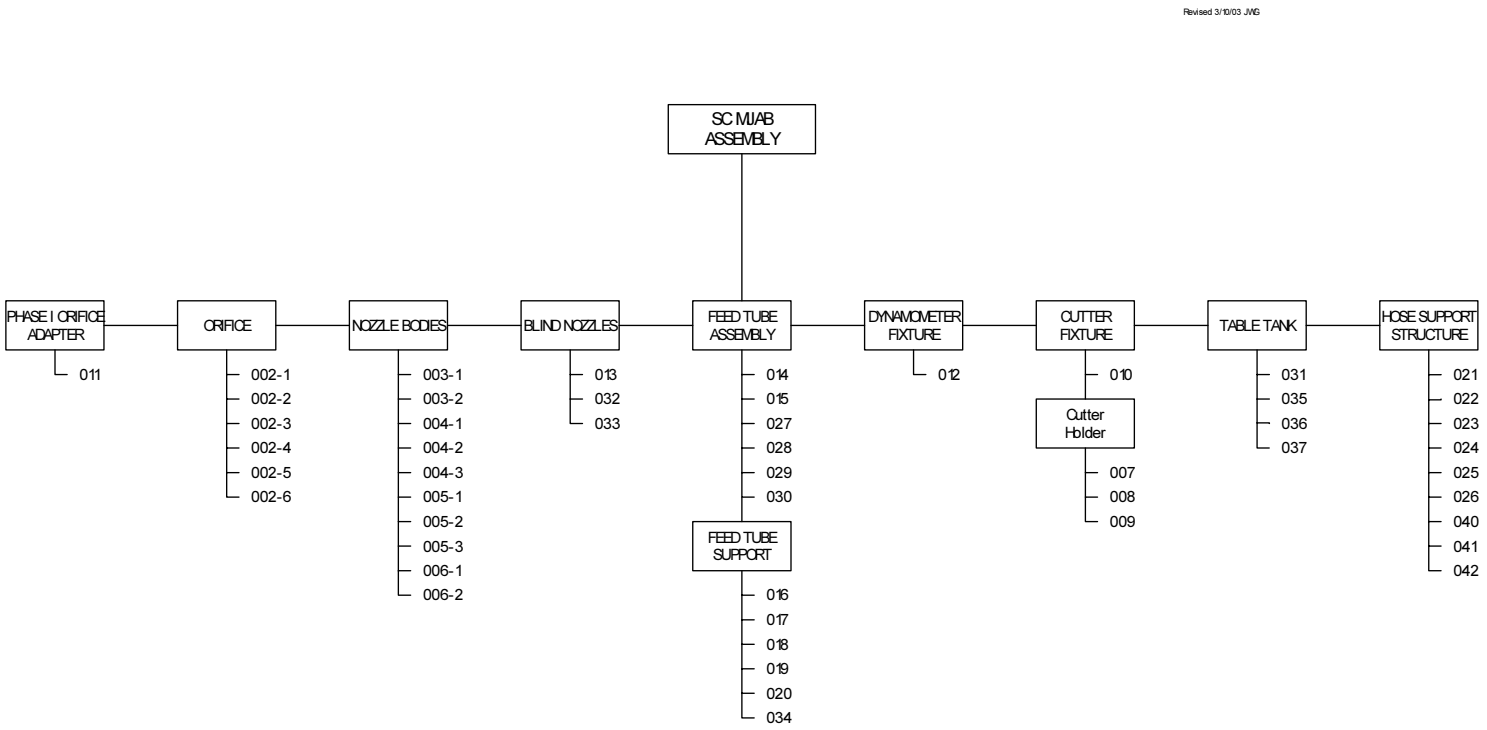

Figure 63: Test Fixture Assembly drawing configuration.

3.2.1 Cutting Structure

The Linear Cutter Test Facility consists of a Kearney & Trecker horizontal mill. The machine is located in the Building 851 Hi-Bay in Technical Area I at Sandia National Laboratories.

The dynamometer is a three-axis force transducer manufactured by Kistler. The cutter holder was designed to adapt to the dynamometer and extend the cutter to a configuration where it could be augmented. The cutter holder was designed to be used with one, two, or three cutters. Stud cutters were used to accommodate close mounting of adjacent cutters and were representative of cutter mounting on an actual bit.

3.2.2 Nozzle Hydraulics

Six nozzle orifice diameters were evaluated. Nozzle feed tube diameters and lengths dictated three different configurations, each accommodating two orifice diameters. Sandia fabricated the orifices using the polycrystalline diamond wire die technology demonstrated in Phase I. A similar approach was employed for the interaction testing in Phase II. However, in this case, the EDM-machined orifices were installed in the test fixture by clamping them into a nozzle assembly. Sandia had successfully machined the orifices for the Phase I work using Electro Discharge Machining (EDM) and found this to be a favorable technique. It has also been used successfully by the wire die industry to profile dies for wire drawing. Woodburn Diamond Die, Woodburn, Indiana, fabricated the orifices for the Phase II testing. Woodburn was chosen as they have machines capable of machining the orifice sections at a lower cost than those produced internally at Sandia in Phase I. The range of orifices fabricated for Phase II is shown in *Figure 64*; a 13mm diameter PDC cutter is also shown.

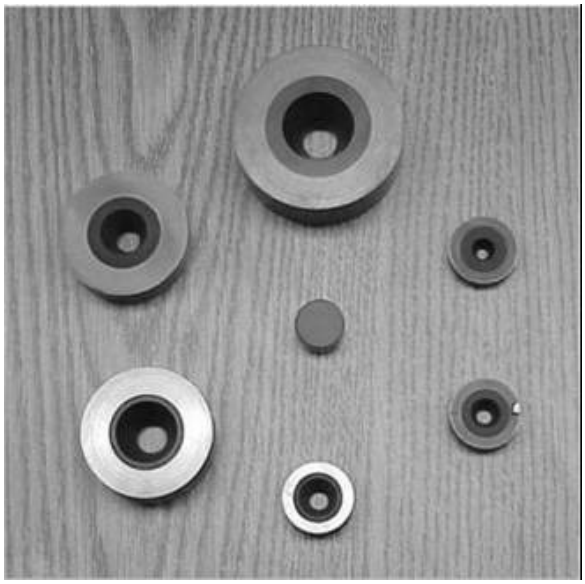

Figure 64: Variety of orifice sizes fabricated by Woodburn Diamond Wire Die for Phase II testing.

3.2.3 Interaction between Cutting Structure & Nozzle Hydraulics

The feed tube support fixture allowed the feed tube assembly to be supported independently of the cutting fixture so that the reaction loads from the nozzle operation were not transmitted into the milling machine assembly and accordingly measured as cutting loads. It also allowed the nozzle to be adjusted with respect to the cutter so that a variety of nozzle/cutter interaction geometries could be evaluated. The feed tube support fixture and its orientation relative to the horizontal mill are shown in *Figure 65*.

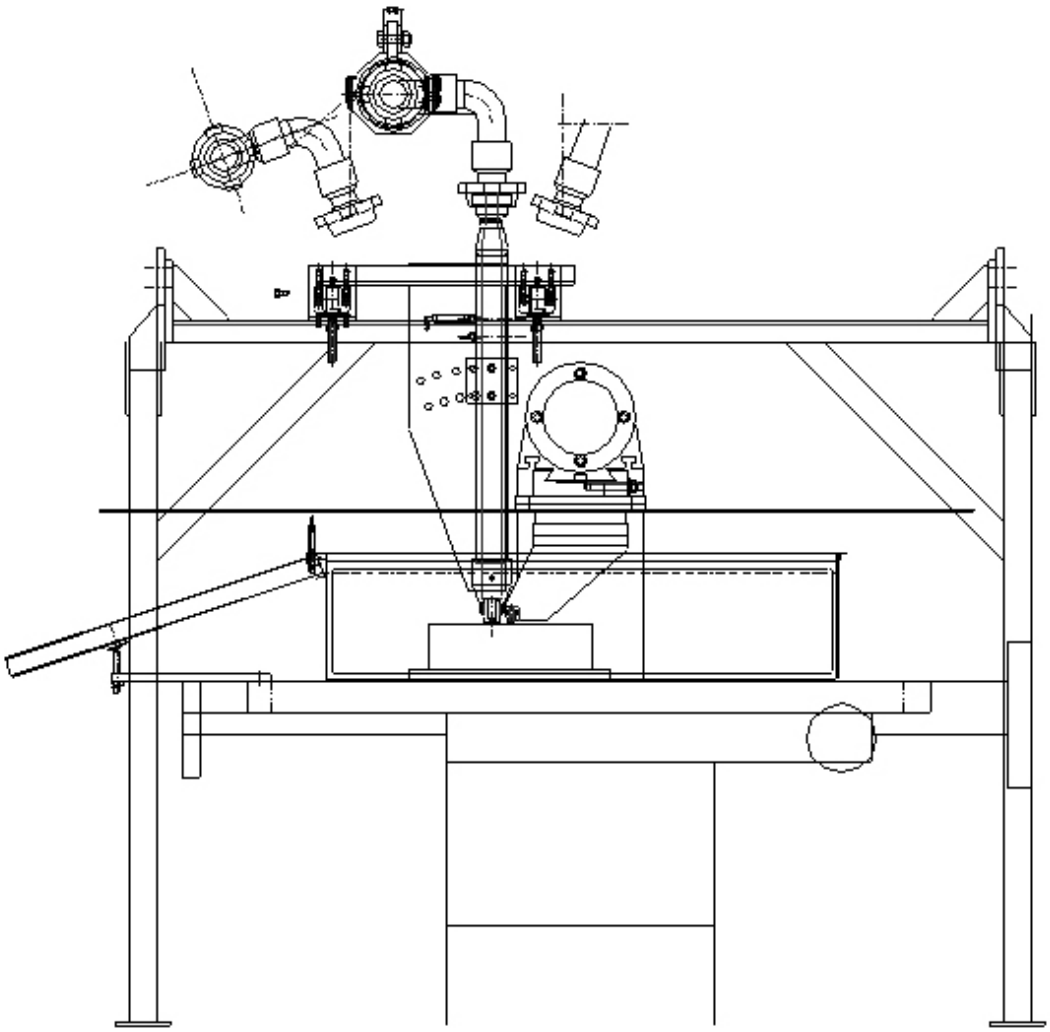

Figure 65: Feed Tube Support Fixture.

3.2.4 Flow Loop

A schematic of the piping network is shown in *Figure 66*. A high-pressure Triplex pump was leased and delivered to Sandia in support of this testing. The pump produced pressures up to 8,000 psi to supply the passively pulsating-cavitating nozzles coupled in a cutting configuration with a PDC cutter in Sandia's Linear Cutter Test Facility. Water was used as the test fluid. This high-pressure pump is similar to the type that may be

used in the field to feed the nozzles on a full-scale PDC bit incorporating this technology. A safety relief device was installed in the system to define the Maximum Allowable Working Pressure (MAWP) and prevent over-pressurization of the fixtures.

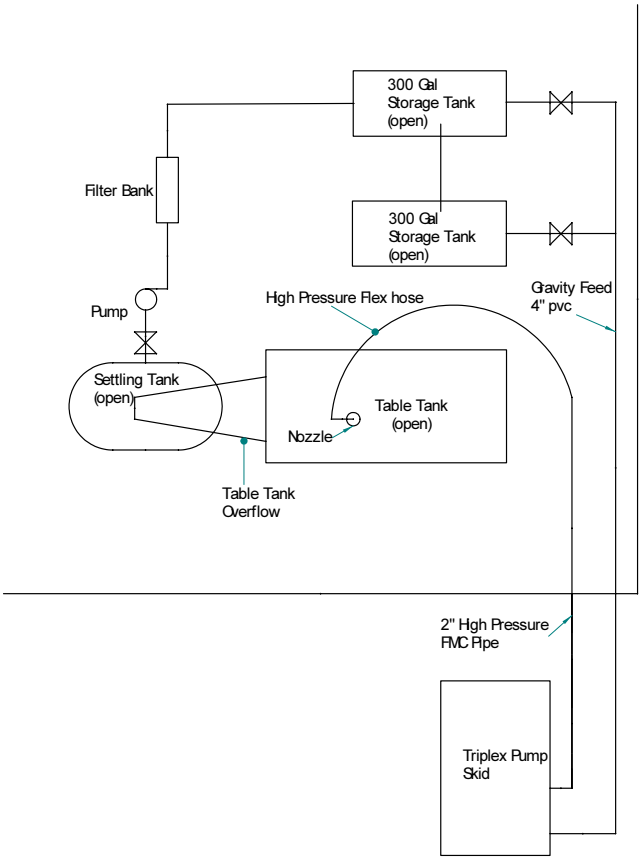

Figure 66: Flow Loop used for Phase II testing.

The high-pressure supply was constructed primarily of commercially available components. The supply piping components were FMC Flowline Products with Figure 1502 connections. The flexible hose is a choke and kill hose fabricated by Nephi Rubber Products Corp. Other components are as follows:

- *High-Pressure Pump* - Sandia rented a high-pressure pump to accomplish the nozzle/cutter interaction testing.

- *Table Tank* - A tank was mounted on the table of the horizontal mill to submerge the rock specimen. It included an overflow weir to maintain a constant fill volume; the weir fed into a settling tank.

- *Settling Tank* - The settling tank collected the overflow fluid from the table tank. It had adequate volume to allow rock cuttings to settle out of the flow before being returned to the storage tanks.

- *Return Pump* - A centrifugal pump returned fluid from the settling tank to the storage tanks.

- *Filter Bank* - The filter bank included replaceable bag filters to screen cutting particulates from the flow.

- *Reservoir Tank* - Supply tanks stored 300 gal of water each.

- *Tank Heaters* – were installed in tank end-wall feed thrus to maintain the supply fluid at constant temperature.

- *Pressure Relief Valves* - PRVs were mounted at the outlet port of the mud pump. Three PRVs were used; each corresponding to the Maximum Allowable Working Pressure for a particular feed tube configuration.

3.2.5 Instrumentation & Data Acquisition

A personal computer with National Instruments PCI-1200 card was used to record cutting loads from the dynamometer. A linear potentiometer was mounted to the table of the milling machine to record table position information as a function of time. This system forms the basis for the Linear Cutter Test Facility and was used here consistent with Sandia's standard test cutting protocol. Additional instrumentation was added to this system to measure parameters pertinent to the hydraulic augmentation.

Two pressure transducers were installed in each feed tube configuration. One of these was a static transducer to measure the mean pressure delivered to the feed tube. The other was a dynamic pressure transducer and was used to measure the range of pressure fluctuations generated by the resonating nozzle. An ultrasonic flow meter was installed on the output from the pump. Fluid temperature was measured with an RTD in the table tank. Data from the dynamic pressure transducer was collected using a Wave Book high rate data acquisition system. A second PCI-1200 card collected data from the other transducers. The three systems were triggered externally by a momentary switch activated by the motion of the mill table and simultaneously started when the cutter had traversed 1 inch of the rock surface. The PCI cards sampled for four seconds at a rate of 4000 samples/channel/sec. The Wave Book sampled for one-half second at a rate of 500,000 samples/sec. A LabView© based computer program was used to configure, acquire, display, and store the data along with other parameters pertinent to the linear cutting process.

3.3 Test Matrix Design

The laboratory testing was divided into phases as summarized in *Table 10*. The first phase (II-A) consisted of testing in the LCTF without jet augmentation to establish the baseline forces for one, two, and three cutters. Then pressure augmentation was added to address low-pressure conditions (II-B & II-C). We had also planned to address medium

pressure conditions (II-D) followed by interaction testing corresponding to the Phase I nominal nozzle configuration (II-E & II-F). Finally, high-pressure conditions (II-G & II-H) were to be addressed. However, as stated, budget restrictions limited the scope of the project. Testing was limited to Phases II-A, II-B, & II-C.

Table 10: Phase II Work Breakdown.

Phase	Orifice Size (#/32 inches)	Description	Parameter Variation
II-A	-	Baseline evaluation	Depth of cut
II-B	12	Large diameter	Low p, high q
II-C	10	Large diameter	Low p, high q
II-D	8	Medium diameter	Nominal p, Nominal q
II-E	6.2	Medium diameter	Nominal p, Nominal q
II-F	6.2	Medium diameter	Interaction testing
II-G	5	Small diameter	High p, low q
II-H	4	Small diameter	High p, low q

Within each phase, various tests were to be conducted with a parameter varied to determine its effect. This results in the unabridged test matrix shown in *Table 11*.

Table 11: Phase II Testing Matrix.

Administrative Summary					Cutter Configuration				Nozzle Configuration		Cutter/Nozzle Interaction				Rock
Test		*Purpose*	*Parameter Variation*	*Description*	*Cutter Type*	*N Cutters*	*doc (in) [2]*	*Linear Speed*	*Orifice No.*	*Pressure Drop (psi)*	*Nozzle Standoff*	*Nozzle Lead*	*Nozzle Incl.*	*Nozzle Tilt*	*Rock Type*
II-A	1	Baseline	depth of cut	No Orifice or Feed Tube	GE	1	lo-hi	nom.	-	-	-	-	-	-	SWG
II-A	2	Baseline	depth of cut	No Orifice or Feed Tube	GE	2	lo-hi	nom.	-	-	-	-	-	-	SWG
II-A	3	Baseline	depth of cut	No Orifice or Feed Tube	GE	3	lo-hi	nom.	-	-	-	-	-	-	SWG
II-B	1	Large nozzle	low p, high q	Large nozzles w/Large FT	GE	1	lo-hi	nom.	12	2000	nom.	nom.	nom.	none	SWG
II-B	2	Large nozzle	low p, high q	Large nozzles w/Large FT	GE	2	lo-hi	nom.	12	2000	nom.	nom.	nom.	none	SWG
II-B	3	Large nozzle	low p, high q	Large nozzles w/Large FT	GE	3	lo-hi	nom.	12	2000	nom.	nom.	nom.	none	SWG
II-C	1	Large nozzle	low p, high q	Large nozzles w/Large FT	GE	1	lo-hi	nom.	10	3000	nom.	nom.	nom.	none	SWG
II-C	2	Large nozzle	low p, high q	Large nozzles w/Large FT	GE	2	lo-hi	nom.	10	3000	nom.	nom.	nom.	none	SWG
II-C	3	Large nozzle	low p, high q	Large nozzles w/Large FT	GE	3	lo-hi	nom.	10	3000	nom.	nom.	nom.	none	SWG
II-D	1	Medium nozzle	nom p, nom q	Medium nozzles w/Med FT	GE	1	lo-hi	nom.	8	4000	nom.	nom.	nom.	none	SWG
II-D	2	Medium nozzle	nom p, nom q	Medium nozzles w/Med FT	GE	2	lo-hi	nom.	8	4000	nom.	nom.	nom.	none	SWG
II-D	3	Medium nozzle	nom p, nom q	Medium nozzles w/Med FT	GE	3	lo-hi	nom.	8	4000	nom.	nom.	nom.	none	SWG
II-E	1	Medium nozzle	nom p, nom q	Medium nozzles w/Med FT	GE	1	lo-hi	nom.	6.2	5000	nom.	nom.	nom.	none	SWG
II-E	2	Medium nozzle	nom p, nom q	Medium nozzles w/Med FT	GE	2	lo-hi	nom.	6.2	5000	nom.	nom.	nom.	none	SWG
II-E	3	Medium nozzle	nom p, nom q	Medium nozzles w/Med FT	GE	3	lo-hi	nom.	6.2	5000	nom.	nom.	nom.	none	SWG
II-F	1	Nozzle geometry	nozzle/cutter interaction	Phase I Nozzles w/Med FT	GE	1	lo-hi	nom.	6.2	5000	min-max	min-max	min-max	min-max	SWG
II-F	2	Nozzle geometry	nozzle/cutter interaction	Phase I Nozzles w/Med FT	GE	1	lo-hi	nom.	6.2	5000	min-max	min-max	min-max	min-max	SWG
II-F	3	Nozzle geometry	nozzle/cutter interaction	Phase I Nozzles w/Med FT	GE	1	lo-hi	nom.	6.2	5000	min-max	min-max	min-max	min-max	SWG
II-G	1	Small nozzle	high p, low q	Small nozzles w/Small FT	GE	1	lo-hi	nom.	5	6000	nom.	nom.	nom.	none	SWG
II-G	2	Small nozzle	high p, low q	Small nozzles w/Small FT	GE	2	lo-hi	nom.	5	6000	nom.	nom.	nom.	none	SWG
II-G	3	Small nozzle	high p, low q	Small nozzles w/Small FT	GE	3	lo-hi	nom.	5	6000	nom.	nom.	nom.	none	SWG
II-H	1	Small nozzle	high p, low q	Small nozzles w/Small FT	GE	1	lo-hi	nom.	4	7000	nom.	nom.	nom.	none	SWG
II-H	2	Small nozzle	high p, low q	Small nozzles w/Small FT	GE	2	lo-hi	nom.	4	7000	nom.	nom.	nom.	none	SWG
II-H	3	Small nozzle	high p, low q	Small nozzles w/Small FT	GE	3	lo-hi	nom.	4	7000	nom.	nom.	nom.	none	SWG

Notes: 1. Depth of cut range is 0.010, 0.020, 0.040, 0.080
2. Nominal values are average position of test fixture.
3. Minimum-maximum values span range allowed by test fixture.
4. All testing is conducted using water.

3.4 Phase II Testing

With delivery of the high pressure pump (*Figure 67*), final assembly of the test system was completed. *Figure 68* shows an overview of the test system on the mill. The large feed tube with the 0.375" orifice and nozzle was installed in the vertical position. *Figure 69* is a closer view of the nozzle, cutter, and rock sample. Several tests were run with the nozzle positioned away from the rock surface to verify the operation of the pump and the data acquisition system, and to evaluate leak mitigation measures.

Figure 67: High pressure pump skid

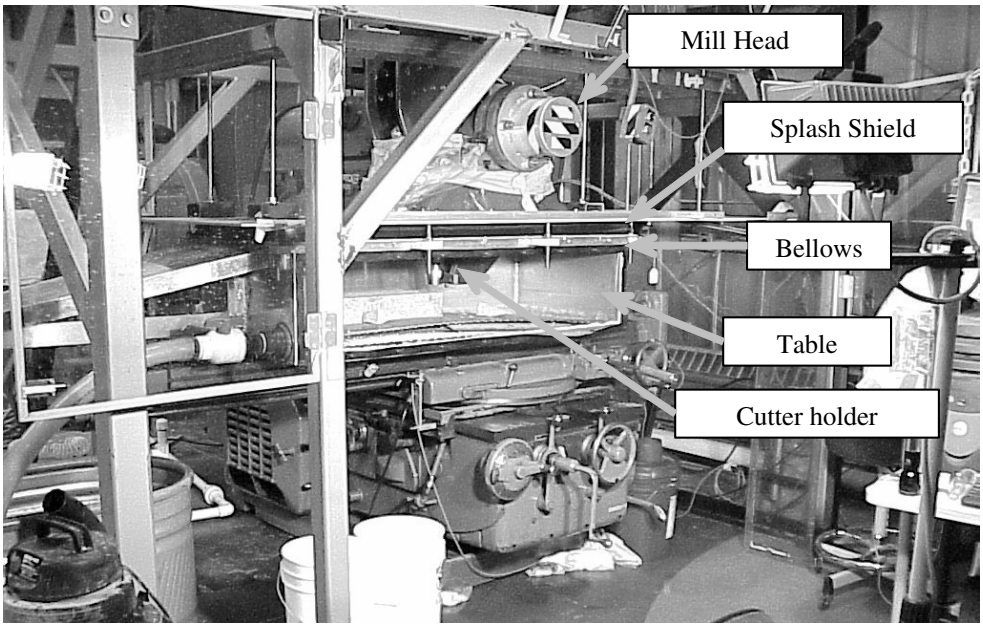

Figure 68: Phase II test system overview.

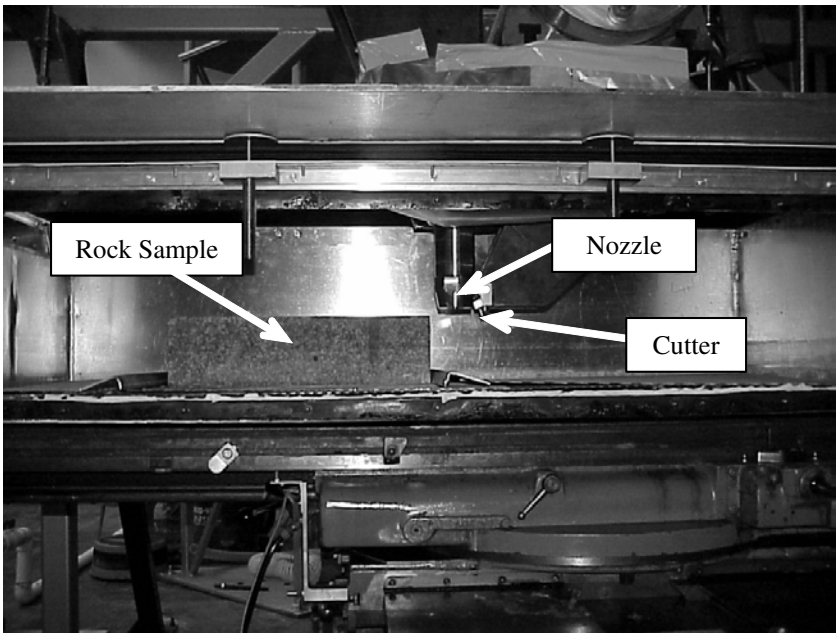

Figure 69: Detail view of cutter, nozzle, and rock sample.

The first test series attempting to make load measurements with pressurized water flow while cutting rock was discontinued when the rock sample separated from its mounting plate. We initially thought undercutting of the rock by the water jet at the edge of the rock/epoxy bond was the cause of the failure (*Figure 70*). When subsequent tests that attempted to shield the interface from the water jet did not eliminate the problem, another failure mode was recognized.

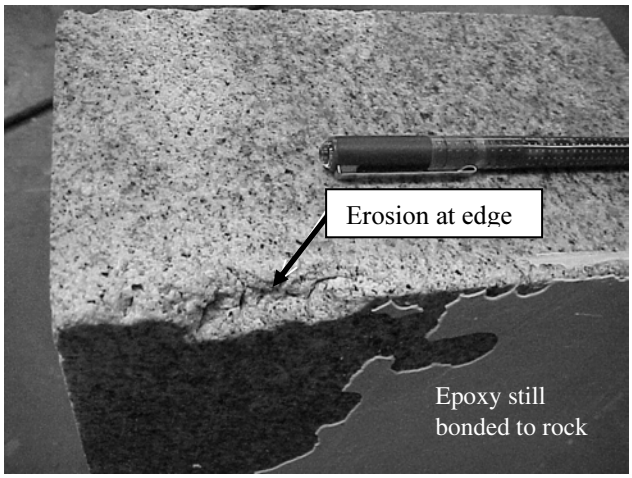

Figure 70: Under cutting of rock edge.

Welding of the aluminum table tank during fabrication created some waviness in the tank bottom. When the rock mounting plate which was secured at the long ends (*Figure 71*) was bolted to the mill table (sandwiching the tank bottom), the waviness deformed the mounting plate and caused localized bond failures that easily propagated through the brittle epoxy. The final mounting configuration was to secure the rock with concrete anchors drilled horizontally into the ends of the rock sample and using the epoxy as a filler (*Figure 72*).

Figure 71: Original rock mounting.

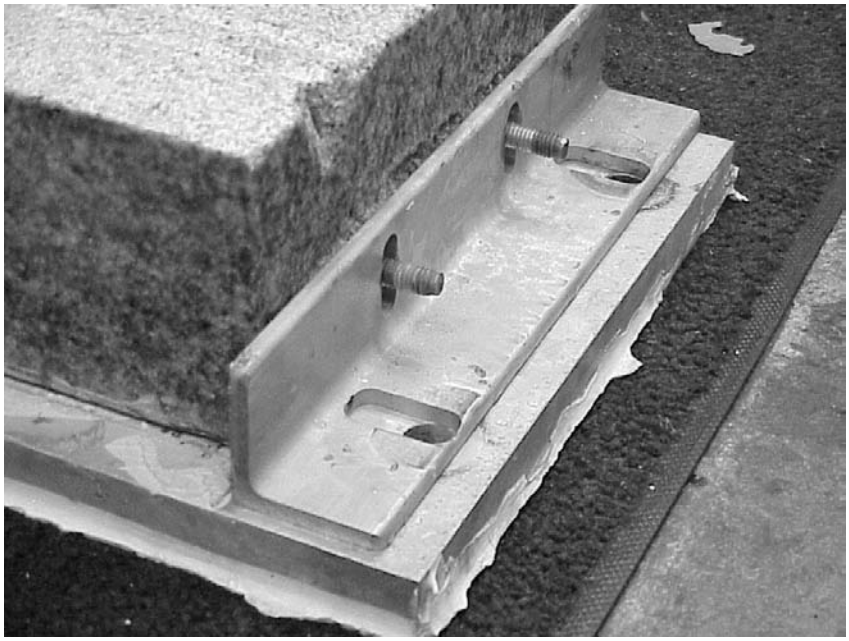

Figure 72: Concrete anchors in rock sample.

Simultaneous with the work on the rock mounting, a visual inspection of the cutter revealed considerable erosion of the cutter face. There was an almost symmetrical crescent shaped erosion pattern centered on the lower tip of the cutter, with the base metal exposed at the outside edge over about a twenty degree arc (Figure 73).

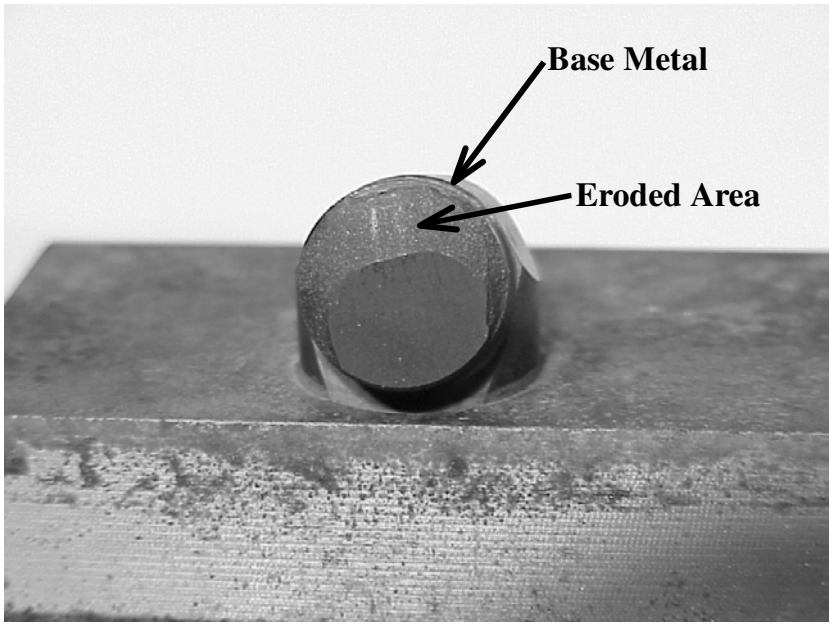

Figure 73: Cutter erosion

The cutter had been exposed to the water jet for only a short time, so the condition of the cutter was a concern. The erosion had occurred so rapidly, it would have been difficult to complete a full set of cuts without seeing a significant degradation in cutter performance. We had a limited number of cutters and there was not any additional production immediately scheduled. The decision was made to discontinue any testing with the nozzle in the vertical position and change the nozzle orientation to a 5^{o} tilt away from the cutter face. In this position, the water jet reflecting off the rock surface would be directed away from the cutter face. One consequence of using this orientation was that the physical configuration of the system limited the closest horizontal distance between the cutter and the nozzle to 7.5”; however, the cutter erosion was eliminated.

With the rock firmly held in place and a new cutter installed, load testing was resumed. The first series of tests was done using the 0.375” diameter orifice operating at 2000 psi with cutting depths of 0.01”, 0.02”, 0.04”, and 0.08”. Two passes on the rock were made at each depth of cut. A two-inch space was maintained between passes as the cutter was repositioned across the rock. This allowed four passes with the single cutter before the rock face had to be resurfaced (fewer for the multi-cutter fixtures). For some test series, additional passes were made at 0 depth of cut to obtain values for the load cell offsets. These tests were followed by tests with the two and three-cutter holders.

Two other test series were conducted with the same cutting depths and cutter holders. The first test series was added to measure the load reductions when a non-cavitating nozzle of the same diameter was used at the same pressure. The second was done with the rock submerged in water but with no flow. This test provided the baseline loads for comparison with all the other tests.

When the nozzle was changed to the 0.3125" diameter and the test pressure increased to 3000 psi, cutter loads began varying between tests at values that were not plausible. Some penetration loads were negative, indicating that the cutter was pulled downward while cutting the rock. This of course was not a realistic result. We discovered that the load cell offsets would vary significantly depending on the cutter position when the system was at 3000 psi, presumably due to momentum effects from the high flow rate around the cutter holder assembly. We installed baffles to isolate the cutter holder from flow loads and made sure there were no components inadvertently loading the holder, but could find no mechanical cause for the offset variations. The solution entailed a small change to the test procedure.

The original procedure for testing had a manual reset of the load cell zero performed in conjunction with entering the test file name. When the program changed screens from the data entry page to the flow monitoring page, the pump would be brought to pressure and stabilized. Once the pressure was stable, the external trigger was armed and the mill table traverse was started. This procedure was used for all the testing at 2000 psi without any difficulties. The variations in the offset at 3000 psi were eliminated by performing another reset of the load cell just prior to arming the external trigger. The offsets became consistent with values from the previous tests (Appendix G).

3.5 Phase II Data Analysis

Each cutter test created a data file with seven data channels (x-axis load, y-axis load, z-axis load, table position, temperature, pressure, and flow) each with 112,000 readings (4 seconds at 4,000 readings /channel /second). These large record sizes made point-by-point comparisons cumbersome. Since we were interested in trends rather than absolute values, the average values calculated for each channel were used in the analysis. While a complete set of data (single, dual, and triple cutters, cavitating nozzle, non-cavitating nozzle, and no flow) was compiled for the 0.375' diameter orifice, time and funding limitations allowed for only single-cutter measurements with the 0.3125" diameter orifice. A summary of all the data is included in Appendix H. For this analysis, we use only the single cutter data. This is sufficient to establish the trend information necessary for the analysis.

For all the data presented here, the raw load averages were adjusted by subtracting an offset value corresponding to the test conditions (no flow, cavitating flow or non-cavitating flow, penetrating or drag load). Since none of the cutter sets had any side rake, y-axis loads were not evaluated.

The first set of graphs, Figures 74 and 75, shows penetrating (z-axis) and drag (x-axis) loads as a function of the nominal depth of cut (doc). The nominal depth of cut is used because cutting on a non-homogeneous material such as granite causes unpredictable variations in the actual depth of cut. *Figure 74* and *Figure 75* give the penetrating and drag forces, respectively, for the 0.375" orifice operating at 2000 psi. *Figure 76 and Figure 77* show the penetrating and drag forces, respectively, for the 0.3125" orifice operating at 3000 psi.

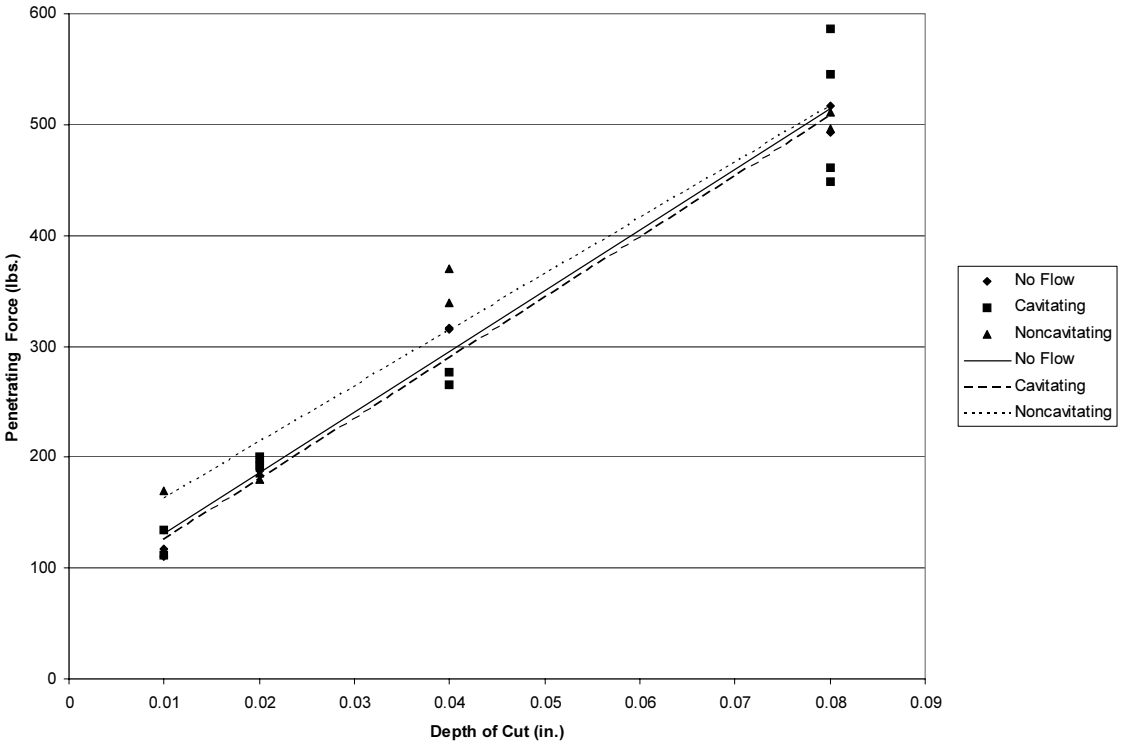

Figure 74: Penetrating forces for the 0.375" diameter orifice at 2000 psi.

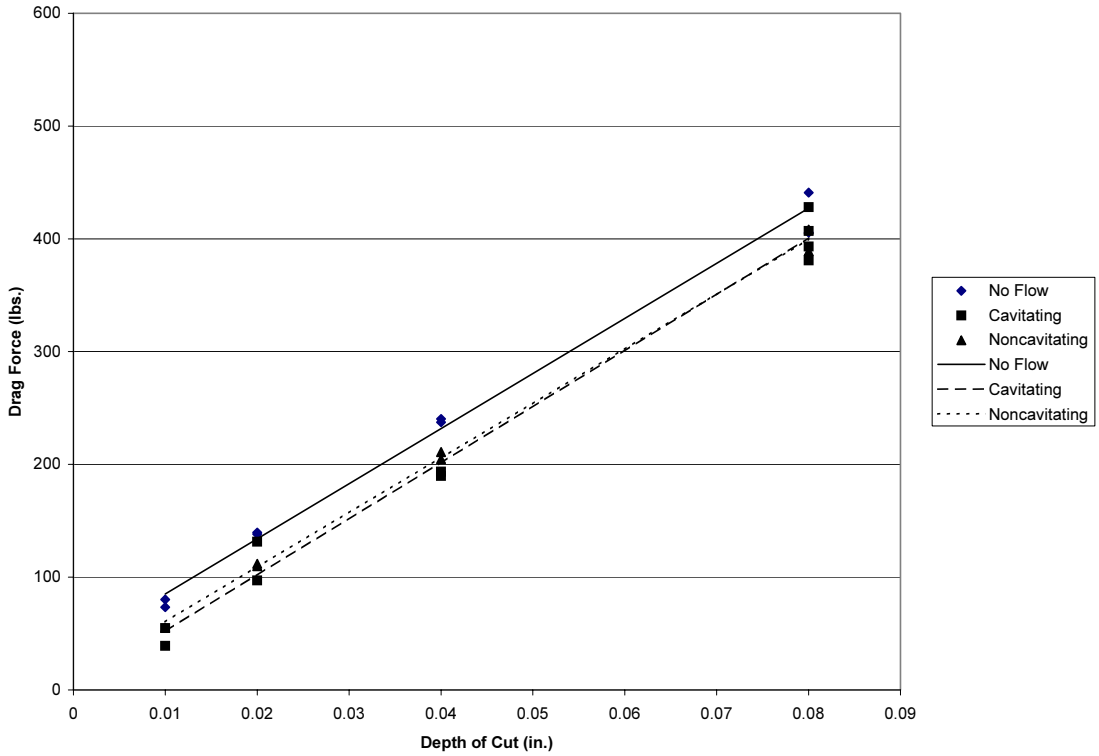

Figure 75: Drag forces for the 0.375" diameter orifice at 2000 psi.

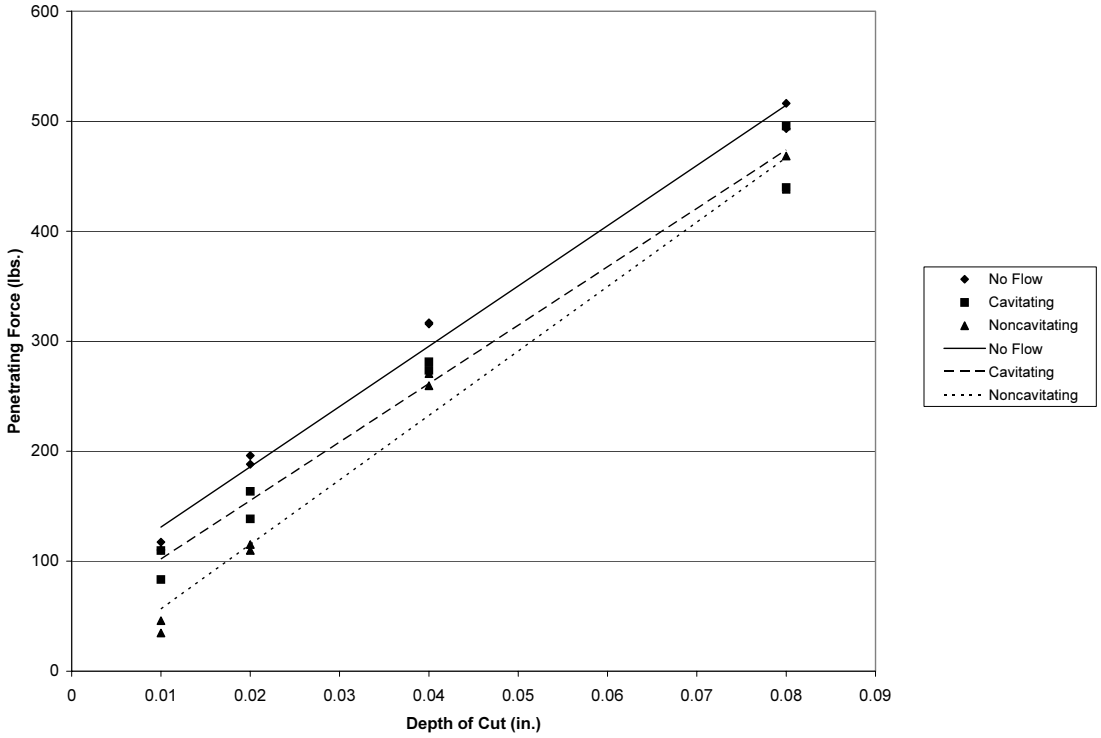

Figure 76: Penetrating forces for the 0.3125" diameter orifice at 3000 psi.

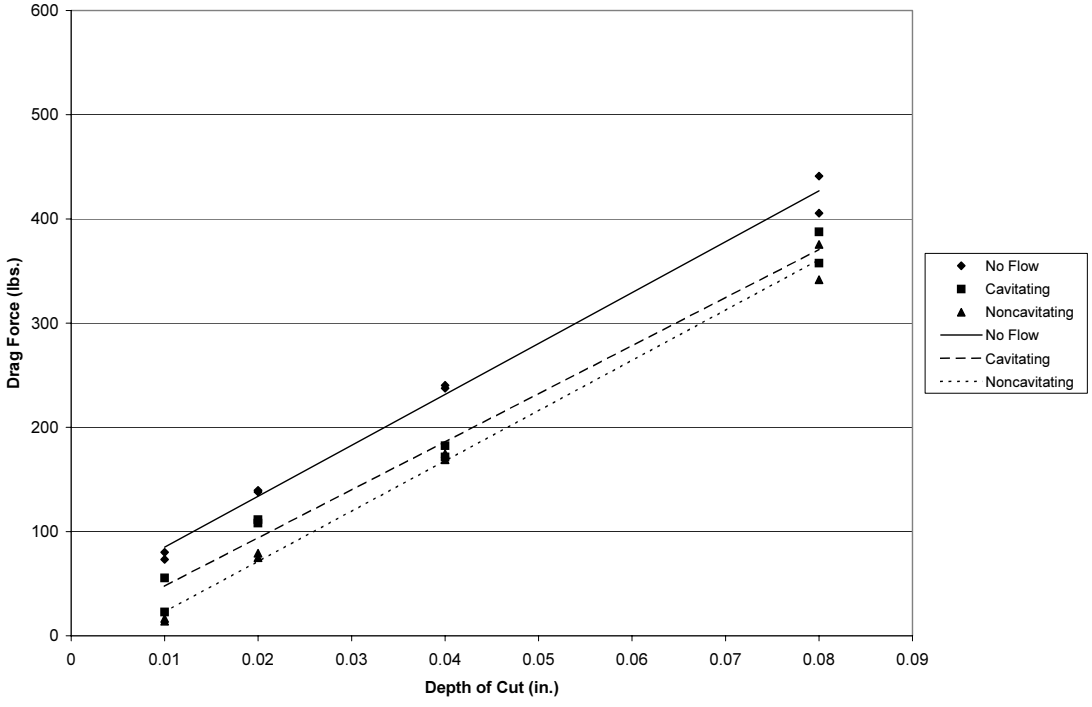

Figure 77: Drag forces for the 0.3125” diameter orifice at 3000 psi.

The penetrating forces in *Figure 74* are essentially the same for all three test conditions, while there seems to be some reduction in the drag forces (*Figure 75*) with high-pressure flow. There is not any trend in the data that indicates a difference between the cavitating and non-cavitating flows. Examination of the higher pressure data (*Figure 76 and Figure 77*) shows that the load reduction with the high-pressure flow is also evident. Again, there is no clear differentiation between cavitating and non-cavitating flow.

The next two figures quantify the trends in terms of a percentage reduction of loads from the baseline no flow tests.

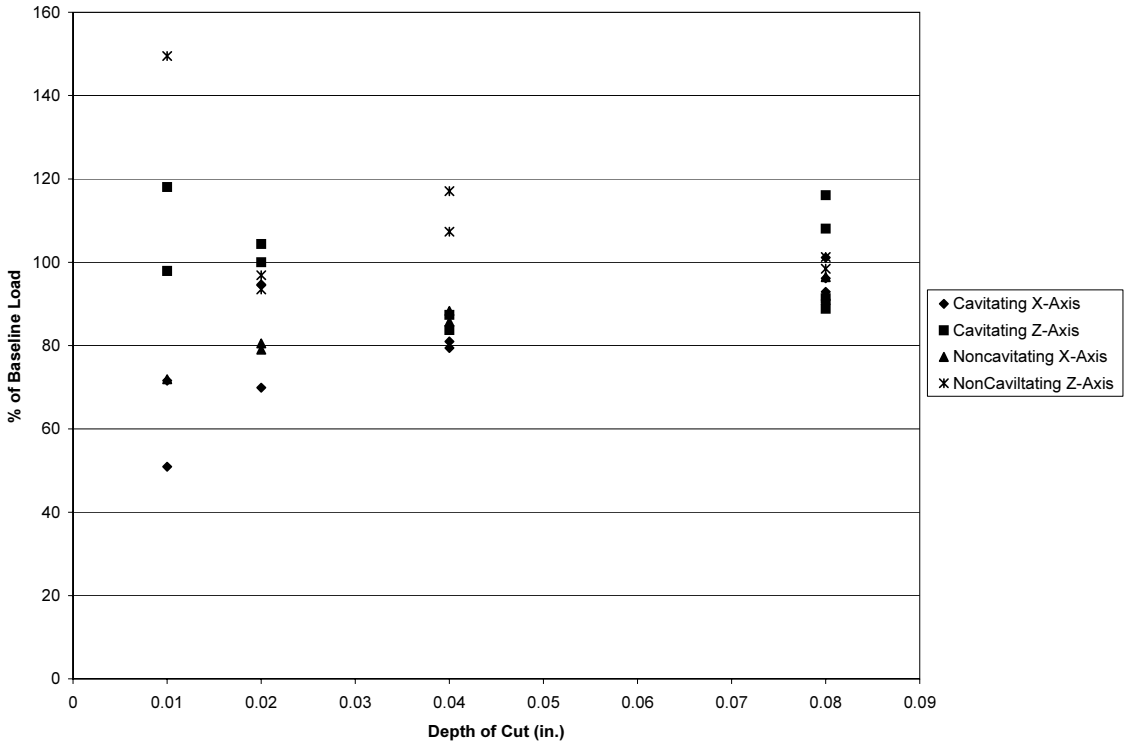

Figure 78: Percentage of no flow loads for the 0.375" diameter orifice at 2000 psi.

Figure 78 shows that when pressurized flows are introduced there is no apparent reduction in penetration loads and on the average a less than 10% reduction in the drag loads with no discernable difference between cavitating and non cavitating flow. Again at 3000 psi (*Figure 79*), there is an average 30% load reduction from the baseline loads with flow but no clear distinction as to which type of flow is more effective.

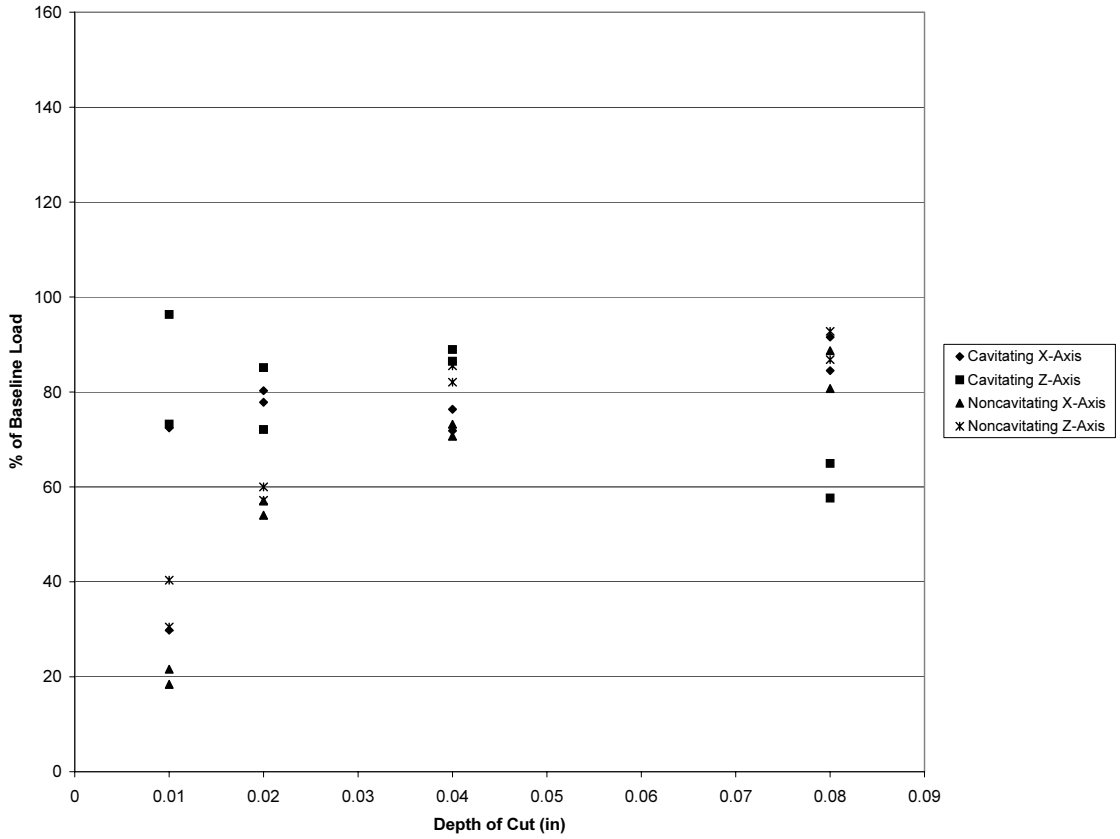

Figure 79: Percentage of no flow loads for the 0.3125" diameter orifice at 3000 psi.

Two additional tests were done that were not included in the original test plan. The first was an offshoot of the inclusion of the non-cavitating flow tests and was used to establish the proper functioning of the feed tube design. There was an audible difference between tests using the cavitating orifice when compared to the non-cavitating orifice. This was more of an anecdotal observation than measurement of cavitation. Placement of the dynamic pressure sensor was dictated by the physical layout of the system and it was not located in a position that was ideally suited for measurement of pressure pulsations created by the cavitation. When the nozzle was over the rock, there was too much noise on the signal to measure any cavitation. To establish the presence of cavitation, measurements were made with the nozzles in the vertical position with the discharge offset from the rock surface. A Fast Fourier Transform (FFT) was performed on the high frequency samples from the dynamic pressure sensor. The results indicated excitation in frequencies above 2000 Hz in the cavitating data that are not present in the non-cavitating data (*Figure 80* and *Figure 81*) thus confirming the existence of resonance in the organ pipe.

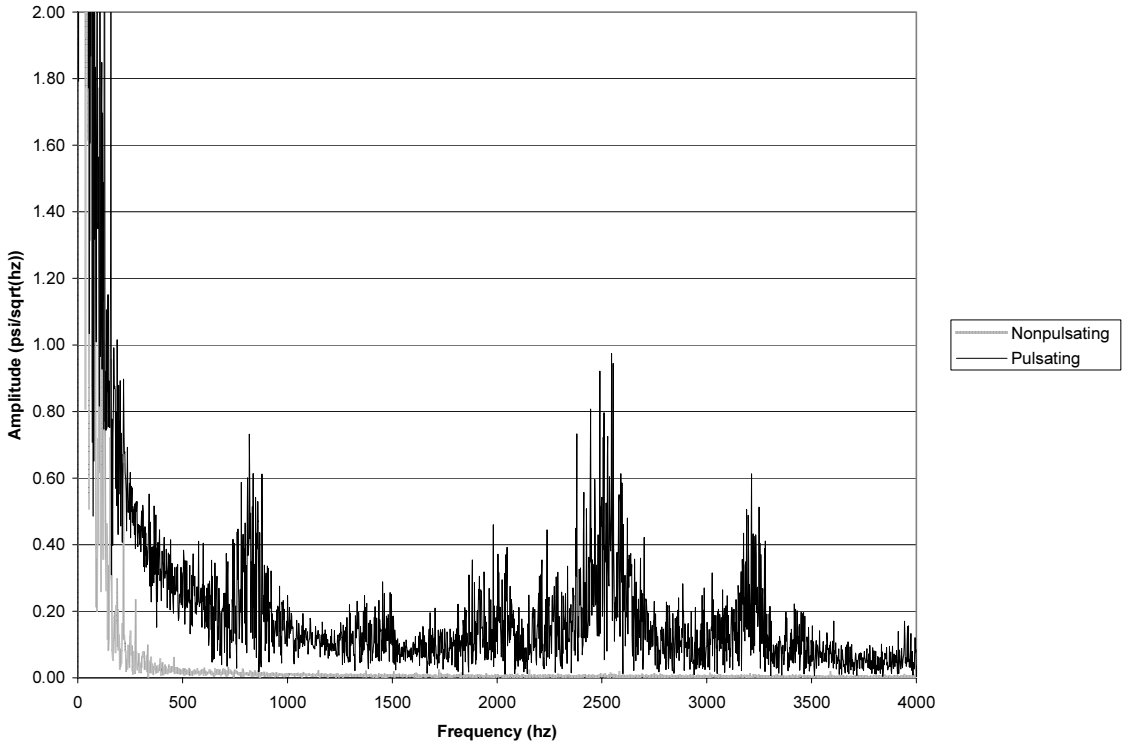

Figure 80: FFT results for 0.375" orifice at 2000 psi.

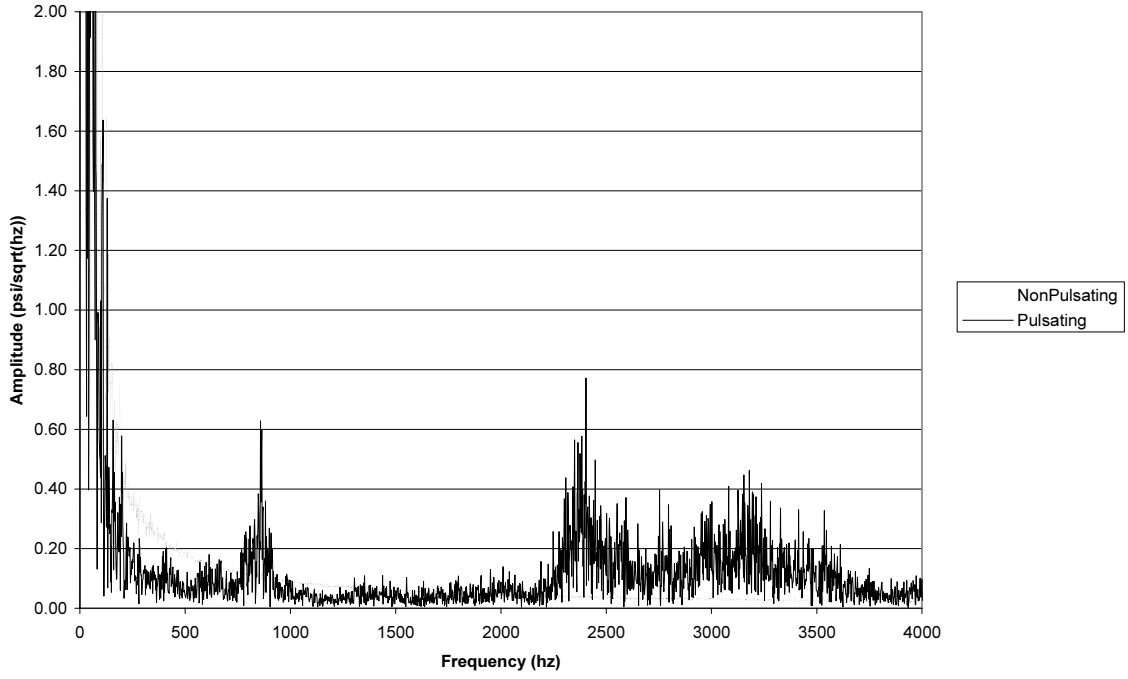

Figure 81: FFT results for 0.3125" orifice at 3000 psi.

The other test that was not included in the original plan was a simple, rather informal test. While operating at full pressure (3000 psi) the nozzle was placed in a stationary position above the rock for one minute. Since the timing of the nozzle operation could not be tightly controlled, the pump pressure tended to drift over a one-minute period, and the data acquisition program was not configured for this test. Hence the results were merely anecdotal. The non-cavitating jet eroded an area ≈0.5" in diameter and .013" to .019" deep, while the cavitating jet eroded an area ≈.38" in diameter and 0.035" to 0.05" deep. This suggests that the cavitating nozzle does generate higher loading but does not quantify it.

Like Glowka's data in Figure 3, this testing shows that cavitating jets operating at low pressures of 2000 psi do not affect cutting loads in Sierra White Granite; even at 3000 psi the cutting loads are not reduced significantly in this hard, non-porous rock. A disparity is noted between the results obtained by DynaFlow, presented in *Figure 6*, and those obtained here. Apparently the test procedures used here did not provide the resolution necessary to quantify the benefit of cavitating jet performance at the limited pressures and flows tested. One explanation is the standoff distance mandated by the test fixture used in the LCTF testing.

4. Fielding and Commercialization

4.1 Stepped vs. Single Nozzle Evaluation

DynaFlow conducted testing to address the stepped organ pipe concept, i.e. a nozzle, based upon multiple organ pipes in series. This work is summarized in Appendix F. The objective here was to extend the pressure operating range beyond the narrow band imposed by a single organ pipe. Although the stepped organ pipe gives a wider operating range, the peak value of the normalized pressure fluctuations is reduced. It is unclear which of the nozzle configurations (i.e., single or stepped) would be best suited for integration into a production bit to be used in field drilling. Although the single organ pipe has demonstrated greater potential for rock erosion, it requires operation within a narrow pressure band to maximize the cavitating action. Conversely, the stepped organ pipe configuration has exhibited a more uniform performance across the required operating pressure range yet offers smaller erosive potential when subject to the geometric constraints of the bit used in the Phase I demonstration. Since the single nozzle exhibits a stronger erosive potential, it was selected for the interaction study in Phase II as well. Future bit developments may consider a stepped organ pipe configuration or some other geometry. DynaFlow has conceived a concept for an organ pipe geometry that would self-tune based upon the pressure differential available at the bit, although this concept has not been developed as of this writing.

4.2 Direct Sintered Orifice Development

US Synthetic has successfully produced prototype orifices using the direct-sintered approach, resulting in a process that may be of significant benefit to this technology application. This work is summarized in Appendix I. Entrance and exit views of one of these prototype orifices are shown in *Figure 82*.

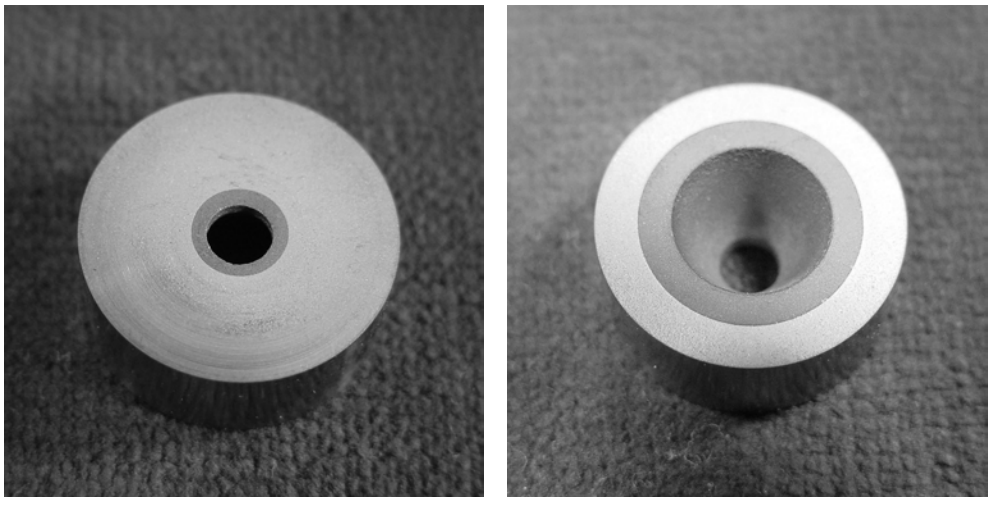

Figure 82: Direct Sintered orifice prototype – entrance and exit views.

5. Conclusions

This project has made progress toward meeting stated goals, and results to date demonstrate significant rate of penetration performance enhancements with this technology.

5.1 Summary

Full-scale testing in the Phase I demonstration was successful in achieving programmatic objectives: increased penetration rates in hard rock, reduced cutter forces as demonstrated by reduced WOB requirements, and enhanced performance at elevated well bore pressures. The increased penetration rates of 20-40 percent achieved by this technology, as shown in Figures 47-56, have significant value relative to drilling costs as seen by the full-scale test results at increased hydrostatic pressures. These gains are available by no substantial changes to the drilling approach but merely through modified bit design. The Phase I proof of concept demonstration has clearly proven the value-added contribution of resonating cavitating nozzles interacting with the rock reduction process.

This demonstration testing has shown that structured cavitating jets add benefit at depth. They are effective in increasing penetration rate in rock even with negligible porosity and permeability. While the Phase II cutter testing showed indiscernible cutting force reductions at the lower pressure ranges (2000-3000 psi) addressed, it is still expected that a bit with passively pulsating-cavitating nozzles would outperform a bit without them in this pressure range considering the effects of down hole cleaning introduced by the Stratojets®. Unfortunately, the Phase II results are inconclusive since funding restrictions limited this phase of the research.

One scenario for deployment is to manufacture a bit that includes organ pipes and has the capability to incorporate enhanced nozzles, yet not necessarily deploy the bit with the enhanced nozzles. The design of the bit is not significantly different and the cost to produce it in this way should not be much greater. This provides the capability for a driller to install enhanced nozzles at his discretion to penetrate a particular formation or to increase ROP in response to other drilling requirements.

Figure 21 suggests the higher ROP available with jet augmentation will not necessarily result in a reduction in the life of the bit. The Phase I bit analysis indicates it will have the same bit life available at twice the ROP. As with conventional bit design, tradeoffs exist between bit life and penetration rate. These should be appropriately balanced when future generation bits are developed.

A significant accomplishment in this project has been the development of orifices fabricated from tungsten carbide supported polycrystalline diamond. Development of direct-sintered cavitation resistant orifices promises great potential for this project and for similar applications. It is anticipated that technology developments in this area will foster greater commercialization of these bit types.

5.2 Recommendations for Further Research

Using information from the developments described herein, the United States drilling industry is encouraged to adopt this technology and develop and test fieldable bits incorporating the best combination of parameters identified in this research. Unlike the Phase I bit development, wherein the bit development evolved from an existing bit, the next generation bit development should be an integrated approach to nozzle/cutting structure design to develop the overall configuration of the bit. This will allow the bit design to accommodate the necessary and favorable nozzle/cutter interaction parameters rather than be constrained by the design of an existing bit. As was done in Phase I, laboratory testing should be continued to investigate lower orifice pressure differentials (i.e., less than 3000 psi) to validate performance improvements that may be readily employed in the field using this technology. The bit design should incorporate an erosion-resistant technology for inclusion during manufacturing of the bit. Some additional research may be required in this area to resolve the issue of bit erosion.

Research should continue in the area of direct-sintered polycrystalline diamond orifices as these will reduce the actualized cost of this technology. Flow testing should be conducted on the direct-sintered polycrystalline diamond orifices to confirm their erosion resistance.

Finally, field testing of a prototype bit should be done to validate these improvements. While laboratory testing is of significant benefit, it does not fully characterize the dynamic events that can occur in the field.

5.3 Acknowledgements

The vision and inspiration of David Glowka in pursuing support for this work is gratefully acknowledged. The efforts of all personnel from the multi-company team are especially appreciated: DynaFlow, Security DBS, TerraTek, and US Synthetic. Special thanks to Alan Black and the drilling crew at TerraTek for completing the Phase I testing; Gordon Tibbits for procuring standard nozzles for testing the roller cone bit; and, Craig Ivie at Reed Hycalog for making the roller cone available for the testing in Sierra White Granite. The contributions of our fellow Sandians are greatly appreciated: José Gonzales and Doug Abrams in the Sandia machine shop, for successfully producing the Phase I nozzles; Elton Wright for an extra set of hands during the Phase I testing; George Staller, for completing the detailed design of the Phase II test fixtures; Pat Gronewald and John Gabaldon, for fabricating these fixtures and completing the requisite testing; T.J. Cook for his editorial contributions to this report; Jack Wise and Doug Drumheller for the editorial review; and many others who supported and contributed to the project.

This work was supported by Sandia National Laboratories, which is a multiprogram laboratory operated by Sandia Corporation, a Lockheed Martin Company, for the United States Department of Energy under Contract DE-AC04-94AL85000.

References

[1] Hart's Exploration & Production, Feb. 2001, "Shopping for the Right Bit," pp. 37-45.

[2] Hood, M.: "Cutting Strong Rock with a Drag Bit Assisted by High-Pressure Water Jets, "J. South African Inst. Min. and Metl., Nov 1976, pp. 97-90.

[3] Dubugnon, O,: "An Experimental Study of Water Assisted Drag Bit Cutting of Rocks," presented at 1st U.S. Water Jet Symp., Golden, CO, April 7-9, 1981.

[4] Glowka, D.A., "Development of a Method for Predicting the Performance and Wear of PDC Bits," Report SAND 86-1977, Sandia National Laboratories, Albuquerque, NM, September, 1986.

[5] Conn, A.F. and Radtke, R. P. "CAVIJET Augmented Deep-Hole Drilling Bits," *Transactions of ASME, Journal of Pressure Vessel Technology*," Vol. 100, No. 1, pp. 52-59, February 1978.

[6] Chahine, G.L., et. al., October 1987, "Internal and External Acoustics and Large Structures Dynamics of Cavitating Self-Resonating Water Jets," SAND86-7176.

[7] Chahine, G.L., and Johnson, V. E., Jr., 1985, "Mechanics and Applications of Self-Resonating Cavitating Jets," Proceedings of the Jets and Cavities International Symposium, pp. 21-33.

[8] Chahine, G. L., Kalumuck, K.M., and Frederick, G.S., 1995, "The Use of Self-Resonating Cavitating Water Jets for Rock Cutting, "Proceedings of the 8th American Water Jet Conference", pp. 765-778.

[9] Telephone conversation between D. Raymond and O. Matthews, 03/15/99.

[10] Email from O. Matthews to D. Glowka, 09/5/97.

[11] Email from K. Kalumuck to D. Raymond, 12/18/98.

[12] GE Superabrasives website: www.ge.com/superabrasives.

[13] Email from O. Matthews to D. Raymond, 05/20/1999.

[14] Telephone conversation between D. Raymond and O. Matthews, 05/21/1999.

[15] Telephone conversation between D. Raymond and K. Kalumuck, 05/24/1999.

[16] Telephone conversation between D. Raymond and O. Matthews, 06/2/1999.

[17] Email from O. Matthews to D. Raymond, 06/07/1999.

[18] Letter from O. Matthews, Security DBS, to D. Raymond, Sandia National Laboratories, 06/14/1999, Subject: Nozzle Design Transmittal.

[19] Email from O. Matthews to D. Raymond, 06/15/1999.

[20] Letter from O. Matthews, Security DBS, to D. Raymond, Sandia National Laboratories, 06/29/1999, Subject: Nozzle Design Transmittal.

[21] Email from O. Matthews to D. Raymond, 09/02/1999.

[22] Email from O. Matthews to D. Raymond, 12/11/2000.

[23] Detournay, E., Defourny, P., 1992, "A Phenomenological Model for the Drilling Action of Drag Bits," Int. J. Rock Mech. Min. Sci. & Geomech. Abstr., Vol. 29, No.1, pp. 13-23.

[24] Email from K. Kalumuck to D. Raymond, 08/20/2001.

[25] D. Raymond, 05/7/2003, "Test Plan: Mudjet-Augmented PDC Bit, Phase II, Nozzle/Cutter Interaction Testing."

This page intentionally left blank

Acronyms and Abbreviations

gpm - gallons per minute
ksi - thousands of pounds per square inch
LCTF - Linear Cutter Test Facility
psi - pounds per square inch
PDC - Polycrystalline Diamond Compact
PCD - Polycrystalline Diamond
PDCWEAR - A computer program developed at Sandia National Laboratories to predict integrated loads on a bit based upon an array of individual cutters
TOB - Torque on Bit
UCS - Unconfined Compressive Strength
WOB - Weight on Bit

Page intentionally left blank

Appendix A: DynaFlow Phase I Development Report, Letter Report 97008-1

Page intentionally left blank

Development of a STRATOJET® Cavitating Mud Jet Nozzle for Use in PDC Bits Operating at Conventional Rig Pressures

Letter Report 97008-1

November 1998

Work Performed for Sandia National Laboratory under Purchase Order No. E39452

This letter report summarizes work performed for Sandia National Laboratories as part of a project team comprising Sandia, DYNAFLOW, Security DBS and Terra Tek for "Development of a Mud Jet-Augmented PDC Bit for Use with Conventional Rig Pressures" [1].

It has been shown in the past that the use of water jets in conjunction with mechanical cutters can increase cutting rates and reduce forces on cutters [2-4] due to the ability of the jets to remove debris and pre-weaken rock. In addition, in the case of PDC bits for geothermal applications, the jets can serve to cool the cutter. The combination of these effects is to reduce the stress on the cutter thereby increasing its lifetime. The STRATOJET® self-resonating cavitating jet technology has been shown to be significantly more erosive than conventional jets in rock cutting under down-hole conditions. (See, for example, [5-7].) The present effort involved design and testing of a STRATOJET® for incorporation into a PDC test bit.

Experimental Setup

Experiments were conducted in DYNAFLOW's High Pressure Cell (HPC) capable of ambient pressures up to approximately 2600 psi. A photograph of the HPC is presented in Figure 1. The HPC is a cylindrical pressure vessel with inside dimensions of approximately 9.5 inch diameter and 28 inch length with three quartz view ports circumferentially spaced and located near its mid length. Constructed for studies of deep hole drilling with cavitating jets, it includes a rotating fixture in which rocks are placed and rotated at various speeds for cutting beneath the jet and a fixture which allows advancement of the rock towards the nozzle at a controlled rate thus enabling actual drilling. The rock surface being cut is visible in the view ports. Ambient pressure is adjusted and maintained by a choke plate which acts as a back pressure valve in the outflow line. The jet flow is driven by a Weatherford five piston positive displacement pump capable of up to 20 gpm at 10,000 psi or 11 gpm at 20,000 psi with a different head.

Nozzle acoustic resonance was assessed with the aid of two Piezotronics 101-A04 (5 mv/psi sensitivity) and one 102-A03 (0.5 mv/psi) pressure transducers used to measure the fluctuating component of the pressure. The transducers were positioned at three different locations. One was inserted in the HPC wall. Initially, one was fitted with a hard casing inserted through the cell and located immediately upstream of the organ pipe. However, we experienced a number of failures of the transducer. Initially, this involved failure of the casing weld to the sensor and of the connection between the sensor and the cable. Following each failure, the transducer was repaired by the vendor. Subsequently, however, we found that the pressure fluctuations were too intense and were overdriving the crystal causing a failure. At this point we abandoned use of

this transducer and, instead, utilized one located upstream of the nozzle in the feed tube just before entering the HPC. The output of the transducers were monitored with both a digital rms meter to obtain the root mean square value of the fluctuating pressure component, p', and with a frequency analyzer to ascertain the frequency content of the fluctuations and determine the peak (resonant) frequencies of the nozzles. These measurements were used to determine whether or not a particular self-resonating nozzle had achieved good acoustic resonance at the design operating conditions - an important factor in achieving good performance.

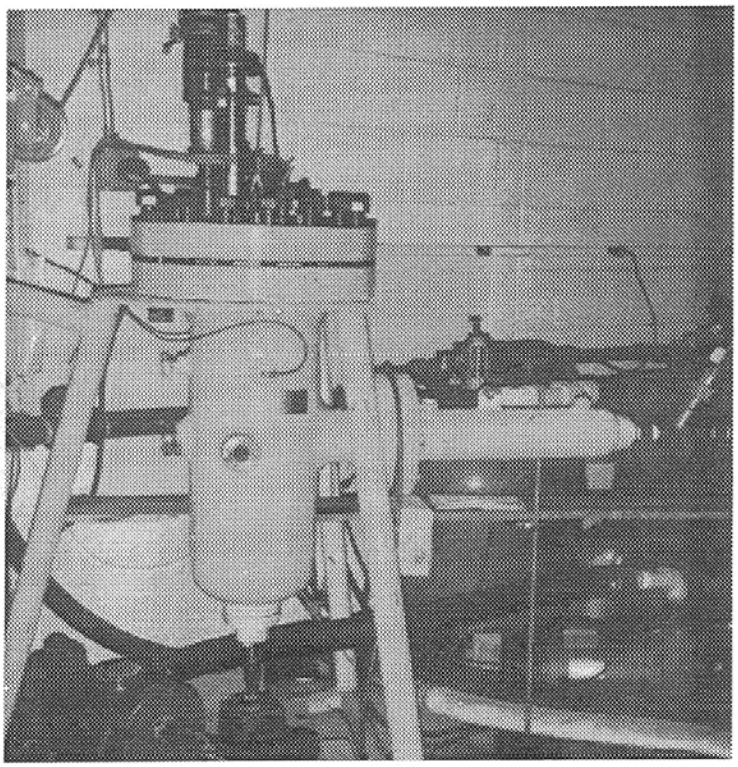

Figure 1. Photograph of High Pressure Cell (HPC).

Test Parameters

Important experimental variables include the nozzle pressure drop, ΔP, the ambient pressure, P_a, the standoff, and the translation velocity of the jet over the target, as well as details of the nozzle geometry. An important parameter to conserve between small scale and full scale is the cavitation number, σ, which is defined as:

$$\sigma = \frac{P_a - P_v}{1/2 \rho V^2}, \tag{1}$$

where P_v is the vapor pressure of the liquid, ρ is the liquid density, and V is the characteristic velocity, the jet mean velocity. In deep-hole drilling, the ambient pressure is hydrostatic and directly related to hole depth. In the case of high-pressure submerged jets used in deep-hole drilling, $P_a >> P_v$, and for well-designed nozzles $1/2\rho V^2$ may be approximated by the pressure drop, ΔP, across the nozzle. Thus

$$\sigma \approx \frac{P_a}{\Delta P}. \tag{2}$$

The cavitation number is an important parameter in determination of the occurrence and behavior of cavitation phenomena. Thus all testing should be conducted under conditions that match the value expected in practice.

Characterization Tests

A series of static cutting tests were conducted in aluminum (6061-T6) plates in which the plate was exposed to the jet for a specified period of time. Aluminum was selected for this work because, based on past experience, it provides a good measure of the performance of an erosive jet. Unlike rock, it is a very homogeneous material with negligible sample to sample variation in its properties. This removes questions of the influence of target sample property variation on nozzle performance and enables one to focus on obtaining a good nozzle design. It also simulates a very hard, nonporous rock, and is thus very useful as a development and screening tool.

The design conditions selected were ΔP = 5,000 psi and P_a = 1,200 psi resulting in a value of σ = 0.24. These represent full-scale pressures. Experiments were conducted, however, at reduced flow rates obtained by scaling the orifice and other nozzle dimensions to accommodate the test facilities available. Thus the majority of the testing was conducted with an orifice diameter, d_o = 0.09 in. producing an initial flow rate, Q, of approximately 12 gpm at ΔP = 5,000 psi. All tests were conducted with water as the working fluid. Previous work has demonstrated the ability to achieve acoustic resonance with drilling mud and has established the relations to scale the tests between the two media [8].

A special holder was utilized that enabled the nozzle assembly to be fabricated in several separate pieces so that these individual component geometries could be varied without remaking the entire nozzle assembly. As shown in Figure 2, the nozzle assembly itself consisted of a nozzle tip in the form of a disk in which are bored the cylindrical exit orifice of diameter, d_o, length, e, and a 21 degree conical expansion section of length, t. Upstream of the orifice are one or two organ pipe sections. The organ pipe immediately upstream of the orifice contains the contraction machined with a ball end mill. Otherwise, it has a constant diameter, d_1, and is of length, L_1. A second organ pipe of larger diameter, d_2, and length, L_2, could be located upstream of the first. This assembly is located in a pipe nipple that serves as the feed tube of diameter, d_f. The feed tube would be the analog of the waterway in the drill bit. Experiments were conducted in varying the lengths and diameters of the organ pipe and with one or two organ pipes.

One problem that arose was erosion of the nozzle tip in the orifice and expansion sections. This is not a new problem in that our experience has been that aggressively erosive nozzles at such

relatively high ambient pressures often experienced rapid self-erosion. The nozzle tips were made of 17-4 pH stainless steel. Nonetheless, they often experienced significant self-erosion after periods as little as 15 min. such that the flow and acoustic characteristics of the nozzle assembly would change resulting ultimately in a loss of resonance and an increase in flow. Examination of the nozzle tips showed significant pitting and gouging of the nozzle that in severe cases increased the orifice size. The result of this was that the useful test time of a given nozzle tip was severely limited. This resulted in the need to make multiple tips and, more importantly, introduced a large element of uncertainty in making comparison tests as to whether a result was due to an actual performance difference or due to the nozzle changing due to erosion. Thus only preliminary testing and screening could be conducted with the stainless steel tips.

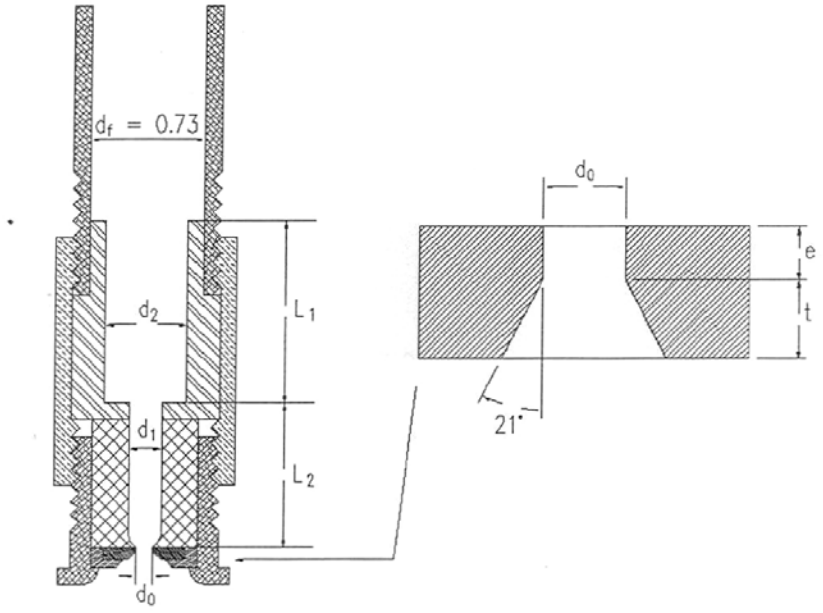

Figure 2. Sketch of the nozzle assembly holder that allowed change out of nozzle tip and variation in organ pipe configuration and dimensions. Also shown is an enlargement of the nozzle tip.

A search was made to find a more erosion resistant material. Our past experience was that tungsten carbide and sapphire each performed better than the stainless steel but did not last as long as desired or needed. Several sources of diamond coating or sleeves were investigated. A single diamond nozzle with a d_o = 0.06 in. was finally obtained and employed for a final set of tests. All other geometric dimensions were scaled to this orifice size.

Design Considerations

The nozzle design was constrained to fit into an 8.5 inch PDC bit whose geometry was provided by Security DBS. Geometric limitations are imposed by the maximum central waterway dimensions. The size and number of nozzles to incorporate into the test bit are constrained by the total flow limit of the pump available for the tests at Terra Tek – 300 gpm. The working fluid was specified to be drilling mud with a density of 10 lb/gal. The pressure, ΔP, was specified to be 5,000 psi. It was initially decided by Sandia to divide the available flow equally between three nozzles. For a typical STRATOJET® discharge coefficient of 0.69, this results in a nozzle size of d_o = 0.25 in. The work was conducted with this taken to be the nozzle diameter. The maximum bit waterway diameter was taken to be the maximum allowable value of the d_f. Initially, this waterway diameter was specified by Security DBS to be 2.0 in. This was later increased to 2.25 in. The tests were setup based on this initial value of 2.0 inch and the ratio d_f/d_o was matched between the test nozzle and the bit nozzle. Note that an increase in d_f can only improve the acoustic resonance. The tests conducted at DYNAFLOW were conducted at full-scale pressures, but at reduced geometric scale and with water instead of mud. Since the speed of sound in drilling mud is not significantly different than in water, the scaling involved linear dimensions, flow, and fluid density.

For a geometric scale factor λ, and a mud specific gravity γ, the scaling is expressed by the following relations where the subscript b refers to the prototype bit scale:

$$\lambda = \frac{d_o}{d_{o,b}} \tag{3}$$

$$d_i = d_{i,b} \times \lambda. \tag{4}$$

By conserving ΔP,

$$V = \frac{V_b}{\sqrt{\gamma}}. \tag{5}$$

To match the acoustic behavior, we match the jet Strouhal Number S_d, given as

$$S_d = \frac{f d_o}{V_j}, \tag{6}$$

where V_j is the jet exit velocity and f is the frequency of oscillation. This results in

$$L = L_b \times \lambda \times \sqrt{\gamma}\,. \tag{7}$$

The organ pipe length L is inversely proportional to the frequency at which it will resonate:

$$L \propto \frac{1}{f} = S_d \frac{V_j}{d_o} \propto \lambda\sqrt{\gamma}. \tag{8}$$

Most recently, Sandia requested that the design be set for 5 nozzles of d_o = 0.194 in. These relations are used in scaling the lab test design to the test bit design and were also employed when switching between the 0.09 in. and 0.06 in. diameter nozzles in the lab tests.

Results and Recommendations

Figure 3 presents results obtained from the 0.06 in. orifice diamond nozzle which did not erode during the tests. Shown are the measured rms pressure fluctuations, p', normalized on pressure drop, ΔP, vs. ΔP. As can be seen in this figure, the normalized rms pressure fluctuation amplitude exhibits a strong peak at about ΔP = 5,000 psi for the sing3le organ pipe case, but only a weak peak for the stepped organ pipe case. Note that the overall small values of $p'/\Delta P$ are due to the position of the transducer far from the orifice.

Exposure of an aluminum plate to the jets for 5 min. produced a cavity with a volume of 8 microliters for the stepped organ pipe case compared to a volume of 35 microliters for the single organ pipe case – a factor of over 4 difference in volume removal.

The geometric dimensions of the configurations tested that produced these results are listed in Table 1 together with the corresponding dimensions for earlier tests of these two configurations with the larger d_o= 0.09 in. stainless steel nozzles that rapidly eroded. Also shown in this table are the dimensions for the single organ pipe design scaled up according to Equations (3-7) above for inclusion into the drill bit for both the initially specified d_o = 0.25 in. and the newly specified d_o = 0.194 in.

	Organ Pipe	Fluid	d_o inches	d_1 inches	d_2 inches	d_f inches	L_1 inches	L_2 inches
Screening Tests	Single	Water	0.09	0.415	--	0.49	1.03	--
	Stepped	Water	0.09	0.315	0.415	0.49	1.03	1.03
Final Tests	Single	Water	0.06	0.278	--	0.73	0.69	--
	Stepped	Water	0.06	0.211	0.278	0.73	0.69	0.69
Full Scale	Single	Mud (γ=1.2)	0.25	1.16	--	$\geq$ 2.0	3.13	--
	Single	Mud (γ=1.2)	0.194	0.90	--	$\geq$ 1.6	2.43	

Table 1. Dimensions for STATOJET® nozzle configurations tested in the HPC and scaled up for inclusion in drill bit. (See Figure 2 for experimental setup.)

These results demonstrate that the single organ pipe design is superior to the stepped organ pipe design both in terms of the resonance achieved – as measured by rms pressure fluctuation – and in terms of the cutting performance in an aluminum plate. We would like to note that the tests were conducted with the geometry subjected to the constraints of the space available in the drill bit. We believe it possible that the stepped configuration could produce improved performance if these constraints were not present.

Based on these results, we recommend use of the single organ pipe design. Scaling this design to fit into the selected drill bit with an orifice size d_o = 0.194 in. results in the configuration

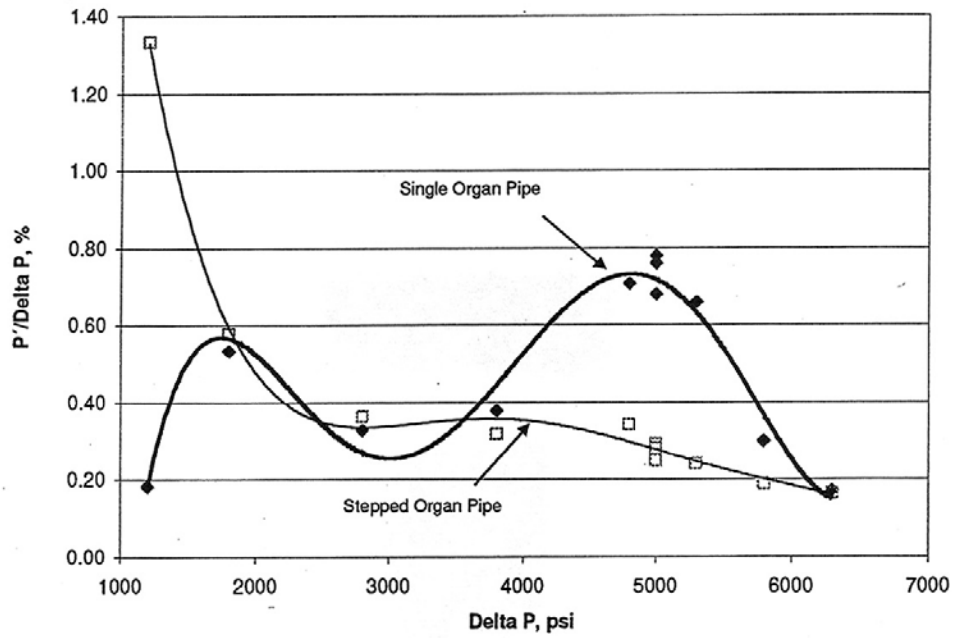

Figure 3. Comparison of normalized rms pressure fluctuations measured in the feed pipe far upstream of the nozzle as a function of pressure drop across the nozzle. The single organ pipe configuration is seen to exhibit a much stronger resonance than the stepped organ pipe at the design pressure of 5,000 psi.

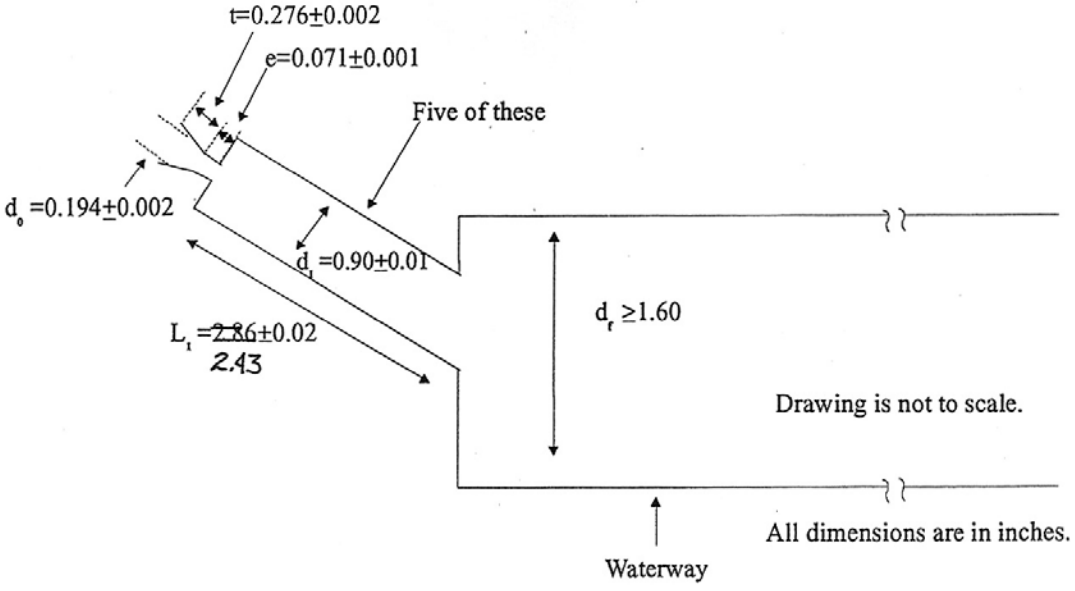

Figure 4. Sketch of selected STATOJET® nozzle and organ pipe design dimensions and location

presented in Figure 4. For simplicity and clarity, only a single nozzle and organ pipe are shown branching from the central waterway in this figure. In the actual bit, five such nozzle/organ pipe combinations would be fed from the waterway.

References

1. "Development of a Mud Jet-Augmented PDC Bit for Use with Conventional Rig Pressures," Sandia proposal to NADET, June 1996.
2. Hood, M., "Cutting Strong Rock with a Drag Bit Assisted by High Pressure Water Jets," J. S. African Inst. Min. and Metal., November 1976.
3. Glowka, D., "Development of a Method for Predicting the Performance and Wear of PDC Drill Bits," Sandia National Labs Rpt. SAND86-1745, September 1987.
4. Dubugnon, O., "An Experimental Study of Water Assisted Drag Bit Cutting of Rocks," Proceedings, 1st U. S. Water Jet Symp., Golden, CO, April 1981.
5. Chahine, G. L., and Johnson, V. E. Jr., "Mechanics and Applications of Self-Resonating Cavitating Jets," Intl. Symp. on Jets and Cavities, ASME, WAM, Miami, FL, November 1985.
6. Chahine, G. L., Kalumuck, K.M., and Frederick, G. S., "Cavitating Water Jets for Deep Hole Drilling in Hard Rock," Proceedings, 8th American Water Jet Conference, Houston, TX, August 1995.
7. Chahine G. L., Liu, H. L., Johnson V.E. Jr., and Frederick G.S., "Development of a STRATOJET® Nozzle for Optimum Resonance in Drilling Mud," Tracor Hydronautics Technical Report 84004, August 1984.
8. Chahine, G. L., Johnson, V. E. Jr., Kalumuck, K.M., Perdue, T. O., Waxman, D. N., Frederick, G. S., and Watson, R. E., "Internal and External Acoustics and Large Structure Dynamics of Cavitating Self-Resonating Water Jets," Sandia National Laboratories, Albuquerque, NM, Contractor Report SAND86-7176, July 1987.

Appendix B: CMM Measurements of Phase I Orifices

Page intentionally left blank

DATE: Mar 03, 2000

MEASUREMENTS REPORT

SHEET 1 OF 1

PROJ. NO.	SERVICE ORDER NO.	LEAD ORG.	SUPPLIER	CITY
	17027		DAVID RAYMOND	SNLA

P. O.	ITEM NO.	REC. NO.	LOT NO.	LOT QUANTITY

NOMENCLATURE	DRAWING NO.	ISSUE	NO. PCS. MEASURED	NO. MEASUREMENTS COMPLETED
NOZZLE ORIFICE	MJAB001	B	5	

DESCRIPTION	OF PLAC	DWG. LOC.	DRAWING DIMENSION	TOLERANCE	1	2	3	4	5
HOLE DIAMETER	1		.194	± .001	.1943	.1942	.1941	.1943 .1955	.1949
CONE ANGLE	1		21°	± 0.5°	21.358° 21.364°	21.323° 21.324°	21.320° 21.331°	21.042°	21.366°
CONICITY	1				.0019	.0015	.0015	.0014	.0017
ANGLE	4		21°	± 0.5°	21.115° 21.698°	21.204° 21.491°	21.104° 21.492°		21.220° 21.394°
LINEAR	4		.071	± .001	.0707 .0735	.0703 .0730	.0701 .0716	.0666	.0687 .0739
OUTSIDE DIAMETER	1		.750	± .001	.7507	.7507	.7510	.7506	.7507
OVERALL HEIGHT	1		.347	± .001	.3450 .3455	.3474 .3487	.3475 .3479	.347	.3468 .3480
				#4	GROOVE IN CONE APPROX. .005" DEEP, RIDGE IN .194 DIA. HOLE APPROX. .0012"				
				#5	MATERIAL VOIDS, TOP IS APPROX. .001, BOTTOM IS APPROX. .003.				

MEASURING EQUIPMENT	CALIB. EXP. DATE
ZEISS CMM UPMC550 S679233	8-19-00

UNITS TO SPEC.	REWORK IN SHOP	APPROVAL	MEASUREMENTS BY	DELIVERED TO	LETTER REQUESTED
					REJECTION
UNITS NOT TO SPEC.	REJECT TO MFG.	NAME	NAME E. J. BARRERAS		PROTEST
	ACCEPTED	ORG.	ORG. 1486-1		NONE

Page intentionally left blank

Appendix C: CMM Measurements of Phase I Bit

Page intentionally left blank

DATE: Nov 30,2000

MEASUREMENTS REPORT

SHEET 1 OF 7

PROJ. NO.	SERVICE ORDER NO.	LEAD ORG.	SUPPLIER	CITY
Mudjet-Augmented PDC Bit			D. RAYMOND ORG. 6211	SNLA

P. O.	ITEM NO.	REC. NO.	LOT NO.	LOT QUANTITY
				1

NOMENCLATURE	DRAWING NO.	ISSUE	NO. PCS. MEASURED	NO. MEASUREMENTS COMPLETED
PDC BIT	PER INSTRUCTION		1	PARTIAL

DESCRIPTION	OF PLCS.	DWG. LOC.	DRAWING DIMENSION	TOLERANCE	X	Y	Z	Ø	FACE ANGLE
LOCATION @ INTERSECTION OF CYLINDER AND FACE.				Blade #1					
Referenced to: Flat @ Top of thread. (Z). Copper cylinder. (X-Y). Stamped Flat on cyl. (Rotation).				1	.302	.263	15.574	.750	ZY: 19.569 XY: -32.854
				3	.968	.699	15.922	.748	ZY: 15.031 XY: -35.457
				6A	1.584	1.036	16.326	.523	ZY: 18.590 XY: -30.194
				8A	2.144	1.394	16.278	.528	ZY: 16.289 XY: -22.341
				10A	2.605	1.666	15.944	.528	ZY: 8.204 XY: -11.383
				12A	3.040	1.821	15.474	.533	ZY: 8.193 XY: -11.434
				14A	3.411	1.841	14.913	.530	ZY: 5.216 XY: -3.297
				16A	3.667	1.783	14.291	.530	ZY: .455 XY: -4.749
				18A	3.775	1.633	13.644	.531	ZY: -4.536 XY: 6.552
				20A					

UNITS TO SPEC.	REWORK IN SHOP	APPROVAL	MEASUREMENTS BY	DELIVERED TO	LETTER REQUESTED
			R. L. ALBERS		REJECTION
UNITS NOT TO SPEC.	REJECT TO MFG.	NAME	NAME		PROTEST
	ACCEPTED		1486-1		

MEASUREMENTS REPORT

DATE: Nov 30,2000 | SHEET: 2 OF 7

PROJ. NO.	SERVICE ORDER NO.	LEAD ORG.	SUPPLIER	CITY
Mudjet-Augmented PDC Bit			D. RAYMOND ORG. 6211	SNLA

P. O.	ITEM NO.	REC. NO.	LOT NO.	LOT QUANTITY
				1

NOMENCLATURE	DRAWING NO.	ISSUE	NO. PCS. MEASURED	NO. MEASUREMENTS COMPLETED
PDC BIT	PER INSTRUCTION		1	PARTIAL

DESCRIPTION	OF PLCS.	DWG. LOC.	DRAWING DIMENSION	TOLERANCE	X	Y	Z	Ø	FACE ANGLE
LOCATION @ INTERSECTION OF CYLINDER AND FACE.				Blade #2					
Referenced to: Flat @ Top of thread. (Z). Copper cylinder. (X-Y). Stamped Flat on cyl. (Rotation).				6B	-.902	1.655	16.326	.524	YfX: 25.253 ZfX: -16.692
				8C	-1.126	2.283	16.270	.527	YfX: 16.621 ZfX: -13.034
				10C	-1.262	2.819	15.953	.531	YfX: 7.587 ZfX: -14.075
				12C	-1.332	3.282	15.480	.534	YfX: -1.638 ZfX: -10.835
				14B	-1.285	3.649	14.918	.530	YfX: -6.900 ZfX: -5.550
				16C	-1.189	3.883	14.292	.534	YfX: -13.639 ZfX: .156
				18C	-1.029	3.969	13.648	.529	YfX: -15.380 ZfX: 4.792
				20C					

UNITS TO SPEC.	REWORK IN SHOP	APPROVAL	MEASUREMENTS BY	DELIVERED TO	LETTER REQUESTED
			R. L. ALBERS		REJECTION
UNITS NOT TO SPEC.	REJECT TO MFG.	NAME	NAME		PROTEST
	ACCEPTED		1486-1		

DATE: Nov 30,2000

MEASUREMENTS REPORT

SHEET 3 OF 7

PROJ. NO.	SERVICE ORDER NO.	LEAD ORG.	SUPPLIER	CITY
Mudjet-Augmented PDC Bit			D. RAYMOND ORG. 6211	SNLA

P. O.	ITEM NO.	REC. NO.	LOT NO.	LOT QUANTITY
				1

NOMENCLATURE	DRAWING NO.	ISSUE	NO. PCS. MEASURED	NO. MEASUREMENTS COMPLETED
PDC BIT	PER INSTRUCTION		1	PARTIAL

DESCRIPTION	OF PLCS.	DWG. LOC.	DRAWING DIMENSION	TOLERANCE	X	Y	Z	Ø	FACE ANGLE
LOCATION @ INTERSECTION OF CYLINDER AND FACE.				Blade #3					
Referenced to: Flat @ Top of thread. (Z). Copper cylinder. (X-Y). Stamped Flat on cyl. (Rotation).				2	-.738	-.276	15.760	.749	ZY: -21.796 XY: -18.062
				4	-1.513	-.401	16.108	.752	ZY: -20.666 XY: -14.868
				7A	-2.221	-.440	16.342	.526	ZY: -15.030 XY: -3.757
				9A	-2.810	-.440	16.124	.529	ZY: -10.411 XY: 2.909
				11A	-3.319	-.390	15.724	.533	ZY: -10.799 XY: 13.076
				13A	-3.714	-.304	15.198	.529	ZY: -2.907 XY: -5.697
				15	-3.984	-.144	14.603	.530	ZY: -2.410 XY: -2.047
				17A	-4.108	.030	13.966	.532	ZY: -1.645 XY: 3.429
				19A					

UNITS TO SPEC.	REWORK IN SHOP	APPROVAL	MEASUREMENTS BY	DELIVERED TO	LETTER REQUESTED
			R. L. ALBERS		REJECTION
UNITS NOT TO SPEC.	REJECT TO MFG.	NAME	NAME		PROTEST
	ACCEPTED		1486-1		

DATE: Nov 30,2000

MEASUREMENTS REPORT

SHEET 4 OF 7

PROJ. NO.	SERVICE ORDER NO.	LEAD ORG.	SUPPLIER	CITY
Mudjet-Augmented PDC Bit			D. RAYMOND ORG. 6211	SNLA

P. O.	ITEM NO.	REC. NO.	LOT NO.	LOT QUANTITY
				1

NOMENCLATURE	DRAWING NO.	ISSUE	NO. PCS. MEASURED	NO. MEASUREMENTS COMPLETED
PDC BIT	PER INSTRUCTION		1	PARTIAL

DESCRIPTION	OF PLCS.	DWG. LOC.	DRAWING DIMENSION	TOLERANCE	X	Y	Z	Ø	FACE ANGLE
LOCATION @ INTERSECTION OF CYLINDER AND FACE.				Blade #4					
Referenced to: Flat @ Top of thread. (Z). Copper cylinder. (X-Y). Stamped Flat on cyl. (Rotation).				5	.372	-1.881	16.335	.523	Y/X: 7.737 Z/X: 21.416
				8B	.417	-2.542	16.265	.528	Y/X: -.628 Z/X: 13.025
				10B	.380	-3.088	15.935	.530	Y/X: -9.324 Z/X: 13.158
				12B	.305	-3.552	15.465	.530	Y/X: -15.611 Z/X: 8.784
				13C	.158	-3.880	14.898	.530	Y/X: -18.687 Z/X: 3.065
				16B	-.007	-4.080	14.277	.528	Y/X: -30.260 Z/X: -.417
				18B	-.179	-4.117	13.633	.535	Y/X: -33.042 Z/X: -5.070
				20B					

UNITS TO SPEC.	REWORK IN SHOP	APPROVAL	MEASUREMENTS BY	DELIVERED TO	LETTER REQUESTED
			R. L. ALBERS		REJECTION
UNITS NOT TO SPEC.	REJECT TO MFG.	NAME	NAME		PROTEST
	ACCEPTED		1486-1		

DATE: Nov 30,2000

MEASUREMENTS REPORT

SHEET 5 OF 7

PROJ. NO.	SERVICE ORDER NO.	LEAD ORG.	SUPPLIER	CITY
Mudjet-Augmented PDC Bit			D. RAYMOND ORG. 6211	SNLA

P. O.	ITEM NO.	REC. NO.	LOT NO.	LOT QUANTITY
				1

NOMENCLATURE	DRAWING NO.	ISSUE	NO. PCS. MEASURED	NO. MEASUREMENTS COMPLETED
PDC BIT	PER INSTRUCTION		1	PARTIAL

DESCRIPTION	OF PLCS.	DWG. LOC.	DRAWING DIMENSION	TOLERANCE	X	Y	Z	Ø	FACE ANGLE
LOCATION @ INTERSECTION OF CYLINDER AND FACE.				Blade #5					
Referenced to: Flat @ Top of thread. (Z). Copper cylinder. (X-Y). Stamped Flat on cyl. (Rotation).				7B	2.106	-.845	16.346	.529	ZfY: 22.234 XfY: 28.683
				9B	2.619	-1.140	16.129	.529	ZfY: 14.713 XfY: 35.680
				11B	3.017	-1.454	15.723	.530	YfX: 15.614 ZfX: 44.608
				13B	3.308	-1.735	15.196	.530	YfX: 41.228 ZfX: 7.985
				14C	3.452	-1.997	14.592	.531	YfX: 39.015 ZfX: .537
				17B	3.465	-2.232	13.965	.531	YfX: 25.461 ZfX: -3.180
				19B					

UNITS TO SPEC.	REWORK IN SHOP	APPROVAL	MEASUREMENTS BY	DELIVERED TO	LETTER REQUESTED
			R. L. ALBERS		REJECTION
UNITS NOT TO SPEC.	REJECT TO MFG.	NAME	NAME		PROTEST
	ACCEPTED		1486-1		

DATE: Nov 30,2000

MEASUREMENTS REPORT

SHEET 6 OF 7

PROJ. NO.	SERVICE ORDER NO.	LEAD ORG.	SUPPLIER		CITY
Mudjet-Augmented PDC Bit			D. RAYMOND	ORG. 6211	SNLA

P. O.	ITEM NO.	REC. NO.	LOT NO.	LOT QUANTITY
				1

NOMENCLATURE	DRAWING NO.	ISSUE	NO. PCS. MEASURED	NO. MEASUREMENTS COMPLETED
PDC BIT	PER INSTRUCTION		1	PARTIAL

DESCRIPTION	OF PLCS.	DWG. LOC.	DRAWING DIMENSION	TOLERANCE	X	Y	Z	DELTA Z	ANGULAR ORIENTATION	DIAMETER	ANGLE OF FACE	Nozzle Center X	Nozzle Center Y	Nozzle Center Z
RELATION IN Z TO HIGHEST POINT OF NOZZLE TO CUTTER				N1	.478	1.261	16.172		69.24°	.889	X/Z: 8.115 Y/Z: 18.643	.660	1.622	16.023
Referenced to: Flat @ Top of thread. (Z). Copper cylinder. (X-Y). Stamped Flat on cyl. (Rotation).				2	-.792	-.119	16.100	-.072	171.46°					
				4	-1.547	-.218	16.451	.279	171.98°					
				N2	-1.155	.701	16.173		148.75°	.888	X/Z: -17.371 Y/Z: 11.123	-1.510	.918	16.022
				2	-.792	-.119	16.100	-.073	171.46°					
				4	-1.547	-.218	16.451	.278	171.98°					
				7B	2.048	-.918	16.592	.419	335.86°					
				7A	-2.240	-.339	16.588	.415	188.61°					
				N3	-.840	-1.306	16.133		237.25°	.890	X/Z: -14.385 Y/Z: -22.507	-1.033	-1.653	15.940
				1	.362	.174	15.926	-.207	25.67°					
				3	1.030	.647	16.282	.149	32.14°					
				6A	1.639	.995	16.570	.437	31.26°					
				6B	-.827	1.712	16.567	.434	115.78°					
				8C	-1.051	2.327	16.517	.384	114.31°					

UNITS TO SPEC.	REWORK IN SHOP	APPROVAL	MEASUREMENTS BY	DELIVERED TO	LETTER REQUESTED
			R. L. ALBERS		REJECTION
UNITS NOT TO SPEC.	REJECT TO MFG.	NAME			
	ACCEPTED		NAME		PROTEST

1486-1

MEASUREMENTS REPORT

DATE: Nov 30,2000 | SHEET 7 OF 7

PROJ. NO.	SERVICE ORDER NO.	LEAD ORG.	SUPPLIER		CITY
Mudjet-Augmented PDC Bit			D. RAYMOND	ORG. 6211	SNLA

P. O.	ITEM NO.	REC. NO.	LOT NO.	LOT QUANTITY
				1

NOMENCLATURE	DRAWING NO.	ISSUE	NO. PCS. MEASURED	NO. MEASUREMENTS COMPLETED
PDC BIT	PER INSTRUCTION		1	PARTIAL

DESCRIPTION	OF PLCS.	DWG. LOC.	DRAWING DIMENSION	TOLERANCE	X	Y	Z	DELTA Z	ANGULAR ORIENTATION	DIAMETER	ANGLE OF FACE	Nozzle Center X	Nozzle Center Y	Nozzle Center Z
RELATION IN Z TO HIGHEST POINT OF NOZZLE TO CUTTER				N4	.735	-1.124	16.194		-56.86°	.887	X/Z: 11.289 Y/Z: -16.863	.963	-1.467	16.045
Referenced to: Flat @ Top of thread. (Z). Copper cylinder. (X-Y). Stamped Flat on cyl. (Rotation).				1	.362	.174	15.926	-.268	25.67°					
				3	1.030	.647	16.282	.088	32.14°					
				6A	1.639	.995	16.570	.376	31.26°					
				6B	-.827	1.712	16.567	.373	115.78°					
				8C	-1.051	2.327	16.517	.323	114.31°					
				N5	1.566	.142	16.167		5.18°	.887	X/Z: 26.218 Y/Z: 2.062	1.959	.145	15.976
				6B	-.827	1.712	16.567	.400	115.78°					

UNITS TO SPEC.	REWORK IN SHOP	APPROVAL	MEASUREMENTS BY	DELIVERED TO	LETTER REQUESTED
			R. L. ALBERS		REJECTION
UNITS NOT TO SPEC.	REJECT TO MFG.	NAME	NAME		PROTEST
	ACCEPTED				

1486-1

Page intentionally left blank

Appendix D: Phase I Test Plan

Page intentionally left blank

Laboratory Testing of Prototype Bit

Laboratory drilling tests will be conducted to determine the penetration rate performance of the prototype jet-augmented PDC bit and to compare its performance with that of a current-technology PDC bit and a roller-cone bit. Although the primary focus of the tests will be the measurement of penetration rates, they will also reveal any tendency for rapid wear or mechanical damage of the bits when drilling in rock of hardness typical of geothermal environments. The tests will be conducted at atmospheric and elevated borehole pressures, to replicate the range of pressures encountered in geothermal drilling applications. Test materials and conditions have been chosen to permit comparison of results with public domain data [D1] previously obtained with a hard-rock roller cone bit drilling under the same conditions.

1) Test Facilities

TerraTek's Drill Rig and Wellbore Simulator will be used. The Drill Rig alone is used for atmospheric pressure drilling tests. Together they permit drilling experiments to be conducted under simulated downhole conditions. They are illustrated in *Figure 41*. Key aspects of their performance specifications are summarized in *Table D1* and *Table D2* below.

Table D1: Drill Rig Performance Specifications.

Parameter	Maximum Capability
Stroke	6 ft
Rate of Penetration	180 ft/hr
Weight on Bit	375,000 lbs (lo-speed) 200,000 lbs (hi-speed)
Rotary Speed	400 rpm (lo-speed) 1000 rpm (hi-speed)
Torque	10,000 ft-lbs (lo-speed) 2,200 ft-lbs (hi-speed)
Mud Pumping Power	1,600 HP

The Drill Rig is a 35 foot tall, moveable gantry that can be positioned over various stations in the test hall for atmospheric or pressure drilling. The conventional electric powered rotary drive system will be used for these tests. A hydraulic servo-controlled, closed-loop feedback system is used to control the weight on bit at values set by the operator during the course of each test.

The Wellbore Simulator consists of a 23 inch inside diameter by 18 feet long pressure vessel with a working length of 7 feet and a certified working pressure of 20,000 psi. Rock samples of up to 17 ½ inch diameter and 5 feet length can be drilled with bits ranging up to 12 ¼ inch diameter. The rock samples can be subjected to independent confining pressure, overburden stress, pore pressure (in permeable rocks only), and wellbore pressure.

Rock samples are mounted between steel end caps and sealed in an elastomeric jacket. They are installed into and removed from the pressure vessel as part of the top sealing plug, thereby facilitating quick turn-around between tests.

Table D2: Wellbore Simulator Performance Specifications.

Parameter	Maximum Capability
Overburden Stress	20,000 psi
Confining Pressure	13,000 psi
Wellbore Pressure	10,000 psi
Pore Pressure	4,000 psi
Bit Diameter Range	6 1/8 to 12 ¼ inches
Mud Temperature	150° F

Confining pressure is applied by hydraulic fluid in the annulus between the jacketed rock sample and the pressure vessel wall. Overburden stress is generated by a ram, which acts on the base of the rock sample and pushes it against the upper seal plug and top closure. As these tests will be conducted in impermeable rock, no pore pressure will be applied to the rock samples.

The Drill Rig has a 1,600 HP triplex mud pump. This will be configured with special high-pressure fluid ends that can provide up to 180 gpm flow rate at delivery pressures of up to 15,000 psi. The output of this pump will be supplemented with rented high-pressure pumping units, to provide a flow rate of 300 gpm at the maximum anticipated delivery pressure of 9,000 psi.

The drilling fluid is pumped from the active tank through a swivel, down the drive shaft, through the bit, back up the drilled annulus and out of the Wellbore Simulator. It then flows through a mesh screen inside a large, pressurized cuttings catch vessel before passing through a choke and returning to the active tank. Wellbore pressure is created and controlled by the choke system downstream of the pressure vessel. Thus, the mud pump delivery pressure is the sum of the wellbore pressure, the bit pressure drop and the (usually small) frictional pressure losses through the circulating system pipe work.

The Rig has a PC-based data collection system, in addition to strip-chart and XY recorders. Data collected during each test consist of time, distance drilled, penetration rate, torque, weight on bit, rotary speed, borehole (wellbore) pressure, swivel (stand-pipe) pressure, overburden stress, confining pressure, mud pump delivery rate, and drilling fluid temperature. These are logged at approximately 1 Hz throughout each test.

After each test, a computer program is used to reduce the time-based data into a concise record consisting of one data set for each interval of steady drilling conditions. Each reduced data set contains: distance drilled, penetration rate, penetration per revolution, torque, weight on bit, rotary speed, borehole pressure, swivel (stand-pipe) pressure, drilling fluid flow rate, drilling fluid temperature,

overburden stress, confining pressure, mechanical horsepower, bit pressure drop, and bit hydraulic horsepower. The mechanical and hydraulic parameters are arithmetic averages over the interval.

2) Test Program

A total of five full-scale drilling tests will be performed. One test will be performed at atmospheric borehole pressure with each of the prototype jet-augmented PDC bit, a current-technology hard rock PDC bit, and a Smith F3 (IADC code 5-3-7) roller cone bit. High borehole pressure tests will also be conducted with the prototype jet-augmented PDC bit and the current technology hard-rock PDC bit. Penetration rate data are already available for the F3 roller cone bit operating at the borehole pressures to be used for these last two tests. *Table D3* summarizes the test program.

Table D3: Test Program.

Test #	Bit	Weights on Bit (klbs)	Rotary Speed (rpm)	Wellbore Pressure (psi)
1	Jet-augmented PDC	10, 20, 30	110	Atmospheric
2	Conventional PDC	10, 20, 30	110	Atmospheric
3	Roller Cone	20, 40, 60	110	Atmospheric
4	Jet-augmented PDC	10, 20, 30	110	2,000 & 4,000
5	Conventional PDC	10, 20, 30	110	2,000 & 4,000
All Tests				
Rock:	Crab Orchard sandstone			
Drilling Fluid:	10 ppg water based mud			
Mud Flow Rate:	300 gpm			
Mud Temperature:	100° F			

The rock samples drilled will be Crab Orchard sandstone, which is a light gray, very fine-grained compact quartzose sandstone. This has 7% porosity, 0.005 mD gas permeability, and an unconfined compressive strength of 21,000 psi. The strength and abrasivity of this rock represent the extreme upper limit of those in which PDC bits can currently drill. They are, however, considered typical of the ranges that the jet-augmented PDC bit must be able to drill successfully if it is to have application for geothermal drilling.

Drilling fluids used in geothermal operations tend not to contain sophisticated shale stabilizing or fluid loss control polymers, nor to be highly weighted. The test will use a simple 10 ppg bentonite / water drilling mud.

Jet cavitation can be suppressed if the jet discharges into an elevated pressure environment. A key element of these tests is that a range of wellbore pressures should be used that replicate those likely to be encountered in geothermal drilling operations, in order to examine the effect of possible suppression of jet cavitation on the prototype PDC bit's performance. It is proposed that both atmospheric and high wellbore pressure tests be conducted with each bit. Each high-pressure test will

involve intervals drilled at two different wellbore pressures, representing shallow and deep geothermal drilling operations. The elevated wellbore pressures proposed are 2,000 and 4,000 psi. Together with the atmospheric tests, data will be collected under conditions that correspond to drilling at surface and at depths of the order of 4,500 and 9,000 feet.

A number of intervals will be drilled at each borehole pressure, under different operating parameters. Three levels of weight on bit, chosen to be representative of those that would be applied to the bit in field operations, will be used. The same rotary speed, 110 rpm, will be used throughout. This is the rotary speed used in the earlier roller cone bit tests. The weight on bit levels will be lower for the PDC bits than for the roller cone bit. The mud flow rate will be held constant for all tests, as will the mud temperature. A repeat interval will be drilled at the end of the test profile, under the same parameters as were used for the first interval in each sample, in order to delineate any loss of penetration rate performance due to rapid wear or damage to the bit during the test.

Reference

[D1] Walker, B.H., Black, A.D., Klauber, W.P., Little, T., and M. Khodaverdian, "Rollerbit Penetration Rate Response as a Function of Rock Properties and Well Depth", SPE paper no. 1560, presented at 1986 SPE Annual Technical Conference and Exhibition, New Orleans, LA (Oct 1986).

Appendix E: Phase I Testing – Test Summaries

Page intentionally left blank

DRILLING & COMPLETIONS LABORATORY

DATA FILE: SANDIA1A.UDS
CLIENT: SANDIA
TEST#: 1A

DATE: 12/ 2/00 TIME: 12:38:16
BIT: 8 1/2" REED HPSM
NOZZLES OR TFA: 3-10/32"

FILE: SANDIA1A.DRP PAGE: 1
MUD: 10.0 PPG WATER-BASE
ROCK: CRAB ORCHARD SANDSTONE #1

DATA PT. #	PENETRATION INTERVAL IN	R.O.P. FT/HR	R.O.P. IN/REV	TEMP DEG-F	TORQUE FT-LB	HP AT BIT HP	BIT WEIGHT LB	ROTARY SPEED RPM	FLOW RATE GPM	BORE PRESS. PSI	SWIVEL PRESS. PSI	SWIV-BORE PSI	HSI HP/SI	BACK PRESS. PSI	BORE-BACK PSI	CONFIN PRESS. PSI	OVRBUR STRESS PSI
1	2.3- 4.0	23.0	.0421	65.7	601	12.5	14948.	109	298	0	1547	1547	4.74	0	0	0	0
2	5.0- 8.0	64.1	.1178	66.7	1341	27.8	29932.	109	298	0	1556	1556	4.77	0	0	0	0
3	9.5-15.3	115.1	.2093	66.7	2287	47.9	44939.	110	299	0	1558	1558	4.78	0	0	0	0
4	16.6-19.1	66.5	.1212	66.8	1331	27.8	29928.	110	298	0	1560	1560	4.79	0	0	0	0
5	20.0-23.0	97.8	.1792	66.8	1950	40.5	39937.	109	299	0	1527	1527	4.69	0	0	0	0
6	23.5-27.9	49.3	.0894	67.5	1073	22.5	25126.	110	298	0	1537	1537	4.72	0	0	0	0

MUD PROPERTIES		
PROPERTIES	BEFORE	AFTER
600	21	21
300	11	10
200	8	8
100	7	6
6	4	4
3	3	3
P.V.	10	11
Y.P.	1	1
A.V.	10.5	10.5
GELS 10SEC/10MIN	3/4	3/5
WEIGHT	9.9+	9.9+
API FILTRATION	9.8	9.8
PH	9.5	9.5

COMMENTS:

TORQUE CORRECTED FOR SEAL FRICTION
FLOW RATE CORRECTED FOR PUMP EFFICIENCY
SWIVEL PRESSURE CORRECTED FOR LINE LOSS
ATMOSPHERIC DRILLING

DRILLING & COMPLETIONS LABORATORY

DATA FILE: SANDIA2.UDS
CLIENT: SANDIA
TEST#: 2

DATE: 12/ 4/00 TIME: 15:08:34
BIT: 8 1/2" SE1150
NOZZLES OR TFA: 5-8/32"

FILE: SNADIA2.DRP PAGE: 1
MUD: 10.0 PPG WATER-BASE
ROCK: CRAB ORCHARD SANDSTONE #1

DATA PT. #	PENETRATION INTERVAL IN	R.O.P. FT/HR	R.O.P. IN/REV	TEMP DEG-F	TORQUE FT-LB	HP AT BIT HP	BIT WEIGHT LB	ROTARY SPEED RPM	FLOW RATE GPM	BORE PRESS. PSI	SWIVEL PRESS. PSI	SWIV-BORE PSI	HSI HP/SI	BACK PRESS. PSI	BORE-BACK PSI	CONFIN PRESS. PSI	OVRBUR STRESS PSI
1	7.1-10.6	114.4	.2088	69.2	2244	46.8	10144.	110	300	0	1704	1704	5.25	0	0	0	0
2	10.8-10.9	8.2	.0149	71.2	304	6.4	2101.	110	298	0	1624	1624	4.98	0	0	0	0
3	11.2-11.7	15.1	.0274	71.2	626	13.1	4160.	110	298	0	1661	1661	5.10	0	0	0	0
4	12.1-13.2	29.9	.0542	71.2	1069	22.5	6150.	110	299	0	1712	1712	5.26	0	0	0	0
5	13.9-16.0	60.0	.1089	71.8	1609	33.7	8136.	110	299	0	1705	1705	5.24	0	0	0	0
6	16.2-17.1	14.1	.0256	71.8	636	13.4	4177.	110	299	0	1695	1695	5.21	0	0	0	0
7	18.2-19.0	33.5	.0606	75.1	1097	23.1	6185.	111	299	0	1717	1717	5.28	0	0	0	0
8	20.2-22.2	57.8	.1048	75.3	1613	33.8	8267.	110	299	0	1696	1696	5.22	0	0	0	0
9	22.8-26.1	94.8	.1732	76.0	2165	45.1	10043.	109	299	0	1709	1709	5.26	0	0	0	0
10	27.7-31.2	174.0	.3169	76.2	2953	61.8	12125.	110	300	0	1729	1729	5.33	0	0	0	0

MUD PROPERTIES		
PROPERTIES	BEFORE	AFTER
600	23	23
300	15	15
200	12	12
100	10	11
6	5	5
3	3	4
P.V.	8	8
Y.P.	7	7
A.V.	11.5	11.5
GELS 10SEC/10MIN	3/6	3/6
WEIGHT	9.95	9.95
API FILTRATION	9.8	9.8
PH	9.5	9.5

COMMENTS:

TORQUE CORRECTED FOR SEAL FRICTION
FLOW RATE CORRECTED FOR PUMP EFFICIENCY
SWIVEL PRESSURE CORRECTED FOR LINE LOSS
ATMOSPHERIC DRILLING

DRILLING RESEARCH LABORATORY

DATA FILE: SANDIA3.UDS
CLIENT: SANDIA
TEST#: 3

DATE: 12/ 4/90 TIME: 17:10:14
BIT: 8 1/2" SE1150
NOZZLES OR TFA: 5-HIGH PRESSURE

FILE: SANDIA3.DRP
MUD: 10.0 PPG WATER-BASE
ROCK: CRAB ORCHARD SANDSTONE #2

DATA PT. #	PENETRATION INTERVAL IN	R.O.P. FT/HR	R.O.P. IN/REV	TEMP DEG-F	TORQUE FT-LB	HP AT BIT HP	BIT WEIGHT LB	ROTARY SPEED RPM	FLOW RATE GPM	BORE PRESS. PSI	SWIVEL PRESS. PSI	SWIV-BORE PSI	HSI HP/SI	BACK PRESS. PSI	BORE-BACK PSI	CONFIN PRESS. PSI	OVRBUR STRESS PSI	MUD PROPERTIES PROPERTIES	BEFORE	AFTER
1	1.6- 1.5	.0	.0000	77.4	.0	.0	0.	43	146	0	1720	1720	2.58	0	0	0	0	600	23	
2	1.6- 1.6	.0	.0000	77.9	.0	.0	0.	31	193	0	2963	2963	5.87	0	0	0	0	300	15	
3	1.6- 1.6	.0	.0000	79.0	.0	.0	0.	31	236	0	4455	4455	10.82	0	0	0	0	200	12	
4	1.6- 1.6	.0	.0000	82.3	.0	.0	0.	32	256	0	5273	5273	13.91	0	0	0	0	100	11	
5	5.8- 6.7	7.1	.0129	87.6	162	3.4	2078.	111	257	0	5253	5253	13.87	0	0	0	0	6	5	
6	6.9- 8.7	14.7	.0266	89.2	440	9.3	4122.	111	255	0	5245	5245	13.76	0	0	0	0	3	4	
7	9.2-12.0	22.0	.0397	90.6	859	18.1	5923.	111	256	0	5204	5204	13.67	0	0	0	0	P.V.	8	
8	12.5-15.3	45.9	.0832	92.0	1438	30.2	8004.	110	256	0	5236	5236	13.76	0	0	0	0	Y.P.	7	
9	16.3-20.2	87.9	.1588	92.6	2028	42.8	9981.	111	256	0	5260	5260	13.83	0	0	0	0	A.V.	11.5	
10	20.9-22.7	24.8	.0450	93.3	924	19.4	5877.	110	256	0	5250	5250	13.80	0	0	0	0	GELS 10SEC/10MIN	3/6	
																		WEIGHT	9.95	
																		API FILTRATION	9.8	
																		PH	9.5	

COMMENTS:

TORQUE CORRECTED FOR SEAL FRICTION
FLOW RATE CORRECTED FOR PUMP EFFICIENCY
SWIVEL PRESSURE CORRECTED FOR LINE LOSS
ATMOSPHERIC DRILLING - NOTE: DATA POINTS 1, 2, 3 & 4 WERE WITH FLOW AND TAKEN OFF BOTTOM

DRILLING & COMPLETIONS LABORATORY

DATA FILE: SANDIA4.UDS
CLIENT: SANDIA
TEST#: 4

DATE: 12/ 5/00 TIME: 10:36:12
BIT: 8 1/2" SE1150
NOZZLES OR TFA: 5-HIGH PRESSURE

FILE: SANDIA4.DRP
MUD: 10 PPG WATER-BASE
ROCK: CRAB ORCHARD #1

DATA PT. #	PENETRATION INTERVAL IN	R.O.P. FT/HR	R.O.P. IN/REV	TEMP DEG-F	TORQUE FT-LB	HP AT BIT HP	BIT WEIGHT LB	ROTARY SPEED RPM	FLOW RATE GPM	BORE PRESS. PSI	SWIVEL PRESS. PSI	SWIV-BORE PSI	HSI HP/SI	BACK PRESS. PSI	BORE-BACK PSI	CONFIN PRESS. PSI	OVRBUR STRESS PSI
1	5.8- 6.2	9.9	.0180	79.5	250	5.2	2101.	110	254	0	5241	5241	13.70	0	0	0	0
2	6.6- 7.4	32.2	.0585	79.9	615	12.9	4077.	110	254	0	5348	5348	13.98	0	0	0	0
3	7.9- 8.6	51.3	.0934	80.3	1022	21.4	6087.	110	255	0	5354	5354	14.01	0	0	0	0
4	9.9-11.9	73.5	.1340	80.3	1500	31.4	8047.	110	255	0	5230	5230	13.70	0	0	0	0
5	13.4-16.0	122.7	.2229	81.3	2064	43.3	9987.	110	255	0	5164	5164	13.53	0	0	0	0
6	16.9-17.8	35.1	.0635	81.3	974	20.5	6003.	111	254	0	5234	5234	13.70	0	0	0	0
7	18.2-19.6	26.0	.0473	87.2	456	9.5	3091.	110	255	0	5197	5197	13.63	0	0	0	0

MUD PROPERTIES		
PROPERTIES	BEFORE	AFTER
600	26	
300	17	
200	14	
100	10	
6	4	
3	3	
P.V.	9	
Y.P.	8	
A.V.	13.0	
GELS 10SEC/10MIN	2/	
WEIGHT	9.95	
API FILTRATION	9.6	
PH	9.5	

COMMENTS:

TORQUE CORRECTED FOR SEAL FRICTION
FLOW RATE CORRECTED FOR PUMP EFFICIENCY
SWIVEL PRESSURE CORRECTED FOR LINE LOSS
ATMOSPHERIC DRILLING NOTE: DATA POINT #7 RUN AT CONSTANT ROP OF 30 FT/HR

DRILLING & COMPLETIONS LABORATORY

DATA FILE: SANDIA5.UDS
CLIENT: SANDIA
TEST#: 5

DATE: 12/ 5/00 TIME: 12:04:24
BIT: 8 1/2" SE1150
NOZZLES OR TFA: 5-8/32"

FILE: SANDIA5.DRP PAGE: 1
MUD: 10 PPG WATER-BASE
ROCK: CRAB ORCHARD SANDSTONE #2

DATA PT. #	PENETRATION INTERVAL IN	R.O.P. FT/HR	R.O.P. IN/REV	TEMP DEG-F	TORQUE FT-LB	HP AT BIT HP	BIT WEIGHT LB	ROTARY SPEED RPM	FLOW RATE GPM	BORE PRESS. PSI	SWIVEL PRESS. PSI	SWIV-BORE PSI	HSI HP/SI	BACK PRESS. PSI	BORE-BACK PSI	CONFIN PRESS. PSI	OVRBUR STRESS PSI	MUD PROPERTIES PROPERTIES	BEFORE	AFTER
1	23.4-23.7	5.6	.0103	90.9	281	5.8	2008.	109	298	0	1677	1677	5.15	0	0	0	0	600	26	
2	23.9-24.4	11.0	.0199	90.8	582	12.2	4067.	110	299	0	1700	1700	5.22	0	0	0	0	300	17	
3	24.7-25.4	19.6	.0356	90.8	941	19.7	6063.	110	299	0	1686	1686	5.18	0	0	0	0	200	14	
4	25.8-27.6	37.9	.0688	91.6	1414	29.6	7926.	110	299	0	1666	1666	5.12	0	0	0	0	100	10	
5	28.3-31.4	70.2	.1276	91.7	1978	41.4	9992.	110	299	0	1677	1677	5.16	0	0	0	0	6	4	
																		3	3	
																		P.V.	9	
																		Y.P.	8	
																		A.V.	13.0	
																		GELS 10SEC/10MIN	2/	
																		WEIGHT	9.95	
																		API FILTRATION	9.6	
																		PH	9.5	

COMMENTS:

TORQUE CORRECTED FOR SEAL FRICTION
FLOW RATE CORRECTED FOR PUMP EFFICIENCY
SWIVEL PRESSURE CORRECTED FOR LINE LOSS
ATMOSPHERIC DRILLING NOTE: DRILLED BOTTOM HALF OF ROCK ALSO USED IN TEST #3

DRILLING & COMPLETIONS LABORATORY

DATA FILE: SANDIA6.UDS
CLIENT: SANDIA
TEST#: 6

DATE: 12/ 7/00 TIME: 11:41:21
BIT: 8 1/2" SE1150
NOZZLES OR TFA: 5-8/32"

FILE: SANDIA6.DRP
MUD: 10.0 PPG WATER-BASE
ROCK: CRAB ORCHARD SANDSTONE

DATA PT. #	PENETRATION INTERVAL IN	R.O.P. FT/HR	R.O.P. IN/REV	TEMP DEG-F	TORQUE FT-LB	HP AT BIT HP	BIT WEIGHT LB	ROTARY SPEED RPM	FLOW RATE GPM	BORE PRESS. PSI	SWIVEL PRESS. PSI	SWIV-BORE PSI	HSI HP/SI	BACK PRESS. PSI	BORE-BACK PSI	CONFIN PRESS. PSI	OVRBUR STRESS PSI	MUD PROPERTIES		
																		PROPERTIES	BEFORE	AFTER
1	6.6- 7.0	8.9	.0161	57.5	712	15.0	5053.	110	296	2013	3353	1339	4.07	0	2013	4996	6055	600	26	
2	7.3- 8.4	16.4	.0300	57.6	1543	32.2	9983.	110	296	2015	3382	1367	4.16	0	2015	5000	6054	300	17	
3	8.7-10.0	29.5	.0535	57.6	3265	68.5	19905.	110	296	2033	3387	1354	4.13	0	2033	5004	6053	200	14	
4	10.8-13.2	49.1	.0886	57.9	5016	105.7	29840.	111	297	2031	3437	1406	4.29	0	2031	4997	6042	100	10	
5	13.8-14.8	28.8	.0518	57.6	3060	64.8	19926.	111	297	2040	3398	1359	4.14	0	2040	4993	6024	6	4	
6	15.0-15.9	18.9	.0342	57.7	2111	44.4	14916.	110	296	2036	3424	1388	4.23	0	2036	5005	6020	3	3	
7	16.6-18.3	42.4	.0771	58.6	4165	87.3	24933.	110	297	2039	3413	1374	4.19	0	2039	4999	6016	P.V.	9	
8	18.6-18.9	7.6	.0138	58.5	642	13.4	4940.	110	296	3967	5314	1347	4.10	0	3967	5017	6116	Y.P.	8	
9	19.2-20.0	15.6	.0281	59.1	1413	29.9	9935.	111	296	3977	5318	1341	4.09	0	3977	5015	6115	A.V.	10.0	
10	20.4-22.1	29.2	.0530	59.3	3186	66.8	19863.	110	297	3998	5331	1333	4.07	0	3998	5014	6119	GELS 10SEC/10MIN	2/6	
11	22.7-25.0	40.9	.0739	59.5	4952	104.5	29820.	111	297	3970	5380	1410	4.31	0	3970	5013	6123	WEIGHT	9.99	
12	25.4-26.6	26.6	.0484	59.5	3045	63.7	19809.	110	297	4001	5317	1316	4.02	0	4001	5011	6112	API FILTRATION	8.6	
13	26.9-27.6	18.1	.0327	59.5	1951	41.1	14931.	111	296	3968	5318	1349	4.11	0	3968	5009	6105	PH	9.5	
14	28.3-29.7	35.4	.0640	59.8	4074	85.7	24827.	110	297	3982	5335	1353	4.13	0	3982	5009	6114			
15	30.4-32.3	30.4	.0551	61.6	3231	67.9	20000.	110	297	4045	5396	1351	4.12	0	4045	5009	6123			

COMMENTS:

TORQUE CORRECTED FOR SEAL FRICTION
SWIVEL PRESSURE CORRECTED FOR LINE LOSS
FLOW RATE SUM OF 180 GPM FROM TERRATEK AND 115 GPM FROM HALLIBURTON
PRESSURE DRILLING AT 2000 AND 4000 PSI BOREHOLE PRESSURE

DRILLING & COMPLETIONS LABORATORY

DATA FILE: SANDIA7.UDS
CLIENT: SANDIA
TEST#: 7

DATE: 12/ 7/00 TIME: 16:12:59
BIT: 8 1/2" SE1150
NOZZLES OR TFA: 5-HIGH PRESSURE

FILE: SANDIA7.DRP
MUD: 10.0 PPG WATER-BASE
ROCK: CARTHAGE MARBLE

DATA PT. #	PENETRATION INTERVAL IN	R.O.P. FT/HR	R.O.P. IN/REV	TEMP DEG-F	TORQUE FT-LB	HP AT BIT HP	BIT WEIGHT LB	ROTARY SPEED RPM	FLOW RATE GPM	BORE PRESS. PSI	SWIVEL PRESS. PSI	SWIV-BORE PSI	HSI HP/SI	BACK PRESS. PSI	BORE-BACK PSI	CONFIN PRESS. PSI	OVRBUR STRESS PSI	MUD PROPERTIES		
																		PROPERTIES	BEFORE	AFTER
1	6.3- 6.8	14.0	.0254	69.0	820	17.2	5029.	110	292	2030	6996	4966	14.90	0	2030	5021	6066	600	26	26
2	7.2- 8.0	22.0	.0399	69.0	1633	34.4	10226.	111	292	2027	6939	4911	14.74	0	2027	5019	6060	300	16	16
3	8.5- 9.8	37.4	.0680	70.7	3426	71.8	20270.	110	292	2036	7028	4992	15.00	0	2036	5017	6058	200	13	14
4	10.7-13.0	71.7	.1282	70.4	5844	124.5	30284.	112	293	2030	6968	4939	14.86	0	2030	5013	6048	100	10	10
5	13.6-14.9	38.1	.0691	68.9	3412	71.6	20109.	110	291	2033	6937	4904	14.67	0	2033	5008	6026	6	4	4
6	15.1-16.0	25.7	.0463	68.1	2294	48.4	15032.	111	290	2020	6841	4821	14.38	0	2020	5005	6012	3	3	4
7	16.9-18.5	54.1	.0973	70.1	4447	94.2	25173.	111	290	1982	6902	4920	14.69	0	1982	5001	6005	P.V.	10	10
8	18.8-19.6	11.6	.0209	76.6	825	17.4	5007.	111	302	3985	8042	4057	12.58	0	3985	5028	6134	Y.P.	4	4
9	19.9-20.7	19.6	.0356	79.7	1400	29.3	10080.	110	302	4008	8026	4018	12.49	0	4008	5027	6137	A.V.	13.0	13.0
10	21.2-22.5	36.7	.0663	77.5	3301	69.6	20119.	111	303	4028	8103	4075	12.69	0	4028	5028	6145	GELS 10SEC/10MIN	3/6	2/6
11	23.0-25.1	51.5	.0920	80.7	5291	112.8	30205.	112	303	3998	8058	4059	12.64	0	3998	5028	6153	WEIGHT	10.0	10.0
12	25.6-27.2	34.8	.0630	79.0	3193	67.3	20118.	111	301	3993	7993	3999	12.38	0	3993	5026	6138	API FILTRATION	8.6	8.6
13	27.4-28.5	27.1	.0484	75.9	2190	46.7	15163.	112	301	3987	8004	4018	12.45	0	3987	5025	6132	PH	9.5	9.5
14	29.0-30.3	43.6	.0785	73.8	4139	87.6	25218.	111	302	3989	7994	4005	12.45	0	3989	5026	6146			
15	30.5-31.7	33.3	.0604	73.3	3096	65.0	20287.	110	302	3987	7972	3985	12.37	0	3987	5025	6142			

COMMENTS:

TORQUE CORRECTED FOR SEAL FRICTION
SWIVEL PRESSURE CORRECTED FOR LINE LOSS
FLOW RATE INCLUDED 121.38 GPM AT 2000 PSI BOREHOLE AND 120.54 GPM AT 4000 PSI BOREHOLE FROM HALLIBURTON PUMP TRUCKS
PRESSURE DRILLING

DRILLING & COMPLETIONS LABORATORY

DATA FILE: SANDIA8.UDS
CLIENT: SANDIA
TEST#: 8

DATE: 12/ 8/00 TIME: 10:27:40
BIT: 8 1/2" SE1150
NOZZLES OR TFA: 5-8/32"

FILE: SANDIA8.DRP
MUD: 10.0 PPG WATER-BASE
ROCK: SIERRA WHITE GRANITE

DATA PT. #	PENETRATION INTERVAL IN	R.O.P. FT/HR	R.O.P. IN/REV	TEMP DEG-F	TORQUE FT-LB	HP AT BIT HP	BIT WEIGHT LB	ROTARY SPEED RPM	FLOW RATE GPM	BORE PRESS. PSI	SWIVEL PRESS. PSI	SWIV-BORE PSI	HSI HP/SI	BACK PRESS. PSI	BORE-BACK PSI	CONFIN PRESS. PSI	OVRBUR STRESS PSI	MUD PROPERTIES PROPERTIES	BEFORE	AFTER
1	6.2- 6.5	4.6	.0085	62.0	457	9.5	5162.	110	302	1998	3390	1392	4.32	0	1998	4980	5986	600	26	25
2	6.7- 7.5	15.1	.0274	62.2	1680	35.3	15183.	110	302	2002	3402	1401	4.34	0	2002	4991	5992	300	15	13
3	7.7- 9.1	21.7	.0394	62.9	2474	52.0	20274.	110	302	2009	3412	1403	4.35	0	2009	4995	5993	200	13	11
4	9.4-11.0	28.0	.0506	62.8	3242	68.3	25254.	111	302	2014	3407	1394	4.32	0	2014	4999	5992	100	9	7
5	11.4-14.4	39.8	.0717	63.1	4142	87.5	30248.	111	302	2016	3415	1399	4.34	0	2016	4996	5986	6	4	4
6	14.7-16.1	28.0	.0503	63.9	3191	67.6	25241.	111	302	2012	3419	1408	4.37	0	2012	4995	5976	3	2	2
7	16.4-17.5	19.0	.0342	63.9	2320	49.3	20101.	112	302	2008	3419	1411	4.38	0	2008	4979	5961	P.V.	11	12
8	17.8-18.5	12.8	.0232	64.5	1625	34.2	15059.	110	302	2004	3419	1414	4.39	0	2004	4992	5966	Y.P.	4	1
9	18.7-19.0	9.4	.0169	64.7	1110	23.4	10080.	111	302	2002	3414	1412	4.38	0	2002	4990	5962	A.V.	13.0	12.5
10	19.2-19.5	4.1	.0073	68.0	635	13.4	5135.	111	301	4017	5320	1303	4.03	0	4017	4989	6033	GELS 10SEC/10MIN	2/3	2/4
11	19.7-20.5	14.5	.0263	68.5	1807	37.9	15159.	110	301	4074	5394	1320	4.08	0	4074	4989	6042	WEIGHT	9.95	10.0
12	20.8-22.0	20.9	.0380	69.0	2417	50.8	20145.	110	301	4114	5451	1337	4.14	0	4114	5007	6055	API FILTRATION	8.6	8.6
13	22.4-24.0	28.5	.0514	69.5	3265	68.8	25200.	111	301	4128	5464	1337	4.14	0	4128	4999	6055	PH	9.5	9.5
14	24.5-27.2	34.6	.0626	70.1	4124	86.8	30191.	110	301	4130	5477	1347	4.17	0	4130	4989	6054			
15	27.5-29.1	25.5	.0457	70.7	3083	65.4	25270.	111	301	4112	5463	1351	4.17	0	4112	4978	6045			
16	29.3-30.6	18.8	.0337	71.6	2300	48.9	20089.	112	301	4086	5427	1341	4.14	0	4086	4978	6040			
17	30.7-31.5	13.8	.0249	71.9	1664	35.3	15100.	111	300	4072	5408	1336	4.13	0	4072	5000	6046			
18	31.7-31.9	8.3	.0148	72.0	1123	23.8	10147.	111	300	4064	5404	1340	4.14	0	4064	4993	6038			

COMMENTS:

TORQUE CORRECTED FOR SEAL FRICTION
SWIVEL PRESSURE CORRECTED FOR LINE LOSS
FLOW RATE INCLUDED 119 GPM AT 2000 AND 4000 PSI BOREHOLE FROM HALLIBURTON PUMP TRUCKS
PRESSURE DRILLING

DRILLING & COMPLETIONS LABORATORY

DATA FILE: SANDIA9.UDS
CLIENT: SANDIA
TEST#: 9

DATE: 12/ 8/00 TIME: 15:56:20
BIT: 8 1/2" SE1150
NOZZLES OR TFA: 5-HIGH PRESSURE

FILE: SANDIA9.DRP
MUD: 10.0 PPG WATER-BASE
ROCK: SIERRA WHITE GRANITE

DATA PT. #	PENETRATION INTERVAL IN	R.O.P. FT/HR	R.O.P. IN/REV	TEMP DEG-F	TORQUE FT-LB	HP AT BIT HP	BIT WEIGHT LB	ROTARY SPEED RPM	FLOW RATE GPM	BORE PRESS. PSI	SWIVEL PRESS. PSI	SWIV-BORE PSI	HSI HP/SI	BACK PRESS. PSI	BORE-BACK PSI	CONFIN PRESS. PSI	OVRBUR STRESS PSI
1	17.1-17.4	9.7	.0176	76.9	1157	24.3	10218.	110	300	1991	7030	5039	15.55	0	1991	4998	6085
2	17.7-18.4	23.4	.0425	77.0	2563	53.6	20186.	110	300	1999	7076	5076	15.67	0	1999	4992	6088
3	18.8-20.4	48.7	.0885	77.5	4508	94.4	30028.	110	300	2014	7046	5032	15.54	0	2014	4986	6089
4	20.7-21.4	22.9	.0413	78.1	2509	52.8	20192.	111	300	2013	7034	5021	15.50	0	2013	4979	6077
5	21.6-21.8	10.1	.0181	78.3	1176	24.9	10221.	111	300	2008	7100	5092	15.72	0	2008	4972	6065
6	22.4-23.8	47.0	.0852	79.1	4423	93.0	30132.	110	300	2017	7091	5074	15.68	0	2017	4966	6074
7	24.1-24.3	9.3	.0168	88.0	1175	24.7	10094.	110	304	4013	7899	3886	12.15	0	4013	4994	6179
8	24.6-25.2	21.8	.0396	88.9	2529	53.1	20092.	110	304	4020	7919	3899	12.17	0	4020	4990	6185
9	25.6-26.7	38.6	.0697	88.9	4114	86.6	30153.	111	303	4013	7861	3848	11.97	0	4013	4986	6192
10	26.9-27.6	21.6	.0388	89.1	2319	49.2	20073.	111	303	4013	7869	3856	11.99	0	4013	4982	6182
11	27.8-28.1	9.8	.0176	89.8	1103	23.4	10290.	111	303	4002	7879	3877	12.07	0	4002	4976	6171
12	28.7-29.8	38.2	.0695	89.9	3986	83.5	30024.	110	303	4019	7841	3823	11.93	0	4019	4971	6186
13	30.3-31.8	41.4	.0753	92.7	4144	86.7	30123	110	304	3051	7372	4320	13.51	0	3051	4998	6173

MUD PROPERTIES

PROPERTIES	BEFORE	AFTER
600	25	25
300	14	14
200	11	11
100	8	7
6	4	3
3	3	2
P.V.	11	11
Y.P.	3	3
A.V.	12.5	12.5
GELS 10SEC/10MIN	2/2	2/4
WEIGHT	10.0	10.0
API FILTRATION	8.6	8.8
PH	9.5	9.5

COMMENTS:

TORQUE CORRECTED FOR SEAL FRICTION
SWIVEL PRESSURE CORRECTED FOR LINE LOSS
FLOW RATE INCLUDED 121 GPM FROM HALLIBURTON PUMP TRUCKS
PRESSURE DRILLING

DRILLING & COMPLETIONS LABORATORY

DATA FILE: SAND10.UDS
CLIENT: SANDIA
TEST#: 10

DATE: 3/27/01 TIME: 10:58:15
BIT: 8 1/2" REED 62A
NOZZLES OR TFA: 3-10/32"

FILE: SAND10.DRP
MUD: 10 PPG WATER-BASE
ROCK: SIERRA WHITE GRANITE

DATA PT. #	PENETRATION INTERVAL IN	R.O.P. FT/HR	R.O.P. IN/REV	TEMP DEG-F	TORQUE FT-LB	HP AT BIT HP	BIT WEIGHT LB	ROTARY SPEED RPM	FLOW RATE GPM	BORE PRESS. PSI	SWIVEL PRESS. PSI	SWIV-BORE PSI	HSI HP/SI	BACK PRESS. PSI	BORE-BACK PSI	CONFIN PRESS. PSI	OVRBUR STRESS PSI	MUD PROPERTIES		
																		PROPERTIES	BEFORE	AFTER
1	1.7- 2.0	4.6	.0083	69.9	429	9.0	20114.	110	300	2008	3388	1380	4.26	0	2008	4989	6026	600	31	42
2	2.3- 2.8	12.6	.0231	70.2	900	18.8	40335.	110	301	2008	3397	1389	4.29	0	2008	4990	6033	300	17	27
3	3.1- 3.9	20.8	.0382	70.9	1447	30.0	60429.	109	301	2020	3410	1390	4.30	0	2020	4990	6039	200	12	19
4	4.1- 4.7	12.0	.0219	70.9	842	17.7	40367.	110	300	2013	3407	1394	4.31	0	2013	4988	6023	100	9	13
5	5.0- 5.6	19.8	.0361	71.7	1377	28.7	60323.	110	299	1998	3384	1386	4.27	0	1998	4990	6030	6	4	6
6	5.8- 6.1	4.2	.0076	71.7	404	8.5	20294.	111	299	1994	3378	1384	4.26	0	1994	4990	6005	3	2	4
7	6.2- 6.5	3.0	.0085	72.5	445	6.0	20343.	71	300	1996	3390	1394	4.30	0	1996	4993	6005	P.V.	14	15
8	6.6- 7.1	9.0	.0257	72.7	901	12.0	40357.	70	300	2003	3389	1386	4.28	0	2003	4991	6013	Y.P.	3	12
9	7.5- 8.2	15.4	.0440	73.3	1451	19.3	60274.	70	300	2012	3404	1392	4.30	0	2012	4987	6020	A.V.	15.5	21.0
10	8.3- 8.8	8.8	.0251	73.1	875	11.7	40376.	70	300	2006	3389	1382	4.27	0	2006	4982	6005	GELS 10SEC/10MIN	2/6	3/15
11	9.0- 9.9	15.1	.0434	73.4	1461	19.3	60329.	69	301	2011	3397	1386	4.28	0	2011	4987	6017	WEIGHT	10.05	10.0
12	9.9-10.2	3.7	.0104	73.8	453	6.1	20191.	71	299	1997	3380	1383	4.26	0	1997	4985	5989	API FILTRATION	8.1	7.8
13	10.4-10.6	4.9	.0090	79.0	425	8.9	20109.	110	300	3950	5394	1444	4.46	0	3950	4987	6130	PH	9.5	9.5
14	10.8-11.2	11.4	.0207	79.8	830	17.4	40333.	110	299	3922	5274	1352	4.16	0	3922	4991	6144			
15	11.4-12.0	17.6	.0320	79.9	1306	27.4	60222.	110	300	3972	5374	1403	4.32	0	3972	4990	6157			
16	12.1-12.6	10.8	.0196	79.9	818	17.1	40393.	110	300	3942	5354	1412	4.35	0	3942	4989	6144			
17	12.8-13.7	17.1	.0312	80.4	1314	27.5	60341.	110	300	3919	5356	1436	4.43	0	3919	4994	6157			
18	13.8-14.1	4.9	.0088	81.3	393	8.3	20266.	111	299	3909	5305	1396	4.30	0	3909	4990	6126			
19	14.1-14.2	3.1	.0089	83.2	427	5.7	20150.	70	302	3945	5361	1415	4.39	0	3945	4992	6131			
20	14.3-14.7	8.5	.0245	83.6	873	11.6	40307.	70	302	3958	5387	1429	4.44	0	3958	4992	6148			
21	14.9-15.4	13.3	.0379	84.6	1339	17.9	60328.	70	302	3971	5360	1389	4.32	0	3971	4991	6164			
22	15.5-15.9	8.7	.0246	84.8	874	11.7	40364.	71	302	3960	5382	1422	4.42	0	3960	4988	6147			
23	16.0-16.2	3.5	.0099	85.4	433	5.9	20184.	71	302	3945	5292	1347	4.18	0	3945	4994	6134			
24	16.3-16.5	6.3	.0115	85.2	518	10.9	20212.	110	301	507	1904	1397	4.32	0	507	4991	6038			
25	16.7-17.3	17.8	.0324	85.2	1030	21.6	40205.	110	301	511	1909	1398	4.33	0	511	4989	6049			
26	17.8-18.7	31.2	.0567	85.3	1664	34.9	60348.	110	301	513	1921	1408	4.36	0	513	4989	6059			
27	18.9-19.6	18.1	.0329	85.2	1012	21.3	40333.	110	301	514	1912	1398	4.33	0	514	4994	6043			
28	20.1-21.1	34.4	.0621	85.2	1694	35.7	60268.	111	301	513	1920	1407	4.36	0	513	4992	6054			
29	21.3-21.7	6.7	.0121	85.2	521	11.0	20202.	111	301	511	1908	1398	4.33	0	511	4988	6015			
30	21.8-22.0	4.3	.0121	85.2	541	7.2	20131.	70	301	509	1903	1394	4.31	0	509	4994	6016			
31	22.2-22.8	13.1	.0374	85.2	1086	14.5	40358.	70	300	505	1896	1391	4.29	0	505	4993	6032			
32	23.0-24.1	24.0	.0685	85.2	1677	22.4	60279.	70	300	508	1899	1391	4.29	0	508	4991	6044			
33	24.3-24.8	13.2	.0371	85.2	1037	14.0	40349.	71	300	507	1896	1389	4.29	0	507	4987	6022			
34	25.1-26.3	23.2	.0662	85.2	1734	23.2	60406.	70	300	501	1901	1400	4.32	0	501	4993	6039			
35	26.3-26.6	4.5	.0127	85.2	531	7.1	20295.	71	300	505	1895	1390	4.29	0	505	4993	6001			
36	26.8-27.3	12.4	.0223	85.2	829	17.5	40299.	111	300	1997	3379	1382	4.26	0	1997	5004	6165			
37	27.6-28.1	19.2	.0347	85.2	1315	27.7	60379.	111	300	2011	3377	1366	4.22	0	2011	5003	6183			
38	28.3-28.8	23.2	.0420	85.2	1605	33.7	70363.	110	300	2017	3400	1383	4.27	0	2017	5002	6192			
39	29.2-29.9	27.4	.0498	85.2	1882	39.5	80254.	110	300	2021	3374	1352	4.18	0	2021	5001	6202			
40	30.5-31.2	23.7	.0434	86.3	1609	33.5	70454.	109	300	2011	3382	1371	4.24	0	2011	4995	6192			

COMMENTS:
TORQUE CORRECTED FOR SEAL FRICTION
FLOW RATE CORRECTED FOR PUMP EFFICIENCY
SWIVEL PRESSURE CORRECTED FOR LINE LOSS

DRILLING & COMPLETIONS LABORATORY

DATA FILE: SAND10A.UDS
CLIENT: SANDIA
TEST#: 10A

DATE: 3/27/01 TIME: 10:58:15
BIT: 8 1/2" REED 62A
NOZZLES OR TFA: 3-10/32"

FILE: SAND10A.DRP
MUD: 10 PPG WATER-BASE
ROCK: SIERRA WHITE GRANITE

DATA PT. #	PENETRATION INTERVAL IN	R.O.P. FT/HR	R.O.P. IN/REV	TEMP DEG-F	TORQUE FT-LB	HP AT BIT HP	BIT WEIGHT LB	ROTARY SPEED RPM	FLOW RATE GPM	BORE PRESS. PSI	SWIVEL PRESS. PSI	SWIV-BORE PSI	HSI HP/SI	BACK PRESS. PSI	BORE-BACK PSI	CONFIN PRESS. PSI	OVRBUR STRESS PSI	MUD PROPERTIES		
																		PROPERTIES	BEFORE	AFTER
41	31.5-32.2	28.8	.0525	86.3	1882	39.3	80414.	110	299	2002	3383	1381	4.25	0	2002	4995	6203	600	31	42
																		300	17	27
																		200	12	19
																		100	9	13
																		6	4	6
																		3	2	4
																		P.V.	14	15
																		Y.P.	3	12
																		A.V.	15.5	21.0
																		GELS 10SEC/10MIN	2/6	3/15
																		WEIGHT	10.05	10.0
																		API FILTRATION	8.1	7.8
																		PH	9.5	9.5

COMMENTS:

TORQUE CORRECTED FOR SEAL FRICTION
FLOW RATE CORRECTED FOR PUMP EFFICIENCY
SWIVEL PRESSURE CORRECTED FOR LINE LOSS

Page intentionally left blank

Appendix F: DynaFlow Phase II Development Report, Letter Report 97008-2

Page intentionally left blank

DEVELOPMENT OF A STRATOJET® CAVITATING MUD JET NOZZLE FOR USE IN PDC BITS OPERATING AT CONVENTIONAL RIG PRESSURES: PHASE II

G. L. Chahine

K. M. Kalumuck

G. S. Frederick

P. D. Aley

January 2002

DYNAFLOW, INC.

10621-J Iron Bridge Road

Jessup, MD 20794

Work Performed for Sandia National Laboratory under Purchase Order No. E39452

Introduction

This letter report summarizes work recently performed for Sandia National Laboratories as part of a project team comprising Sandia, DYNAFLOW, Security DBS and Terra Tek for "Development of a Mud Jet-Augmented PDC Bit for Use with Conventional Rig Pressures" [1]. This effort represents part of our Phase II work that seeks to further improve and refine the design developed in Phase I [2] and enable operation over a broader range of operating conditions. The STRATOJET® self-resonating cavitating jet technology has been shown to be significantly more erosive than conventional jets in rock cutting under down-hole conditions. (See, for example, [3-6].)

Experimental Setup

Experiments were conducted in DYNAFLOW's High Pressure Cell (HPC) capable of ambient pressures up to approximately 2600 psi. A photograph of the HPC is presented in Figure 1. The HPC is a cylindrical pressure vessel with inside dimensions of approximately 9.5 inch diameter and 28 inch length with three quartz view ports circumferentially spaced and located near its mid length. Constructed for studies of deep hole drilling with cavitating jets, it includes a rotating fixture in which rocks are placed and rotated at various speeds for cutting beneath the jet and a fixture which allows advancement of the rock towards the nozzle at a controlled rate thus enabling actual drilling. The rock surface being cut is visible in the view ports. Ambient pressure is adjusted and maintained by a choke plate which acts as a back pressure valve in the outflow line. The jet flow is driven by a Weatherford five piston positive displacement pump capable of up to 80 gpm at 2,500 psi, 20 gpm at 10,000 psi or 11 gpm at 20,000 psi with different heads.

Nozzle acoustic resonance was assessed with the aid of one Piezotronics 101-A04 (5 mv/psi sensitivity) and one 102-A03 (0.5 mv/psi) pressure transducers used to measure the fluctuating component of the pressure. One transducer was inserted in the HPC wall, and one was located upstream of the nozzle in the feed tube just before entering the HPC. In addition, a hydrophone (made in-house from piezocomposite material obtained from Materials Systems, Inc.) was mounted on a plate onto which the jet was impacted. The output of the transducers and hydrophone were monitored with both a digital rms meter to obtain the root mean square value of the fluctuating pressure component, p', and with a frequency analyzer to ascertain the frequency content of the fluctuations and determine the peak (resonant) frequencies of the nozzles. These measurements were used to determine whether or not a particular self-resonating nozzle had achieved good acoustic resonance at particular operating conditions - an important factor in achieving good performance. The hydrophone and cell wall transducers gave very similar results. However, the data from the upstream transducer was not always consistent with these. It was thus determined to suspend use of this transducer.

Two types of experiments were run: those in which only pressure fluctuation/resonance measurements were made and those with static cuts in aluminum (6061-T6) plate. Cut volume

in the aluminum plat was measured by filling the crater with a measured volume of water (with surfactant added) from a hypodermic syringe.

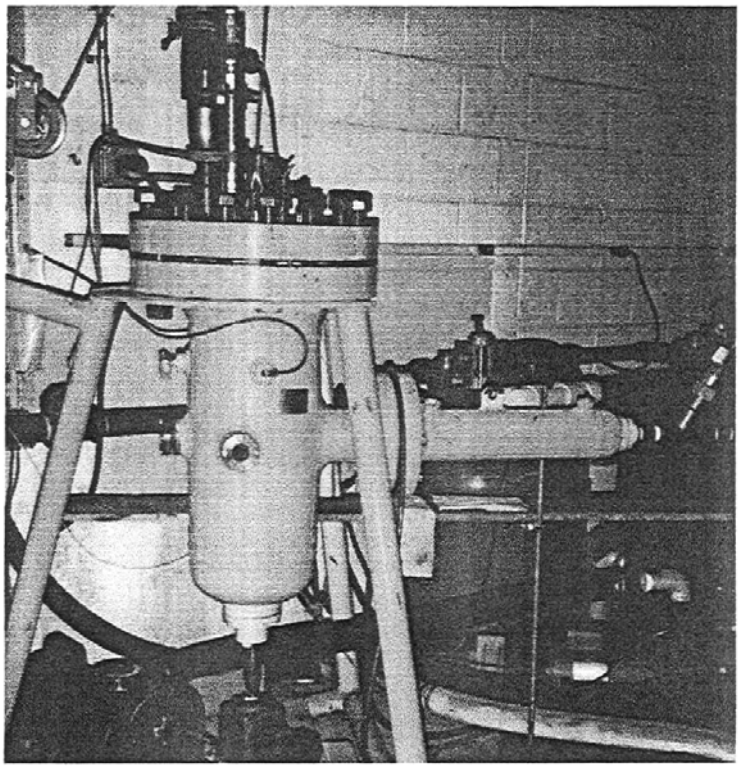

Figure 1. Photograph of High Pressure Cell (HPC).

Important experimental variables include the nozzle pressure drop, ΔP, the ambient pressure, P_a, the standoff, and the translation velocity of the jet over the target, as well as details of the nozzle geometry. An important parameter to conserve between small scale and full scale is the cavitation number, σ, which is defined as:

$$\sigma = \frac{P_a - P_v}{1/2\rho V^2}, \tag{1}$$

where P_v is the vapor pressure of the liquid, ρ is the liquid density, and V is the characteristic velocity, the jet mean velocity. In deep-hole drilling, the ambient pressure is hydrostatic and directly related to hole depth. In the case of high-pressure submerged jets used in deep-hole drilling, $P_a >> P_v$, and for well-designed nozzles $1/2\rho V^2$ may be approximated by the pressure drop, ΔP, across the nozzle. Thus

$$\sigma \approx \frac{P_a}{\Delta P}. \tag{2}$$

The cavitation number is an important parameter in determination of the occurrence and behavior of cavitation phenomena. Thus all testing should be conducted under conditions that match the value expected in practice.

Figure 2 provides a sketch of holder utilized to enable the nozzle assembly to be fabricated in several separate pieces so that these individual component geometries could be varied without remaking the entire nozzle assembly. The nozzle assembly itself consisted of a nozzle tip in the form of a disk in which are bored the cylindrical exit orifice of diameter, d_o, length, e, and a 21 degree conical expansion section of length, t. Upstream of the orifice are one or two organ pipe sections. The organ pipe immediately upstream of the orifice contains the contraction machined with a ball end mill. Otherwise, it has a constant diameter, d_1, and is of length, L_1. A second organ pipe of larger diameter, d_2, and length, L_2, could be located upstream of the first. This assembly is located in a pipe nipple that serves as the feed tube of diameter, d_f. Experiments were conducted varying the lengths and diameters of the organ pipe and with one or two organ pipes.

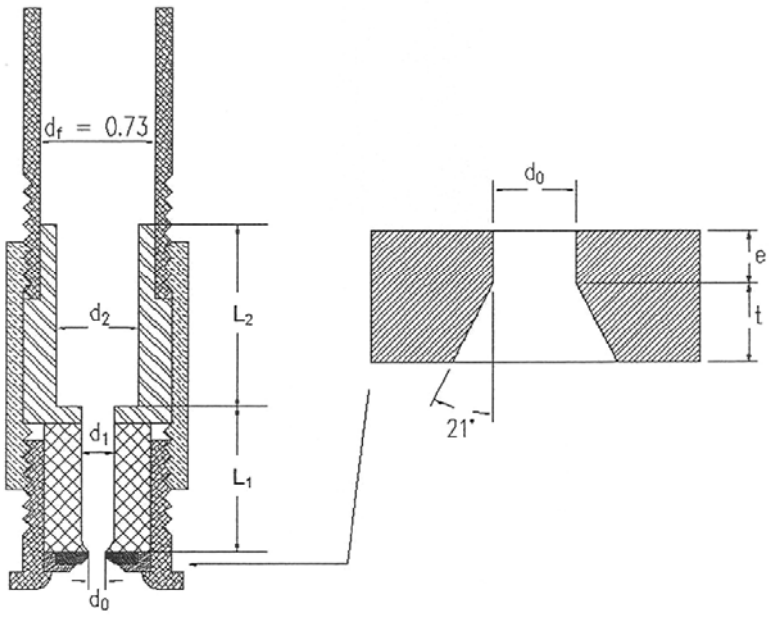

Figure 2. Sketch of the nozzle assembly holder that allowed change out of nozzle tip and variation in organ pipe configuration and dimensions. Also shown is an enlargement of the nozzle tip.

Since we no longer had access to the diamond coated nozzle tip used in Phase I, we initially sought to utilize 17-4 stainless steel nozzle tips until a more erosion resistant nozzle tip could be obtained. In order to reduce the propensity for erosion during this time, the operating pressure conditions were scaled down by a factor of 5. Thus the design point of Phase I, ΔP=5,000 psi and P_a=1,200 psi resulting in a value of $\sigma = 0.24$, was scaled to ΔP=1,000 psi and P_a=240 psi with $\sigma = 0.24$ conserved. This enabled us to screen various configurations and to impact the jet on a hydrophone for resonance measurements. (At the full scale pressures, the jet is too erosive for direct impact on the hydrophone.) Although nozzle life was extended at these lower pressures (relative to that of the full scale pressures), nozzle erosion remained a problem. Ultimately we obtained a 0.060 in. diameter diamond orifice made to our specifications by Woodburn Diamond Die (recommended by David Raymond of Sandia).

Our initial testing with the diamond nozzle did not produce magnitude of rms pressure fluctuation anticipated when seeking to reproduce the Phase I results. We discovered that this was due to the entrance to the cylindrical orifice (upstream edge of "e") being too sharp. By operating the diamond tip for approximately 2 hours, this edge became slightly rounded and the rms pressure fluctuation increased significantly. We confirmed this explanation by fabricating a new stainless steel orifice and noting that after a few minutes the rms pressure fluctuation increased about a factor of two. We also sectioned this orifice and inspected it under a microscope. A small amount of rounding was found to be present which occurs in a few minutes for stainless steel, but takes about 2 hours for the diamond. No additional changes – including no changes in flow rate – were noted with the diamond nozzle after the initial 2 hours of operation.

Results and Discussion

Reduced Pressure Results

As noted above, initial screening experiments were conducted with stainless steel nozzle tips while we awaited the diamond nozzle tip. In order to extend their lifetime, scaled operating conditions were employed. The design pressures from Phase I (ΔP=5,000 psi, Pa=1200 psi) were reduced by a factor of 5 to ΔP=1,000 psi, P_a=240 psi.. This scaling has the important effect of preserving the cavitation number (eq.2 above). The geometric parameters of the single and dual organ pipe configurations are presented in Table 1.

Organ Pipe Type	d_o inches	d_1 inches	d_2 inches	d_f inches	L_1 inches	L_2 inches
Single	0.06	0.278	--	0.72	1.57	--
Dual-Equal Lengths	0.06	0.278	0.50	0.72	1.57	1.57
Dual-Unequal Lengths	0.06	0.278	0.50	0.72	1.77	1.37

Table 1. Geometric details of dual and single organ pipe configurations employed in the reduced pressure screening tests.

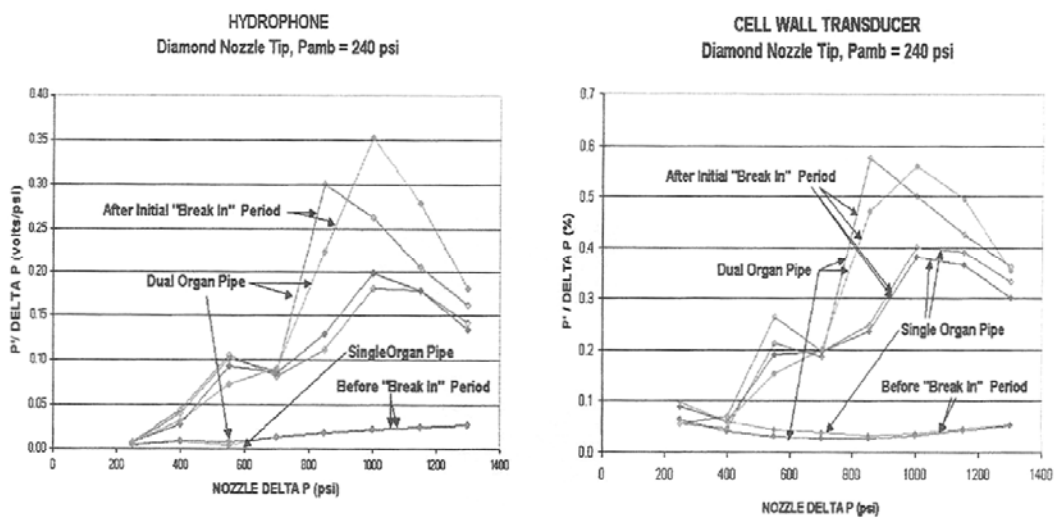

Figure 3. Influence of "break in" period on diamond nozzle performance: normalized rms pressure fluctuations measured with hydrophone below jet and transducer in HPC wall.

As noted above, the initial experiments with the diamond nozzle tip produced very low values of the rms pressure fluctuation. This can be seen in Figure 3 which presents the values of $p'/\Delta P$ vs. ΔP for both the single and dual organ pipe configurations. Measurements are shown for both the hydrophone located beneath the jet (left) and the pressure transducer located in the cell wall (right). Measurements with the diamond nozzle as received are compared to those made after allowing a "break-in period" of two hours operation at ΔP=5,000 psi, P_a=1200 psi which resulted in a slight rounding of the upstream edge (top in Figure 2) of the orifice "e". The difference in behavior following this "break-in" period is enormous. A can be seen in Figure 3, prior to this rounding, there was no resonance peak – rather the curves were relatively flat. Following the "break-in", the broad peaks occurred in the data with magnitudes of the normalized pressure fluctuations more than an order of magnitude larger than those obtained prior to the "break-in" period.

Figure 3 also compares the results for the single and dual organ pipe configurations (following "break-in"). Shown are two repeats of each test series. Good repeatability is exhibited in both the hydrophone and cell wall transducers measurements with only modest differences in the magnitude and location of the resonance peak for the dual organ pipe configuration. The single orifice configuration exhibits extremely good repeatability. Comparison of the data from the hydrophone and the cell wall transducer measurements show very similar behavior. Based on this and similar results throughout the reduced pressure testing, use of the hydrophone was suspended when we later moved to full scale testing in order to avoid damaging this hydrophone, and data from the cell wall transducer together with cutting were utilized.

Figure 3, shows that the peaks for both the single and dual organ pipe configurations are relatively broad – a few hundred psi. The peak values due to the dual organ pipe configuration are 50-100 % higher than those of the single organ pipe configuration.

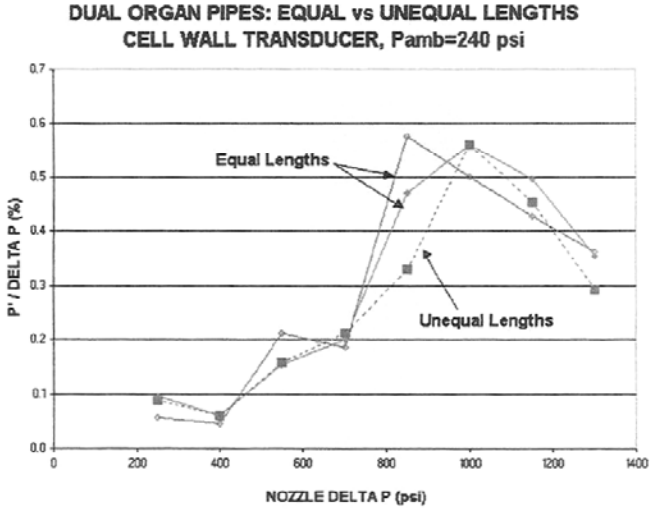

Figure 4. Effect of unequal organ pipe lengths on performance of dual organ pipe configuration.

In an attempt to further broaden the peak performance of the dual organ pipe configuration, we fabricated a configuration in which the combined length of the two organ pipe sections remained the same but in which the upstream organ pipe length (L_2) was decreased by 13% while the downstream organ pipe length (L_1)was increased by 13%. It was thought then that we would, in effect, be able to achieve resonance at three different lengths corresponding to three different frequencies and pressure drops – in effect creating a band of resonating pressure drops rather than a single value. The results are shown in Figure 4. The desired broadening of the peak values of the rms pressure fluctuation was not achieved. In fact, the data indicate a slight narrowing, although this difference is of the same order as the data scatter.

We also investigated the sensitivity of the design to ambient pressure by keeping the nozzle pressure drop constant while varying the ambient pressure (and thus the cavitation number). These results are presented in Figure 5 for measurements made with both the hydrophone and the HPC wall transducer. Experiments were conducted for $180 \le P_a \le 320$ psi at ΔP=850 and 1000 psi. These correspond to $0.21 \le \sigma \le 0.38$ for ΔP=850 and $0.18 \le \sigma \le 0.32$ for ΔP=1000 psi. As can be seen in these figures, the dual organ pipe configuration had increased pressure fluctuations over a broader range than the single organ pipe configuration. This indicates that the dual organ pipe configuration is more sensitive to ambient pressure or cavitation number than the single organ pipe configuration, but that away from its peak, its pressure fluctuations are comparable to those of the single organ pipe configuration. The shift of the peak to lower P_a at the lower ΔP suggests an optimal cavitation number in the vicinity of $\sigma \approx 0.26$-0.28.

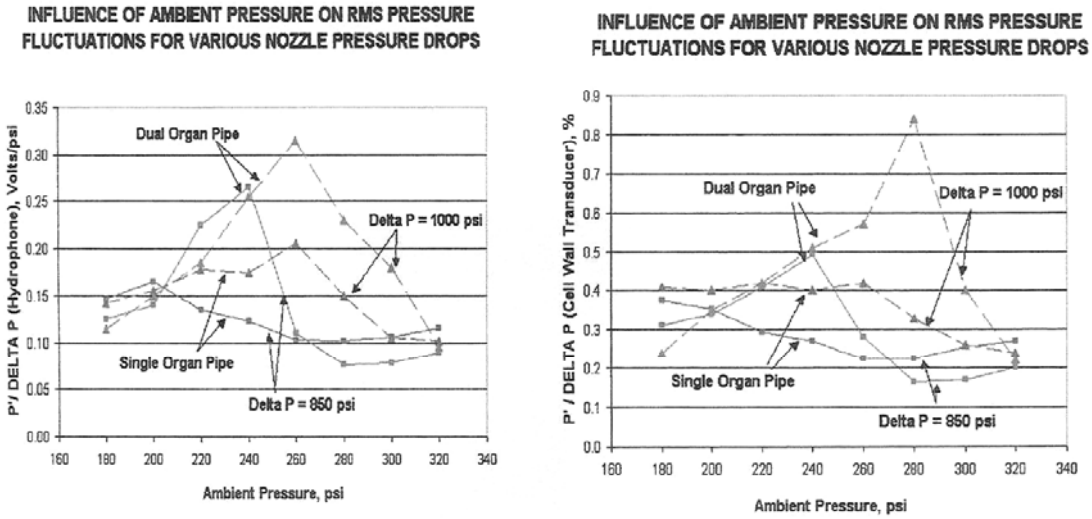

Figure 5. Influence of ambient pressure on rms pressure fluctuations for the single and dual organ pipe configurations. Left: measurements from hydrophone located beneath the jet. Right: measurements from pressure transducer in HPC wall.

Full Scale Pressure Results and Ersosion Tests

Figure 6 presents results of resonance testing (as measured by the HPC wall transducer) and static cutting in aluminum plate at a fixed ambient pressure of 1,200 psi for values of ΔP between 1,200 and 6,300 psi corresponding to values of σ between 1 and 0.19, respectively. Cutting in aluminum was performed at a standoff of 0.25 in. (0.42 d_0). The results of four nozzle configurations are presented in this figure: one with dual ("stepped") organ pipes and three with a single organ pipe which differs in its length and diameter. The geometric details of these configurations are presented in Table 2.

As can be seen in Figure 6a, the largest values of the normalized rms pressure fluctuations, $p'/\Delta P$, are produced by the single organ pipe configuration with the larger diameter. In addition, as shown in Figure 6b, this configuration achieves the largest measured cut volumes at all pressures at which measurable cutting occurred during the 5 min. exposure (4,800 psi and above). Measured cut volumes were nearly twice as large as the volumes achieved with the other configurations at ΔP=4,800, 5,300, and 5,800 psi 50% larger at ΔP =6300 psi. In terms of cut volume, the other three configurations were fairly similar with the dual organ pipe producing slightly better cutting than the other two at all but the highest pressure. In all cases the cut volume rapidly increases in a nonlinear fashion with ΔP.

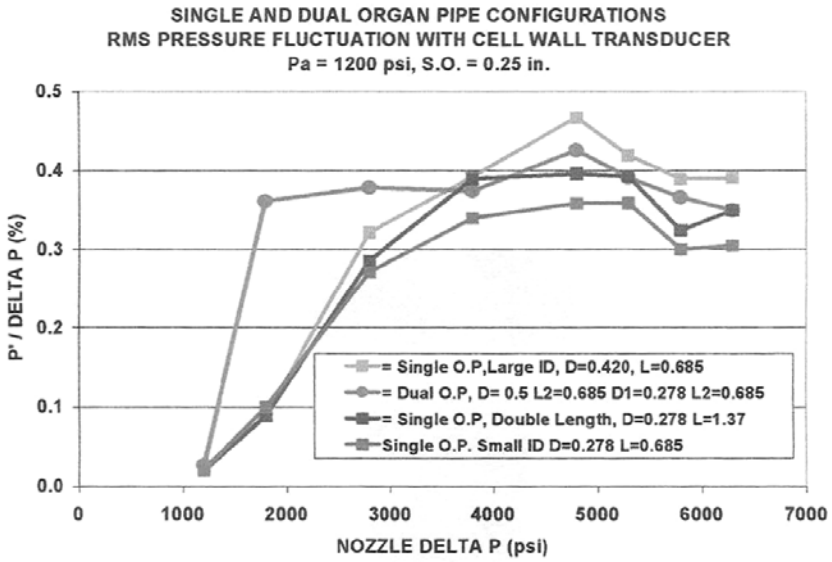

Figure 6a. Results of full scale pressure tests for single and dual organ pipe configurations of Table 2. Measured rms pressure over range of nozzle pressure drops.

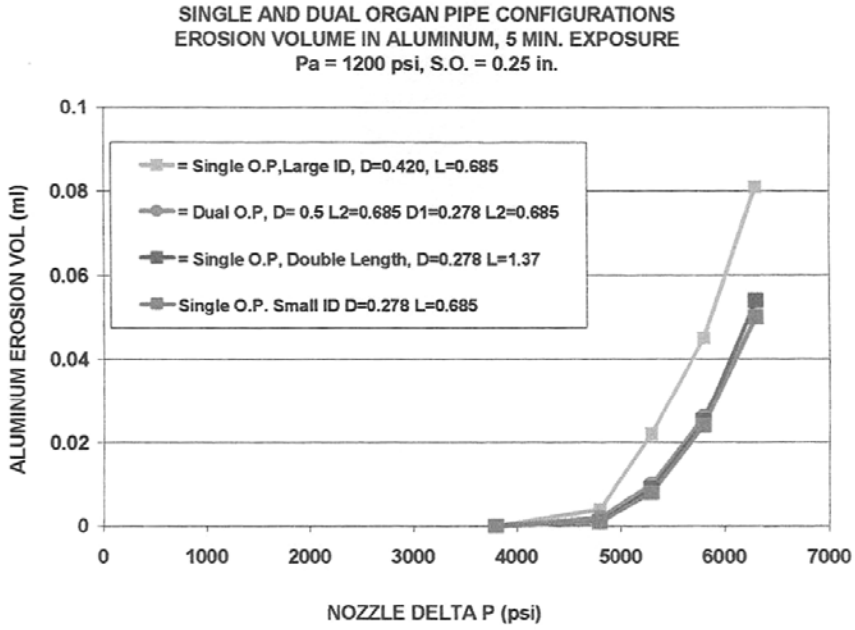

Figure 6b. Results of full scale pressure tests for single and dual organ pipe configurations of Table 2. Measured aluminum plate cut volumes (5 min. static exposure) over range of nozzle pressure drops

Organ Pipe Type	d_o inches	d_1 inches	d_2 inches	d_f inches	L_1 inches	L_2 inches
Single	0.06	0.278	--	0.72	0.685	--
Single – Large ID	0.06	0.420	--	0.72	0.685	--
Single – Double length	0.06	0.278	--	0.72	1.37	--
Dual	0.06	0.278	0.50	0.72	0.685	0.685

Table 2. Geometric details of dual and single organ pipe configurations employed to create the data of Figure 6.

Conclusions

It appears form our tests that the configuration with $p'/\Delta P$, and thus resonance, least sensitive to ΔP, is the dual organ pipe configuration which has a value that is over 80% of its peak value throughout the entire range of ΔP between 1,800 and 6,300 psi. However, all the single organ pipe configurations are also broadly peaked so that while their operating envelopes may not be as broad as that of the dual organ pipe, they are not narrow. In addition, the single, large diameter, organ pipe has larger values of $p'/\Delta P$ than the dual organ pipe configuration at all pressures of 3,800 psi and above.

Other observations from our tests (Figure 6) are that the single organ pipe configuration with the smaller diameter generally has the lowest values of $p'/\Delta P$ and also the smallest cut volumes. Doubling the length of this organ pipe (such that its length is the same as the sum of the two lengths of the dual organ pipe configuration) produces an improvement, but is not as much as attained with the dual organ pipe configuration nor with the larger diameter for the single organ pipe.

References

1. "Development of a Mud Jet-Augmented PDC Bit for Use with Conventional Rig Pressures," Sandia proposal to NADET, June 1996.
2. Chahine, G. L., Kalumuck, K.M., Aley, P. D. and Frederick, G. S., "Development of STRATOJET® Cavitating Mud Jet Nozzle for Use in PDC Bits Operating at Conventional Rig Pressures," DYNAFLOW, INC. Letter Report 97008-1, November 1998.
3. Chahine, G. L., and Johnson, V. E. Jr., "Mechanics and Applications of Self-Resonating Cavitating Jets," Intl. Symp. on Jets and Cavities, ASME, WAM, Miami, FL, November 1985.
4. Chahine, G. L., Kalumuck, K.M., and Frederick, G. S., "Cavitating Water Jets for Deep Hole Drilling in Hard Rock," Proceedings, 8th American Water Jet Conference, Houston, TX, August 1995.
5. Chahine G. L., Liu, H. L., Johnson V.E. Jr., and Frederick G.S., "Development of a STRATOJET® Nozzle for Optimum Resonance in Drilling Mud," Tracor Hydronautics Technical Report 84004, August 1984.
6. Chahine, G. L., Johnson, V. E. Jr., Kalumuck, K.M., Perdue, T. O., Waxman, D. N., Frederick, G. S., and Watson, R. E., "Internal and External Acoustics and Large Structure Dynamics of Cavitating Self-Resonating Water Jets," Sandia National Laboratories, Albuquerque, NM, Contractor Report SAND86-7176, July 1987.

Page intentionally left blank

Appendix G: Phase II Summary of Offset Measurements

Page intentionally left blank

Drag and Penetrating Load Offsets at 2000 psi.

No Flow									Average
Drag	53.2	59.0	53.9	52.6	58.0	62.0	60.3	58.7	57.2
Penatrating	9.6	9.6	10.2	8.8	6.1	5.7	5.2	4.5	7.4
Cavitating									
Drag	53.0	61.3	57.7	58.6					57.6
Penatrating	-74.7	-20.0	-19.2	-5.7					-29.9
Non Cavitating									
Drag	59.7	63.1							61.4
Penatrating	-45.1	-42.7							-43.9

Drag and Penetrating Load Offsets at 3000 psi.

No Flow											Average
Drag	64.0	60.3	64.9	61.5	65.3	64.3	64.0				63.5
Penatrating	6.3	5.7	6.4	4.0	7.4	6.4	6.2				6.1
Cavitating											
Drag	63.1	76.5	71.0	70.4	69.5	82.1	77.4	68.8	74.9	70.8	72.4
Penatrating	55.0	6.5	6.3	-1.3	3.6	7.9	-0.4	30.6	1.1	6.4	11.6
Non Cavitating											
Drag	79.9	79.0									79.5
Penatrating	7.0	20.1									13.6

Page intentionally left blank

Appendix H: Phase II Test Data Summary

Page intentionally left blank

Single Cutter with 0.375" Cavitating Orifice at 2000 psi.

Stats	Average	Minimum	Maximum	Average	Minimum	Maximum
DoC-#	010-1			010-2		
X axis (lb)	96.69312	-23.1934	261.2305	112.5503	-15.8691	308.8379
Y axis (lb)	-18.0382	-62.0117	33.20313	12.19147	-41.5039	61.52344
Z axis (lb)	104.3578	7.324219	310.0586	81.47789	-41.5039	283.2031
Velocity (in/sec)	2.343896	0	0	2.341455	0	0
Temperature (Deg F)	86.46541	84.70673	89.17557	84.73437	82.47355	88.05805
Pressure (psia)	2149.822	1864.729	2368.298	2092.728	1796.233	2309.646
Flow (gpm)	111.9767	107.415	117.2098	110.2677	104.0526	115.821
DoC-#	020-1			020-2		
X axis (lb)	189.0175	-85.4492	550.5371	154.6571	-29.2969	426.0254
Y axis (lb)	11.75687	-74.707	98.14453	-13.7311	-69.8242	42.96875
Z axis (lb)	162.179	-57.373	571.2891	170.5915	2.441406	441.8945
Velocity (in/sec)	2.343896	0	0	2.341455	0	0
Temperature (Deg F)	85.0469	82.47355	88.05805	83.73186	81.35727	85.82363
Pressure (psia)	2099.661	1810.911	2314.533	2194.047	1903.87	2422.063
Flow (gpm)	110.2934	105.4414	114.3591	111.3192	103.3947	116.3327
DoC-#	020-3			040-1		
X axis (lb)	156.6454	-14.6484	430.9082	247.3879	-112.305	793.457
Y axis (lb)	3.281311	-58.1055	63.96484	11.2449	-91.7969	115.7227
Z axis (lb)	63.37006	-107.422	373.5352	234.8897	-98.877	881.3477
Velocity (in/sec)	2.343896	0	0	2.343896	0	0
Temperature (Deg F)	86.84767	82.47355	89.17557	86.22362	82.47355	89.17557
Pressure (psia)	2125.493	1835.374	2334.084	2233.066	1952.796	2456.277
Flow (gpm)	109.9581	104.7835	114.7977	111.4802	102.5906	116.2596
DoC-#	040-2			080-1		
X axis (lb)	251.061	-117.188	804.4434	485.6313	-181.885	1418.457
Y axis (lb)	4.067535	-108.398	109.8633	-9.0509	-184.082	184.082
Z axis (lb)	246.2974	-109.863	748.291	556.1414	-106.201	1434.326
Velocity (in/sec)	2.343896	0	0	2.348779	0	0
Temperature (Deg F)	86.01452	83.59004	88.05805	83.81973	81.35727	85.82363
Pressure (psia)	2162.165	1864.729	2387.849	2089.501	1801.126	2294.982
Flow (gpm)	109.6387	103.4678	116.552	109.054	105.149	112.8972
DoC-#	080-2			080-3		
X axis (lb)	464.6272	-268.555	1452.637	450.728	-168.457	1314.697
Y axis (lb)	-17.5352	-188.477	158.6914	-14.0426	-180.664	129.8828
Z axis (lb)	418.3493	-328.369	1271.973	515.5879	-36.6211	1247.559
Velocity (in/sec)	2.343896	0	0	2.351221	0	0
Temperature (Deg F)	84.72495	82.47355	88.05805	84.71776	82.47355	88.05805
Pressure (psia)	1948.281	1659.24	2133.688	2025.194	1732.629	2216.779
Flow (gpm)	106.4621	100.2516	110.5581	108.4677	102.9561	112.5317

Stats	Average	Minimum	Maximum	Average	Minimum	Maximum

DoC-#	080-4			000-1		
X axis (lb)	438.5081	-224.609	1326.904	52.97348	28.07617	85.44922
Y axis (lb)	-13.6225	-186.523	124.5117	7.784668	-28.8086	42.96875
Z axis (lb)	431.2757	-195.313	1263.428	-74.734	-89.1113	-51.2695
Velocity (in/sec)	2.348779	0	0	2.175429	0	0
Temperature (Deg F)	86.69902	83.59004	89.17557	88.01322	85.82363	89.17557
Pressure (psia)	2155.23	1859.837	2368.298	2241.949	1952.796	2470.94
Flow (gpm)	109.0749	103.3216	112.6048	110.0096	104.2718	116.4789

DoC-#	000-2		
X axis (lb)	61.26144	29.29688	111.084
Y axis (lb)	-19.3875	-39.5508	5.371094
Z axis (lb)	-20.0478	-45.166	45.16602
Velocity (in/sec)	2.346338	0	0
Temperature (Deg F)	84.75071	81.35727	88.05805
Pressure (psia)	2149.74	1850.052	2373.186
Flow (gpm)	110.1326	106.9764	114.8708

Double Cutter with 0.375" Cavitating Orifice at 2000 psi.

Stats	Average	Minimum	Maximum	Average	Minimum	Maximum
DoC-#	010-1			010-2		
X axis (lb)	141.0312	0	332.0313	161.2837	7.324219	368.6523
Y axis (lb)	-13.7792	-55.1758	31.73828	-16.3868	-62.5	34.66797
Z axis (lb)	184.3103	58.59375	402.832	2.801056	-150.146	229.4922
Velocity (in/sec)	2.343896	0	0	2.346338	0	0
Temperature (Deg F)	85.74629	82.47355	89.17557	86.85137	83.59004	88.05805
Pressure (psia)	2139.381	1845.159	2343.859	1940.965	1649.455	2138.576
Flow (gpm)	110.0833	104.8566	116.4789	106.6851	97.16797	110.5581

DoC-#	010-3			020-1		
X axis (lb)	111.5897	14.64844	255.127	274.9241	8.544922	656.7383
Y axis (lb)	-2.1199	-37.1094	35.64453	-5.89969	-69.8242	60.05859
Z axis (lb)	148.9031	32.95898	308.8379	253.4489	-15.8691	633.5449
Velocity (in/sec)	2.346338	0	0	2.343896	0	0
Temperature (Deg F)	88.17462	85.82363	91.41122	86.95764	84.70673	90.29329
Pressure (psia)	1987.135	1693.489	2192.341	2053.245	1757.092	2255.881
Flow (gpm)	109.2088	103.1754	114.0667	108.6002	103.9795	112.8972

DoC-#	020-2			040-1		
X axis (lb)	221.1616	9.765625	532.2266	385.9528	-50.0488	889.8926
Y axis (lb)	-13.5068	-68.8477	72.26563	-17.8532	-110.352	64.45313
Z axis (lb)	155.9004	-84.2285	511.4746	394.7141	1.220703	977.7832
Velocity (in/sec)	2.341455	0	0	2.341455	0	0
Temperature (Deg F)	87.6982	84.70673	91.41122	88.99655	84.70673	91.41122
Pressure (psia)	2103.527	1810.911	2319.421	2033.313	1722.844	2241.218
Flow (gpm)	110.4369	104.3449	115.821	108.2457	101.6404	114.1398
Stats	Average	Minimum	Maximum	Average	Minimum	Maximum
DoC-#	040-2			080-1		

X axis (lb)	405.7457	-78.125	1047.363	757.664	-140.381	1818.848
Y axis (lb)	-20.0312	-134.277	84.47266	1.490936	-211.426	201.1719
Z axis (lb)	483.432	37.8418	1099.854	821.3059	-83.0078	1888.428
Velocity (in/sec)	2.341455	0	0	2.343896	0	0
Temperature (Deg F)	87.84506	84.70673	91.41122	85.75969	82.47355	89.17557
Pressure (psia)	2072.599	1771.77	2280.319	2003.687	1688.596	2216.779
Flow (gpm)	109.1886	102.4444	114.2129	107.7483	100.9825	112.9703

DoC-#	080-2		
X axis (lb)	770.284	-83.0078	1921.387
Y axis (lb)	10.73612	-193.359	223.1445
Z axis (lb)	841.6989	1.220703	1972.656
Velocity (in/sec)	2.343896	0	0
Temperature (Deg F)	85.93576	82.47355	88.05805
Pressure (psia)	2030.453	1713.059	2236.33
Flow (gpm)	107.9584	102.5906	113.2627

Triple Cutter with 0.375" Cavitating Orifice at 2000 psi.

Stats	Average	Minimum	Maximum	Average	Minimum	Maximum
DoC-#	010-1			010-2		
X axis (lb)	153.9497	-6.10352	421.1426	172.1478	13.42773	424.8047
Y axis (lb)	-15.068	-58.5938	32.71484	14.82428	-50.7813	66.89453
Z axis (lb)	172.1909	17.08984	491.9434	131.6282	-20.752	437.0117
Velocity (in/sec)	2.341455	0	0	2.343896	0	0
Temperature (Deg F)	87.07516	83.59004	90.29329	86.86882	83.59004	88.05805
Pressure (psia)	1985.827	1673.918	2177.678	2082.552	1786.448	2285.207
Flow (gpm)	108.0079	103.9795	113.9205	109.6208	105.5145	113.3358

DoC-#	020-1			020-2		
X axis (lb)	410.5199	35.40039	958.252	418.7412	29.29688	928.9551
Y axis (lb)	-14.6587	-89.3555	70.3125	18.41663	-73.2422	106.9336
Z axis (lb)	511.3744	151.3672	1110.84	489.6849	80.56641	1046.143
Velocity (in/sec)	2.343896	0	0	2.343896	0	0
Temperature (Deg F)	88.69266	85.82363	92.52936	88.80141	86.94074	92.52936
Pressure (psia)	2018.424	1713.059	2221.667	2125.441	1806.018	2348.747
Flow (gpm)	107.6977	101.7135	112.6048	110.8062	104.0526	116.6251

DoC-#	040-1			040-2		
X axis (lb)	693.5649	268.5547	1127.93	719.243	231.9336	1215.82
Y axis (lb)	-19.027	-117.188	57.61719	10.66284	-113.281	115.2344
Z axis (lb)	852.4799	297.8516	1403.809	886.7223	295.4102	1496.582
Velocity (in/sec)	2.343896	0	0	2.346338	0	0
Temperature (Deg F)	87.40645	84.70673	90.29329	87.09744	84.70673	89.17557
Pressure (psia)	2010.935	1693.489	2211.892	2124.706	1820.696	2343.859
Flow (gpm)	107.4344	103.1023	110.7043	108.6097	101.8597	113.9205

Stats	Average	Minimum	Maximum	Average	Minimum	Maximum
DoC-#	080-1			080-2		
X axis (lb)	1244.306	273.4375	2241.211	1287.672	368.6523	2558.594

Y axis (lb)	-18.4313	-188.477	166.0156	8.593933	-194.336	177.7344
Z axis (lb)	1475.954	358.8867	2519.531	1542.464	505.3711	2905.273
Velocity (in/sec)	2.343896	0	0	2.343896	0	0
Temperature (Deg F)	86.34336	83.59004	89.17557	85.96948	84.70673	89.17557
Pressure (psia)	2100.857	1732.629	2329.196	1999.42	1693.489	2202.116
Flow (gpm)	111.229	106.9033	116.552	107.5587	103.8333	112.8241
DoC-#	000-1			000-2		
X axis (lb)	57.65289	48.82813	68.35938	58.591	46.38672	73.24219
Y axis (lb)	-10.5784	-20.5078	0	-0.38532	-10.7422	10.74219
Z axis (lb)	-19.1786	-31.7383	-7.32422	-5.7045	-17.0898	7.324219
Velocity (in/sec)	2.343896	0	0	2.343896	0	0
Temperature (Deg F)	85.00878	82.47355	88.05805	85.94379	82.47355	89.17557
Pressure (psia)	2004.292	1703.274	2202.116	2058.926	1757.092	2265.656
Flow (gpm)	106.8865	101.7866	111.6545	108.2358	104.7835	111.2891

Single Cutter with 0.375" Noncavitating Orifice at 2000 psi.

Stats	Average	Minimum	Maximum	Average	Minimum	Maximum
DoC-#	010-1			010-2		
X axis (lb)	116.6318	48.82813	195.3125	107.3766	43.94531	187.9883
Y axis (lb)	-13.395	-29.2969	1.953125	3.095947	-15.625	21.48438
Z axis (lb)	126.2103	34.17969	241.6992	57.76596	-34.1797	173.3398
Velocity (in/sec)	2.343896	0	0	2.341455	0	0
Temperature (Deg F)	87.54108	86.94074	91.41122	85.75564	82.47355	89.17557
Pressure (psia)	2097.148	1815.803	2309.646	2117.502	1850.052	2324.309
Flow (gpm)	119.6606	113.6281	124.4463	121.4182	114.8708	126.7062
DoC-#	020-1			020-2		
X axis (lb)	171.1696	41.50391	329.5898	173.2494	46.38672	378.418
Y axis (lb)	14.10754	-20.5078	41.01563	9.333008	-18.5547	35.15625
Z axis (lb)	135.6932	-31.7383	349.1211	142.213	-24.4141	410.1563
Velocity (in/sec)	2.341455	0	0	2.339013	0	0
Temperature (Deg F)	86.01396	82.47355	89.17557	87.14674	84.70673	90.29329
Pressure (psia)	2118.749	1840.266	2329.196	2177.157	1903.87	2387.849
Flow (gpm)	119.4542	111.5814	126.779	122.6455	118.5256	126.4149
DoC-#	040-1			040-2		
X axis (lb)	272.4222	21.97266	534.668	266.1443	4.882812	498.0469
Y axis (lb)	-19.2307	-86.9141	36.13281	-0.4718	-66.4063	59.57031
Z axis (lb)	326.322	17.08984	683.5938	295.6963	-26.8555	573.7305
Velocity (in/sec)	2.346338	0	0	2.343896	0	0
Temperature (Deg F)	87.19779	84.70673	90.29329	89.03553	85.82363	91.41122
Pressure (psia)	2116.951	1830.481	2329.196	2122.318	1845.159	2334.084
Flow (gpm)	122.1587	111.8738	128.6727	122.8532	116.3327	128.0172
Stats	Average	Minimum	Maximum	Average	Minimum	Maximum
DoC-#	080-1			080-2		
X axis (lb)	450.5267	-39.0625	1005.859	469.7192	-68.3594	1135.254
Y axis (lb)	4.948792	-110.352	127.9297	7.470642	-114.258	131.8359

Z axis (lb)	452.9761	-114.746	1022.949	467.2125	-144.043	1132.813
Velocity (in/sec)	2.343896	0	0	2.343896	0	0
Temperature (Deg F)	90.29127	86.94074	93.6477	91.31934	88.05805	93.6477
Pressure (psia)	1958.766	1659.24	2177.678	2139.961	1845.159	2358.523
Flow (gpm)	116.0732	108.8769	120.2068	124.7519	118.7449	129.6196

Double Cutter with 0.375" Noncavitating Orifice at 2000 psi.

Stats	Average	Minimum	Maximum	Average	Minimum	Maximum
DoC-#	010-1			010-2		
X axis (lb)	141.9711	75.68359	224.6094	148.1105	83.00781	231.9336
Y axis (lb)	-14.1277	-27.3438	0	11.12982	-3.90625	24.41406
Z axis (lb)	160.5923	58.59375	290.5273	152.5671	56.15234	280.7617
Velocity (in/sec)	2.346338	0	0	2.341455	0	0
Temperature (Deg F)	87.2878	83.59004	91.41122	86.20645	82.47355	86.94074
Pressure (psia)	2033.47	1747.307	2246.105	2049.254	1766.878	2260.769
Flow (gpm)	120.164	115.017	123.7885	118.1481	110.7774	123.5692
DoC-#	020-1			020-2		
X axis (lb)	265.278	112.3047	412.5977	242.3466	83.00781	397.9492
Y axis (lb)	11.72412	-21.4844	39.0625	-11.5384	-44.9219	17.57813
Z axis (lb)	274.4344	58.59375	488.2813	293.0141	68.35938	515.1367
Velocity (in/sec)	2.341455	0	0	2.346338	0	0
Temperature (Deg F)	87.40449	83.59004	91.41122	91.05432	86.94074	93.6477
Pressure (psia)	2074.775	1791.34	2285.207	1942.269	1644.563	2163.015
Flow (gpm)	115.9003	109.1693	124.6656	117.0376	108.8038	122.5458
DoC-#	040-1			040-2		
X axis (lb)	432.1831	70.80078	747.0703	464.2264	144.043	827.6367
Y axis (lb)	5.319519	-72.2656	77.14844	17.41272	-56.6406	96.67969
Z axis (lb)	505.9332	17.08984	891.1133	533.2069	102.5391	983.8867
Velocity (in/sec)	2.343896	0	0	2.341455	0	0
Temperature (Deg F)	90.14547	86.94074	93.6477	91.22565	88.05805	94.76626
Pressure (psia)	2095.558	1810.911	2309.646	2117.049	1835.374	2334.084
Flow (gpm)	120.9083	112.4586	125.5408	124.734	113.9936	129.3282
DoC-#	080-1			080-2		
X axis (lb)	782.4902	168.457	1618.652	822.0222	151.3672	1848.145
Y axis (lb)	-7.53748	-134.766	100.5859	6.902161	-129.883	140.625
Z axis (lb)	893.1421	217.2852	1711.426	952.5485	175.7813	1906.738
Velocity (in/sec)	2.339013	0	0	2.339013	0	0
Temperature (Deg F)	87.17209	84.70673	90.29329	87.22823	83.59004	90.29329
Pressure (psia)	2090.951	1806.018	2304.758	2051.622	1781.555	2260.769
Flow (gpm)	118.9037	112.9703	124.958	118.1131	113.0434	122.2535

Triple Cutter with 0.375" Noncavitating Orifice at 2000 psi.

Stats	Average	Minimum	Maximum	Average	Minimum	Maximum
DoC-#	010-1			010-2		
X axis (lb)	152.5078	61.03516	280.7617	188.3612	95.21484	378.418
Y axis (lb)	-42.8385	-61.5234	-26.3672	4.073975	-15.625	17.57813
Z axis (lb)	281.0953	144.043	478.5156	79.06067	-61.0352	373.5352
Velocity (in/sec)	2.390286	0	0	2.353663	0	0
Temperature (Deg F)	86.74818	83.59004	90.29329	86.85514	85.82363	89.17557
Pressure (psia)	2072.293	1806.018	2280.319	2065.156	1757.092	2285.207
Flow (gpm)	118.7851	114.2129	122.3997	119.0098	112.0931	125.3223
DoC-#	010-3			010-4		
X axis (lb)	182.6161	102.5391	324.707	193.9561	80.56641	314.9414
Y axis (lb)	-20.2435	-40.0391	-3.90625	10.60339	-10.7422	28.32031
Z axis (lb)	227.0308	104.9805	437.0117	105.5246	-61.0352	285.6445
Velocity (in/sec)	2.343896	0	0	2.341455	0	0
Temperature (Deg F)	85.35216	83.59004	86.94074	89.67205	88.05805	90.29329
Pressure (psia)	2105.565	1840.266	2314.533	1938.94	1654.348	2143.464
Flow (gpm)	119.4378	113.555	124.3732	114.9063	106.7571	120.353
DoC-#	020-1			020-2		
X axis (lb)	387.1477	97.65625	693.3594	403.7492	92.77344	693.3594
Y axis (lb)	-19.5465	-59.5703	26.36719	2.482971	-43.9453	73.24219
Z axis (lb)	661.1255	249.0234	1074.219	288.5356	-131.836	700.6836
Velocity (in/sec)	2.341455	0	0	2.343896	0	0
Temperature (Deg F)	88.48613	85.82363	91.41122	88.47167	86.94074	89.17557
Pressure (psia)	1987.341	1703.274	2197.228	2082.191	1806.018	2294.982
Flow (gpm)	116.4076	109.681	120.4261	118.2118	112.3124	122.2535
DoC-#	020-3			020-4		
X axis (lb)	310.3203	114.7461	571.2891	333.6122	100.0977	629.8828
Y axis (lb)	-41.9183	-83.0078	9.765625	-8.9353	-51.7578	36.13281
Z axis (lb)	416.2546	151.3672	749.5117	378.0348	58.59375	788.5742
Velocity (in/sec)	2.378078	0	0	2.375637	0	0
Temperature (Deg F)	85.22846	82.47355	88.05805	86.72953	83.59004	89.17557
Pressure (psia)	2129.989	1820.696	2353.635	2089.898	1806.018	2304.758
Flow (gpm)	120.5246	116.0403	124.8118	120.3316	115.017	126.0507
DoC-#	040-1			040-2		
X axis (lb)	698.8734	175.7813	1154.785	715.2623	178.2227	1459.961
Y axis (lb)	-30.0319	-93.75	56.64063	5.107788	-85.9375	98.63281
Z axis (lb)	954.044	236.8164	1508.789	774.1901	70.80078	1691.895
Velocity (in/sec)	2.341455	0	0	2.341455	0	0
Temperature (Deg F)	86.04412	84.70673	88.05805	85.31872	81.35727	86.94074
Pressure (psia)	1991.927	1717.952	2202.116	2069.273	1801.126	2280.319
Flow (gpm)	116.6121	111.8738	122.3997	118.5651	114.5053	122.3997

Stats	Average	Minimum	Maximum	Average	Minimum	Maximum

DoC-#	080-1			080-2		
X axis (lb)	1271.357	466.3086	2229.004	1296.667	192.8711	2565.918
Y axis (lb)	-28.7296	-205.078	168.9453	-1.42822	-173.828	154.2969
Z axis (lb)	1611.651	705.5664	2597.656	1459.105	168.457	2719.727
Velocity (in/sec)	2.343896	0	0	2.339013	0	0
Temperature (Deg F)	85.93067	82.47355	89.17557	87.91845	86.94074	89.17557
Pressure (psia)	2044.575	1766.878	2255.881	2065.213	1786.448	2275.432
Flow (gpm)	119.4749	111.6545	123.1306	117.9959	110.5581	123.8616

DoC-#	000-1			000-2		
X axis (lb)	59.70795	48.82813	68.35938	63.13767	53.71094	75.68359
Y axis (lb)	-9.24445	-16.6016	0	-2.61609	-9.76563	5.859375
Z axis (lb)	-45.0864	-56.1523	-36.6211	-42.6588	-51.2695	-34.1797
Velocity (in/sec)	2.339013	0	0	2.336572	0	0
Temperature (Deg F)	87.33249	85.82363	88.05805	88.69867	85.82363	91.41122
Pressure (psia)	2059.844	1786.448	2270.544	2008.627	1727.737	2226.555
Flow (gpm)	117.6115	110.9236	122.0342	117.4112	112.6048	122.3997

Single Cutter with No Flow.

Stats	Average	Minimum	Maximum	Average	Minimum	Maximum
DoC-#	010-1			010-2		
X axis (lb)	130.5754	43.94531	239.2578	137.3611	39.0625	239.2578
Y axis (lb)	-4.73712	-19.5313	11.71875	-1.69617	-17.5781	10.74219
Z axis (lb)	117.6062	-4.88281	290.5273	124.8239	-12.207	290.5273
Velocity (in/sec)	2.339013	0	0	2.339013	0	0
Temperature (Deg F)	72.2407	71.31997	72.43441	72.16074	71.31997	73.54905
Pressure (psia)	18.57897	10.43493	25.11273	18.9349	10.43493	25.11273
Flow (gpm)	0.228521	0.074072	0.296287	0.229812	0.148144	0.370359

DoC-#	020-1			020-2		
X axis (lb)	196.846	24.41406	368.6523	195.3464	31.73828	339.3555
Y axis (lb)	1.880676	-34.1797	38.08594	-6.74719	-38.0859	28.32031
Z axis (lb)	195.6084	-39.0625	405.2734	203.4578	-17.0898	417.4805
Velocity (in/sec)	2.339013	0	0	2.339013	0	0
Temperature (Deg F)	72.19007	71.31997	73.54905	72.15023	71.31997	73.54905
Pressure (psia)	18.95203	10.43493	25.11273	18.64288	10.43493	25.11273
Flow (gpm)	0.230812	0.148144	0.296287	0.230618	0.148144	0.370359

DoC-#	040-1			040-2		
X axis (lb)	294.6895	-7.32422	668.9453	297.5687	-2.44141	681.1523
Y axis (lb)	-2.17163	-72.2656	79.10156	-1.1648	-75.1953	72.26563
Z axis (lb)	323.2115	-48.8281	715.332	324.2853	-46.3867	776.3672
Velocity (in/sec)	2.339013	0	0	2.339013	0	0
Temperature (Deg F)	72.13567	71.31997	73.54905	72.14493	71.31997	73.54905
Pressure (psia)	18.60465	10.43493	25.11273	19.13978	10.43493	25.11273
Flow (gpm)	0.231683	0.148144	0.296287	0.231747	0.148144	0.370359

Stats	Average	Minimum	Maximum	Average	Minimum	Maximum
DoC-#	080-1			080-2		

X axis (lb)	498.2755	-92.7734	1284.18	462.7397	24.41406	1215.82
Y axis (lb)	-4.94714	-137.695	127.9297	-0.67658	-146.484	103.5156
Z axis (lb)	523.8136	-141.602	1323.242	500.7944	14.64844	1176.758
Velocity (in/sec)	2.336572	0	0	2.336572	0	0
Temperature (Deg F)	72.10063	71.31997	73.54905	72.08399	71.31997	72.43441
Pressure (psia)	19.11685	10.43493	25.11273	19.52263	10.43493	30.00532
Flow (gpm)	0.232132	0.148144	0.370359	0.232113	0.148144	0.370359

Double Cutter with No Flow.

Stats	Average	Minimum	Maximum	Average	Minimum	Maximum
DoC-#	010-1			010-2		
X axis (lb)	179.6739	73.24219	285.6445	183.0405	70.80078	302.7344
Y axis (lb)	-0.69739	-18.5547	18.55469	0.740967	-19.5313	16.60156
Z axis (lb)	199.2502	39.0625	349.1211	198.5344	41.50391	354.0039
Velocity (in/sec)	2.339013	0	0	2.339013	0	0
Temperature (Deg F)	71.74269	71.31997	72.43441	71.77174	71.31997	72.43441
Pressure (psia)	20.29627	10.43493	30.00532	19.9226	10.43493	30.00532
Flow (gpm)	0.23253	0.148144	0.370359	0.232794	0.074072	0.370359
DoC-#	020-1			020-2		
X axis (lb)	299.5566	46.38672	546.875	294.503	85.44922	485.8398
Y axis (lb)	-0.08856	-33.2031	36.13281	-3.36859	-39.0625	36.13281
Z axis (lb)	356.8164	7.324219	688.4766	350.2492	56.15234	642.0898
Velocity (in/sec)	2.339013	0	0	2.341455	0	0
Temperature (Deg F)	71.80621	71.31997	72.43441	71.8494	71.31997	72.43441
Pressure (psia)	19.89936	10.43493	30.00532	19.93422	10.43493	25.11273
Flow (gpm)	0.232891	0.148144	0.370359	0.23303	0.148144	0.370359
DoC-#	040-1			040-2		
X axis (lb)	510.537	107.4219	913.0859	464.6585	78.125	849.6094
Y axis (lb)	-5.42609	-82.0313	92.77344	1.216064	-84.9609	73.24219
Z axis (lb)	623.7997	97.65625	1123.047	552.0502	61.03516	1044.922
Velocity (in/sec)	2.336572	0	0	2.336572	0	0
Temperature (Deg F)	71.92804	71.31997	72.43441	74.70515	73.54905	75.77894
Pressure (psia)	20.20698	10.43493	30.00532	18.27104	10.43493	30.00532
Flow (gpm)	0.233613	0.148144	0.296287	0.234331	0.074072	0.296287
DoC-#	080-1			080-2		
X axis (lb)	941.7831	-19.5313	2006.836	902.8619	92.77344	1850.586
Y axis (lb)	-7.9184	-154.297	137.6953	-13.0389	-173.828	132.8125
Z axis (lb)	1064.842	-26.8555	2026.367	1029.596	97.65625	1979.98
Velocity (in/sec)	2.339013	0	0	2.336572	0	0
Temperature (Deg F)	74.66083	73.54905	75.77894	74.66354	73.54905	75.77894
Pressure (psia)	18.7126	10.43493	25.11273	19.04071	10.43493	30.00532
Flow (gpm)	0.23515	0.074072	0.370359	0.234558	0.148144	0.370359

Triple Cutter with No Flow.

Stats	Average	Minimum	Maximum	Average	Minimum	Maximum
DoC-#	010-1			010-2		
X axis (lb)	262.168	131.8359	405.2734	246.9647	107.4219	412.5977
Y axis (lb)	-8.03326	-30.2734	13.67188	-2.54663	-25.3906	14.64844
Z axis (lb)	314.6509	124.5117	517.5781	293.2285	83.00781	527.3438
Velocity (in/sec)	2.336572	0	0	2.341455	0	0
Temperature (Deg F)	72.29462	71.31997	73.54905	72.26905	71.31997	72.43441
Pressure (psia)	17.58944	10.43493	25.11273	17.09376	10.43493	25.11273
Flow (gpm)	0.238442	0.148144	0.296287	0.238002	0.148144	0.296287
DoC-#	020-1			020-2		
X axis (lb)	482.1368	207.5195	778.8086	467.4754	163.5742	705.5664
Y axis (lb)	-8.56854	-61.5234	39.0625	-2.0108	-50.7813	39.0625
Z axis (lb)	625.8086	234.375	1042.48	599.4035	185.5469	915.5273
Velocity (in/sec)	2.339013	0	0	2.336572	0	0
Temperature (Deg F)	72.27511	71.31997	73.54905	70.89322	70.20574	71.31997
Pressure (psia)	17.51085	10.43493	25.11273	20.40635	10.43493	30.00532
Flow (gpm)	0.238502	0.148144	0.370359	0.226368	0.148144	0.296287
DoC-#	040-1			040-2		
X axis (lb)	806.8303	163.5742	1420.898	812.9974	258.7891	1472.168
Y axis (lb)	-6.65143	-102.539	117.1875	-1.8299	-112.305	105.4688
Z axis (lb)	1037.178	144.043	1789.551	1043.299	336.9141	1777.344
Velocity (in/sec)	2.336572	0	0	2.339013	0	0
Temperature (Deg F)	70.78918	69.09172	71.31997	70.30463	69.09172	71.31997
Pressure (psia)	20.52133	10.43493	30.00532	20.54212	15.32753	30.00532
Flow (gpm)	0.227322	0.148144	0.296287	0.23296	0.148144	0.370359
DoC-#	080-1			080-2		
X axis (lb)	1413.809	363.7695	2836.914	1485.394	380.8594	2819.824
Y axis (lb)	-9.11145	-242.188	202.1484	-7.54425	-220.703	207.0313
Z axis (lb)	1735.325	493.1641	3076.172	1835.481	590.8203	3125
Velocity (in/sec)	2.339013	0	0	2.339013	0	0
Temperature (Deg F)	73.51415	72.43441	74.66389	72.9656	71.31997	73.54905
Pressure (psia)	19.7009	10.43493	30.00532	19.51926	10.43493	30.00532
Flow (gpm)	0.232817	0.148144	0.296287	0.233007	0.148144	0.296287

Single Cutter with 0.3125" Cavitating Orifice at 3000 psi.

Stats	Average	Minimum	Maximum	Average	Minimum	Maximum
DoC-#	010-1			010-2		
X axis (lb)	127.6762	-1.2207	349.1211	94.94408	-6.10352	283.2031
Y axis (lb)	-10.4409	-59.082	34.17969	-16.7991	-83.0078	38.08594
Z axis (lb)	122.0191	13.42773	399.1699	95.74242	-18.3105	296.6309
Velocity (in/sec)	2.336572	0	0	2.339013	0	0
Temperature (Deg F)	85.07091	83.59004	86.94074	86.34685	84.70673	88.05805
Pressure (psia)	3086.176	2857.068	3282.298	3160.162	2901.057	3384.94
Flow (gpm)	97.33148	91.73283	102.079	98.05297	93.49558	101.4211
DoC-#	020-1			020-2		
X axis (lb)	180.1813	-42.7246	477.2949	183.5562	-53.7109	515.1367
Y axis (lb)	-0.94568	-65.4297	73.73047	-1.68082	-73.2422	69.33594
Z axis (lb)	150.8917	-23.1934	471.1914	175.945	-20.752	565.1855
Velocity (in/sec)	2.33413	0	0	2.336572	0	0
Temperature (Deg F)	87.35079	85.82363	89.17557	87.39423	85.82363	89.17557
Pressure (psia)	3112.101	2861.956	3321.4	3114.141	2866.843	3326.287
Flow (gpm)	97.29557	91.95317	101.4942	95.3682	89.30905	100.7632
DoC-#	040-1			040-2		
X axis (lb)	254.4645	-135.498	756.8359	243.6941	-126.953	780.0293
Y axis (lb)	-13.0067	-128.418	101.0742	-20.4936	-115.234	75.68359
Z axis (lb)	293.7366	-40.2832	760.498	285.8839	-10.9863	777.5879
Velocity (in/sec)	2.33413	0	0	2.336572	0	0
Temperature (Deg F)	81.02426	79.12532	82.47355	81.23499	80.24119	82.47355
Pressure (psia)	3097.038	2857.068	3301.849	3179.929	2910.833	3399.603
Flow (gpm)	98.59502	91.43904	105.9531	99.44461	91.95317	105.4414
DoC-#	080-1			080-2		
X axis (lb)	459.6188	-181.885	1308.594	429.6947	-220.947	1289.063
Y axis (lb)	-9.19278	-176.27	161.6211	-7.26209	-178.223	154.2969
Z axis (lb)	508.0917	-169.678	1328.125	452.2115	-235.596	1320.801
Velocity (in/sec)	2.339013	0	0	2.33413	0	0
Temperature (Deg F)	81.17821	79.12532	82.47355	82.34525	81.35727	83.59004
Pressure (psia)	3023.212	2798.416	3218.758	3015.586	2793.528	3199.207
Flow (gpm)	97.41744	92.54076	101.2749	96.48354	89.74974	100.617
DoC-#	000-1			000-2		
X axis (lb)	74.90852	46.38672	107.4219	70.77133	43.94531	107.4219
Y axis (lb)	-11.0227	-51.2695	25.87891	10.51294	-14.1602	40.03906
Z axis (lb)	1.078262	-20.752	25.63477	6.44516	-8.54492	28.07617
Velocity (in/sec)	2.33413	0	0	2.336572	0	0
Temperature (Deg F)	83.07345	82.47355	84.70673	83.39054	82.47355	84.70673
Pressure (psia)	3011.378	2783.753	3194.319	3086.918	2842.405	3287.186
Flow (gpm)	96.76722	91.21869	102.1521	99.25736	91.29214	105.2221

Single Cutter with 0.3125" Noncavitating Orifice at 3000 psi.

Stats	Average	Minimum	Maximum	Average	Minimum	Maximum
DoC-#	010-1			010-2		
X axis (lb)	93.601	17.08984	241.6992	96.05202	31.73828	252.6855
Y axis (lb)	5.920258	-31.25	46.875	-6.36417	-41.5039	29.78516
Z axis (lb)	59.45366	-15.8691	227.0508	48.27034	-20.752	214.8438
Velocity (in/sec)	2.336572	0	0	2.336572	0	0
Temperature (Deg F)	78.60758	76.8942	80.24119	79.81458	79.12532	81.35727
Pressure (psia)	3039.919	2695.774	3306.736	3048.15	2715.325	3301.849
Flow (gpm)	111.3388	104.0526	116.2596	110.916	102.883	115.017
DoC-#	020-1			020-2		
X axis (lb)	158.6743	-8.54492	413.8184	154.5306	10.98633	406.4941
Y axis (lb)	3.043335	-50.293	72.26563	-3.43076	-61.5234	53.71094
Z axis (lb)	123.4073	-39.0625	424.8047	128.7878	-9.76563	440.6738
Velocity (in/sec)	2.336572	0	0	2.336572	0	0
Temperature (Deg F)	81.23945	80.24119	82.47355	81.76108	80.24119	82.47355
Pressure (psia)	2926.705	2563.806	3194.319	2955.583	2583.357	3223.646
Flow (gpm)	111.3877	106.3185	115.3824	109.6203	105.149	114.5053
DoC-#	040-1			040-2		
X axis (lb)	254.367	-48.8281	697.0215	248.39	-68.3594	717.7734
Y axis (lb)	-6.1182	-103.027	99.12109	11.59366	-91.3086	98.63281
Z axis (lb)	273.1341	-47.6074	697.0215	284.072	-23.1934	742.1875
Velocity (in/sec)	2.339013	0	0	2.341455	0	0
Temperature (Deg F)	82.21639	81.35727	83.59004	81.9745	81.35727	83.59004
Pressure (psia)	2948.611	2588.244	3218.758	3032.856	2690.886	3301.849
Flow (gpm)	108.4431	102.883	113.7743	110.3799	105.2952	114.7977
DoC-#	080-1			080-2		
X axis (lb)	421.101	-150.146	1252.441	454.9582	-150.146	1472.168
Y axis (lb)	-10.1166	-191.406	167.9688	3.467407	-175.781	162.5977
Z axis (lb)	451.7622	-101.318	1289.063	481.9379	-148.926	1325.684
Velocity (in/sec)	2.33413	0	0	2.336572	0	0
Temperature (Deg F)	82.55373	81.35727	83.59004	83.5532	82.47355	84.70673
Pressure (psia)	3009.831	2656.672	3272.523	3056.704	2710.437	3321.4
Flow (gpm)	110.3401	105.2221	115.7479	110.1736	98.49003	115.6748
DoC-#	000-1			000-2		
X axis (lb)	79.0139	54.93164	115.9668	79.9398	56.15234	106.2012
Y axis (lb)	-12.7388	-34.1797	10.74219	9.017334	-24.4141	40.03906
Z axis (lb)	20.07927	1.220703	41.50391	7.028656	-17.0898	29.29688
Velocity (in/sec)	2.336572	0	0	2.339013	0	0
Temperature (Deg F)	83.27205	82.47355	85.82363	82.85525	80.24119	86.94074
Pressure (psia)	3045.069	2695.774	3306.736	3052.688	2695.774	3321.4
Flow (gpm)	112.716	107.3419	117.8677	111.9773	106.0992	114.7246

Page intentionally left blank

Appendix I: Direct Sintered Orifice Development

Page intentionally left blank

Direct-Sintered Orifice Development

U.S. Synthetic Corp
1260 South 1600 West
Orem, Utah 84058
801-235-9001

Letter Report
January 7, 2004

Fabrication of Nozzle

The nozzle assemblies were fabricated using single-piece carbide with in-situ sintering of the diamond to the carbide support structure. The carbide and the diamond feedstock material proper were placed onto a refractory can system common to the process of sintering diamond. This can assembly was placed into a heater assembly which was subsequently placed into a cube assembly consisting of the pressure transfer medium. This cube assembly was placed into a cubic press and run at a temperature and pressure consistent with the sintering of diamond to tungsten carbide. Upon completion of the sintering cycle, the cube assembly was removed from the press and the can assembly was extracted from the heater assembly. The can material was removed to visually inspect the quality of the diamond material. This visual method was employed to inspect the diamond and determine the press parameters required to produce an acceptable sintered diamond material. The size of the sintered piece was inspected using digital calipers. The remaining assemblies were run at the press using the selected parameters. The can material was removed by employing a lapping technique and also by a centerless grinding method. The throat and conic sections of the nozzle were formed using electric discharge machining (EDM).

Inspection reports

The nozzle assemblies were inspected visually for sintered diamond quality, support carbide integrity, and with calipers for dimensional stability. The proprietary information of these inspections was noted in the press run log and in the experimental notebook of the Principal Investigator.

Cost estimates for commercial production quantities of this nozzle:

$2,000.00 (US dollars) per nozzle assembly

Page intentionally left blank

Distribution:

Ken Bertagnolli, Ph.D., P.E.
U S Synthetic Corporation
1260 South 1600 West
Orem, UT 84058

Craig H. Cooley, P.E.
Manager, Test and Evaluation
U S Synthetic Corporation
1260 South 1600 West
Orem, UT 84058

Marcel Boucher
ReedHycalog
6501 Navigation
Houston, TX 77011

Bill Calhoun
ChevronTexaco Drilling Technology Center
2202 Oil Center Court
Houston, TX 77073

Louis E. Capuano, Jr.
ThermaSource, Inc.
PO Box 1236
Santa Rosa, CA 95402

Tom Champness
Drill-Cool Systems
627 Williams Street
Bakersfield, CA 93305

Robert I. Clayton
Security DBS
15815 Waverly Road
Houston, TX 77032

John H. Cohen
Maurer Technology Inc.
13135 South Dairy Ashford Rd.
Suite 800
Sugar Land, TX 77478

Ted Clutter
Executive Director
Geothermal Resources Council
P.O. Box 1350
Davis, CA 95617

Gary J. Collins
Staff Engineer
Drilling Technology
ConocoPhillips
P.O. Box 2197
Houston, TX 77250-2197

Jim Combs
Geo-Hills Associates
2395 Catamaran Drive
Reno, NV 89509-5731

Dr. George Cooper
UC – Berkeley
595 Evens Hall
Berkeley, CA 94720

Hal B. Curlett, COB/CEO
Deep Heat Energy Corporation
3101 - A Big Horn Ave
Cody, WY 82414

J. David Dowell
ChevronTexaco Exploration & Production Technology Co.
Floating Drilling
2811 Hayes Road, Room 4121
Houston, TX 77082

Mike Elsayed
University of Southwestern Louisiana
P.O. Box 44170
Lafayette, LA 70504-4170

Stephen Ernst
Hughes Christensen
9110 Grogan's Mill Road
The Woodlands, TX 77380-3615

Coy M. Fielder
Vice President of Technology
Diamond Products International
15955 West Hardy, Suite 300
Houston, TX 77060

Phil Frink
Blade Energy Partners
1415 Halsey Way, Suite 300
Carrollton, TX 75007

Marvin Gearhart
RBI-Gearhart
7601 Will Rogers Blvd.
Fort Worth, TX 76140-6023

Dave Glowka
Consultant
P.O. Box 415
Red Rock, TX 78662

Geir Hareland, Ph.D.
Harcon Inc.
803 Caine St.
Socorro, NM 87801

Craig Ivie
ReedHycalog
6501 Navigation
Houston, TX 77011

Allan Jelacic, Physical Scientist
EE-2C/Forrestal Building
U.S. Department of Energy
1000 Independence Ave. SW
Washington, DC 20585

Raymond J. LaSala, General Engineer
EE-2C/Forrestal Building
U.S. Department of Energy
1000 Independence Ave. SW
Washington, DC 20585

Dennis Kaspereit
Calenergy Operating Company
950 W. Lindsey Rd.
Calipatria, CA 92233

Buddy King
Noble Engineering
13135 South Dairy Ashford, Suite 800
Sugar Land, TX 77478

Roy Ledgerwood, III
Hughes Christensen
9110 Grogan's Mill Road
The Woodlands, TX 77380-3615

Bill Livesay
Livesay Consultants
126 Countrywood Lane
Encinitas, CA 92024-3109

James W. Lovekin
GeoThermex Inc.
5221 Central Ave., Suite 201
Richmond, CA 94804

Julian Luckett
Geothermal Energy Team
Shell Int'l Exploration & Production,
STV-GE
P.O. Box 60
2280AB Rijswijk
The Netherlands

Oliver Matthews
Hughes Christensen
9110 Grogan's Mill Road
The Woodlands, TX 77380-3615

William C. Maurer, Ph.D.
President
Maurer Technology Inc.
13135 South Dairy Ashford Rd. Suite
800
Sugar Land, TX 77478

Graham Mensa-Wilmot
Director
Smith Bits – GeoDiamond
16740 Hardy Street
Houston, TX 77032

Michael L. Payne, P.E., Ph.D.
c/o BP
501 Westlake Park Blvd.
Houston, TX 77079

Wyatt A. Pritchard
Security DBS
3000 N. Sam Houston Parkway E.
Houston, TX 77032

Robert P. Radtke, President
Technology International Inc.
2103 River Falls Drive
Kingwood, TX 77339-3154

Scott Randolph
Operations Manager
GTI Catoosa Test Facility Inc.
P.O. Box 1590
Catoosa, OK 74015

Richard Raney
RA-TECH
2800 Fannin Ave.
Midland, TX 79705

Bill Rickard
Resource Group
40201 Sagewood Drive
Palm Desert, CA 92260

Tom Roberts
ReedHycalog
6501 Navigation
Houston, TX 77011
Jim Senger
Diamond Products International
15500 International Plaza Drive
Houston, TX 77032

Gary L. Smith
Conoco Inc.
Leader, Drilling Technology
Offshore, 1006
P.O. Box 2197
Houston, TX 77252-2197

Paul Spielman
Coso Operating Co.
P.O. Box 1690
Inyokern, CA 93527-1690

Marc W. Steffen
Calpine, Drilling Manager
10350 Socrates Mine Road
Middletown, CA 95461

Bob Swanson
Unocal Corporation
1160 North Dutton Ave
Suite 200
Santa Rosa, CA 95401

Tommy M. Warren
Director, Research & Development
TESCO Drilling Technology
Rt. 1, Box 130-10
Coweta, OK 74429

Bob Worrall
Shell Int'l Exploration and Production
Research and Technical Services (RTS)
Volmerlaan 8
2280 AB Rijswijk
The Netherlands

Dennis L. Yeager, President
Diamond Oil Well Drilling Co. Inc.
P.O. Box 7843
Midland, TX 79708

Jeff Brami
Research Specialist
Exxon Production Research Company
P.O. Box 2189
Houston, TX 77252-2189

Tim Tilon
Vice President - Technology
Weatherford International Inc.
11909 Spencer Road (FM 529)
Houston, TX 77041-3011

Rhonda Lindsey
National Energy Technology Laboratory
Advanced Drilling, Completion and
Stimulation Systems
One West Third, Ste. 1400
Tulsa, OK 74103

John Rogers
National Energy Technology Laboratory
P.O. Box 880, MS E06
Morgantown, WV 26507-0880

Vishwas Gupta
ExxonMobil Upstream Research
Company
P.O. Box 2189
Houston, TX 77252-2189

Arnis Judsis
Terratek
1935 S. Fremont Dr.
Salt Lake City, UT 84104

Alan Black
Terratek
1935 S. Fremont Dr.
Salt Lake City, UT 84104

Leland L. (Roy) Mink
Program Manager
EE-2C/Forrestal Building
U.S. Department of Energy
1000 Independence Ave. SW
Washington, DC 20585

2	MS 9018	Central Technical Files	8945-1
2	MS 4536	Technical Library	4536
1	MS 0114	Kevin McMahon	1304
1	MS 0741	M. L. Tatro	6200
1	MS 0741	Rush Robinett	6210
1	MS 1033	Craig Tyner	6211
1	MS 1033	S. J. Bauer	6211
1	MS 1033	J. A. Henfling	6211
1	MS 1033	Jim Grossman	6211
25	MS 1033	David Raymond	6211
1	MS 1033	Douglas Blankenship	6211
1	MS 1033	R. A. Normann	6211
1	MS 1033	A. J. Mansure	6211
1	MS 1181	J. L. Wise	1646
1	MS 1033	Scott S. Kuszmaul	6211
1	MS 1033	Steve Knudsen	6211
1	MS 0706	Allen Sattler	6113
1	MS 0751	David Holcomb	6117
1	MS 0719	Jim Pierce	6142
1	MS 0161	Russell Elliot	11500
1	MS 1033	Yarom Polsky	6211
1	MS 1033	Charles Hickox	6211
1	MS 1033	Elton Wright	6211